WL-TR-91-4103

AD-A250 332

CHEMICAL VAPOR SYNTHESIS OF NIOBIUM ALUMINIDES

J. Chin, J.H.Norman, G.H. Reynolds
MSNW, Inc.
P.O. Box 865
San Marcos, California 92079

DTIC
ELECTE
MAY 06 1992
S D

January 1992

Final Report for Period April 1989 - July 1991

Approved for public release; distribution unlimited.

MATERIALS DIRECTORATE
WRIGHT LABORATORY
AIR FORCE SYSTEMS COMMAND
WRIGHT-PATTERSON AIR FORCE BASE, OHIO 45433-6533

92-12249

92

NOTICE

When Government drawings, specifications, or other data are used for any purpose other than in connection with a definitely government-related procurement, the United States Government incurs no responsibility or any obligation whatsoever. The fact that the government may have formulated or in any way supplied the said drawings, specifications, or other data, is not to be regarded by implication or otherwise in any manner construed, as licensing the holder or any other person or corporation, or as conveying any rights or permission to manufacture, use, or sell any patented invention that may in any way be related thereto.

This report is releasable to the National Technical Information Service (NTIS). At NTIS, it will be available to the general public, including foreign nations.

This technical report has been reviewed and is approved for publication.

William R Kerr

WILLIAM R. KERR
Project Engineer
Materials Behavior Branch
Metals and Ceramics Division

FOR THE COMMANDER

Allan W Gunderson

ALLAN W. GUNDERSON, Chief
Materials Behavior Branch
Metals and Ceramics Division

If your address has changed, if you wish to be removed from our mailing list, or if the addressee is no longer employed by your organization, please notify WL/MLLN, Wright-Patterson AFB OH 45433-6533 to help us maintain a current mailing list.

Copies of this report should not be returned unless return is required by security considerations, contractual obligations, or notice on a specific document.

UNCLASSIFIED

SECURITY CLASSIFICATION OF THIS PAGE

REPORT DOCUMENTATION PAGE

Form Approved OMB No. 0704-0188

1a. REPORT SECURITY CLASSIFICATION: UNCLASSIFIED	1b. RESTRICTIVE MARKINGS: None
2a. SECURITY CLASSIFICATION AUTHORITY	3. DISTRIBUTION/AVAILABILITY OF REPORT: Approved for public release: distribution is unlimited
2b. DECLASSIFICATION/DOWNGRADING SCHEDULE	
4. PERFORMING ORGANIZATION REPORT NUMBER(S): 91-01-12-11	5. MONITORING ORGANIZATION REPORT NUMBER(S): WL-TR-91-4103
6a. NAME OF PERFORMING ORGANIZATION: MSNW, Inc. / 6b. OFFICE SYMBOL (If applicable)	7a. NAME OF MONITORING ORGANIZATION: Materials Directorate (WL/MLLN) Wright Laboratory
6c. ADDRESS (City, State, and ZIP Code): P.O. Box 865 San Marcos, CA 92079	7b. ADDRESS (City, State, and ZIP Code): Wright-Patterson AFB, OH 45433-6533
8a. NAME OF FUNDING/SPONSORING ORGANIZATION / 8b. OFFICE SYMBOL (If applicable)	9. PROCUREMENT INSTRUMENT IDENTIFICATION NUMBER: F33615-89-C-5607
8c. ADDRESS (City, State, and ZIP Code)	10. SOURCE OF FUNDING NUMBERS

PROGRAM ELEMENT NO.	PROJECT NO.	TASK NO.	WORK UNIT ACCESSION NO.
65502F	3005	52	32

11. TITLE (Include Security Classification): hemical Vapor Synthesis of Niobium Aluminides

12. PERSONAL AUTHOR(S): J. Chin, J.H. Norman, G.H. Reynolds

13a. TYPE OF REPORT	13b. TIME COVERED	14. DATE OF REPORT (Year, Month, Day)	15. PAGE COUNT
Final	FROM 4/89 TO 7/91	January 1992	129

16. SUPPLEMENTARY NOTATION

17. COSATI CODES			18. SUBJECT TERMS (Continue on reverse if necessary and identify by block number)
FIELD	GROUP	SUB-GROUP	Intermetallic Compounds, Vapor Deposition

19. ABSTRACT (Continue on reverse if necessary and identify by block number)

Chemical vapor deposition of niobium aluminides, niobium silicides, metal-rich compositions containing dispersed metallic phases, and ternary compositions in the titanium-niobium-aluminum system was performed by several techniques. Process chemistry models were used to select deposition conditions and for correlation with experimental results on deposit compositions. Conditions were identified which permitted direct chemical vapor deposition of small samples of intermetallic foils.

20. DISTRIBUTION/AVAILABILITY OF ABSTRACT	21. ABSTRACT SECURITY CLASSIFICATION
☐ UNCLASSIFIED/UNLIMITED ☐ SAME AS RPT ☒ DTIC USERS	UNCLASSIFIED
22a. NAME OF RESPONSIBLE INDIVIDUAL: William R. Kerr	22b. TELEPHONE (Include Area Code): (513) 255-9834 / 22c. OFFICE SYMBOL: WL/MLLN

DD Form 1473, JUN 86 *Previous editions are obsolete.*

SECURITY CLASSIFICATION OF THIS PAGE
UNCLASSIFIED

TABLE OF CONTENTS

Section		Page
	LIST OF FIGURES	iv
	LIST OF TABLES	ix
1.	PROGRAM OVERVIEW	1
2.	TASK DESCRIPTIONS	3
3.	MODELING STUDIES	4
	3.1 AlCl(g) AS AN Al SOURCE FOR $NbAl_x$ DEPOSITION	4
	3.1.1 Basic Thermochemistry	4
	3.1.2 Reaction Mechanisms of $NbAl_x$ Deposition	13
	3.1.3 $NbAl_x$ from $NbCl_5$ and AlCl Generated from MAl_x	17
	3.2 HYDROGEN REDUCTION OF ALUMINUM AND NIOBIUM CHLORIDES TO PRODUCE INTERMETALLIC COMPOUNDS	19
	3.3 CONCLUSIONS	24
4.	DEPOSITION STUDIES	26
	4.1 $NbAl_x$ DEPOSITION WITH AlCl AS Al SOURCE	28
	4.1.1 Deposition on Doubly Supported Substrates	32
	4.1.2 Deposition on Singly Supported Substrates	48
	4.2 $NbAl_x$ DEPOSITION BY H_2 REDUCTION	69
	4.2.1 Deposition on Doubly Supported Substrates	69
	4.2.2 Deposition on Singly Supported Niobium Substrates	72
	4.3 DEPOSITION OF Nb_xSi_y FROM H_2, $NbCl_5$, AND $SiCl_4$	85
	4.4 DEPOSITION OF $Nb_xAl_yTi_z$ TERNARY ALLOYS	93
5.	COMPOSITE MATERIAL FORMATION (CVI)	103
6.	MECHANICAL TESTING OF FOILS	111
7.	SUMMARY	115
8.	REFERENCES	118

Codes
Dist | Avail and/or Special
A-1

LIST OF FIGURES

Figure		Page
3-1.	Phase diagram of the Nb-Al system	5
3-2.	Al-Nb activity diagram according to Malets' data (900 K)	7
3-3.	Equilibrium constant for AlCl(g) formation from Al(l) + $AlCl_3$(g)	18
3-4.	Derivable Al activities from $AlCl_3$, $NbCl_3$, H_2 mixtures as compared with Nb-Al activities	22
4-1.	Schematic diagram of the molten aluminum system chamber	30
4-2.	The molten aluminum deposition system showing (a) the assembled deposition chamber, heated chloride sources, and vacuum system and (b) the gas flow control panel and temperature monitors	31
4-3.	Typical temperature distribution in the molten aluminum system deposition chamber	33
4-4.	Surface features of porous, discontinuous Nb_xAl_y which are typical of gas phase nucleated deposits from AlCl, $NbCl_5$, and H_2 (sample JB200-86)	37
4-5.	Optical photomicrograph of the cross section of a porous, discontinuous Nb_xAl_y deposit from AlCl, $NbCl_5$, and H_2 (sample JB200-94)	38
4-6.	A continuous film of Nb_xAl_y deposited from the AlCl reduction of $NbCl_5$ without hydrogen (sample JB200-98)	39
4-7.	Niobium aluminide deposited from a moderate increase in the flow rates of $NbCl_5$, AlCl, and He over samples JB300-84 to JB300-96 (sample JB200-108)	40
4-8.	Surface morphology of niobium aluminide deposited on niobium from moderate flow rates of $NbCl_5$, AlCl, and He (sample JB200-110)	41
4-9.	Film fractures due to CTE mismatch between CVD niobium aluminide and the tantalum substrate (sample JB200-106)	42

LIST OF FIGURES (continued)

Figure		Page
4-10.	Overview of a CVD Nb_xAl_y film on tantalum with variable niobium and aluminum contents end to end (sample JB200-112)	43
4-11.	High niobium content, nearly crack-free Nb-$NbAl_x$ films deposited on tantalum by the AlCl reduction process (sample JB200-114)	44
4-12.	High niobium content, nearly crack-free Nb-$NbAl_x$ films deposited by the AlCl reduction process (sample JB200-118)	45
4-13.	SEM photomicrograph of a Nb_xAl_y deposit on tantalum with a high niobium content surface and lower niobium content deposit/substrate interface (sample JB200-120)	46
4-14.	Schematic diagram of the molten aluminum system deposition chamber with a tube furnace heated substrate	49
4-15.	Schematic diagram of the inert gas injection system showing the added helium inlets directed at the molten aluminum or at the substrate	50
4-16.	Schematic diagram of the added helium gas injection system, directed at right angles to the substrate, showing its relationship to the deposition chamber	51
4-17.	Optical photomicrographs at 1000X of deposit samples (a) JB200-128 and (b) JB200-130 on tantalum	55
4-18.	SEM photomicrographs of (a) a typical porous niobium-aluminum deposit (JB200-134) as viewed normal to the substrate and (b) a fractured cross section of the deposit	56
4-19.	SEM photomicrograph of a fractured cross section of deposit JB200-136 on a 25-μm thick niobium foil substrate	57
4-20.	Optical photomicrographs of niobium-aluminum deposits showing (a) reactivity with a tantalum substrate at 960°C (sample JB200-124, 500X) and (b) no reactivity with a niobium substrate at 950°C sample JB200-138, 200X)	58

LIST OF FIGURES (continued)

Figure		Page
4-21.	SEM photomicrographs of sample JB200-140, an isolated grain columnar deposit of niobium-aluminum on niobium	59
4-22.	Porous niobium-aluminum sample JB200-144 deposited on niobium at 7 torr	60
4-23.	Variation in the morphology of deposit JB200-146 across the length of the niobium foil substrate	61
4-24.	SEM photomicrographs of a thick niobium-aluminum deposit (JB200-148) formed with auxiliary helium impinging on the substrate	63
4-25.	SEM photomicrographs of niobium-aluminum sample JB200-150 deposited with auxiliary helium flow parallel to the substrate surface	64
4-26.	Niobium and aluminum contents, end to end, of deposits formed (1) without auxiliary helium in the reactive gas (sample JB200-124), (2) with auxiliary helium directed at the molten aluminum (sample JB200-146), and (3) with auxiliary helium parallel to the substrate (sample JB200-150)	66
4-27.	Niobium and aluminum contents of deposit JB200-148 taken from the substrate surface to the deposit surface	67
4-28.	Schematic diagram of the resistance heated reactor used for $NbAl_x$ deposition from $NbCl_5 + AlCl_3 + H_2$	70
4-29.	SEM photomicrographs of a subatmospheric 1500°C $NbAl_x$ deposit	73
4-30.	Schematic diagram of the isothermal CVD deposition system used for the formation of Nb_xAl_y by the hydrogen reduction of the halides	75
4-31.	Optical photomicrographs at 1000X of cross sections of niobium-aluminum deposited at 1600°C on niobium at (a) moderate $NbCl_5$ flow (sample JD300-40) and (b) low $NbCl_5$ flow (sample JD300-42)	78
4-32.	SEM photomicrographs of niobium-aluminum sample JD300-42 showing mud cracking of the deposit due to the differential coefficient of thermal expansion between the substrate and deposit	79

LIST OF FIGURES (continued)

Figure		Page
4-33.	Porous niobium-aluminum deposit (JD300-43) due to excess aluminum in the reactive gas mixture	80
4-34.	Dense niobium-aluminum deposit (JD300-44) formed on a niobium substrate	81
4-35.	Morphology of niobium-aluminum deposited with (a) excess niobium (sample JD300-44) and (b) excess aluminum (sample JD300-52)	82
4-36.	Optical photomicrographs of niobium-aluminum deposited samples. (a) JD300-53, niobium rich; (b) JD300-54, aluminum rich	83
4-37.	Nb_xSi_y from the hydrogen reduction of the halides showing large void formation (sample JD300-34)	88
4-38.	Nb_xSi_y from the hydrogen reduction of the halides showing large void formation (sample JD300-35)	89
4-39.	SEM photomicrographs of thick Nb_xSi_y films deposited on niobium from the hydrogen reduction of the halides showing minimal void formation (sample JD300-33) . . .	90
4-40.	Thick Nb_xSi_y films deposited on niobium from the hydrogen reduction of the halides showing minimal void formation (sample JD300-33): (a) SEM photomicrograph (1000X); (b) optical photomicrograph (1000X)	91
4-41.	Thick Nb_xSi_y films deposited on niobium from the hydrogen reduction of the halides showing minimal void formation (sample JD300-36): (a) SEM photomicrograph (1000X); (b) optical photomicrograph (1000X)	92
4-42.	The 1200°C section of the Nb-Ti-Al system phase diagram (Ref. 4-1)	94
4-43.	SEM photomicrograph of an NbTiAl intermetallic film containing 58.6 at. % Nb, 35.5 at. % Al, and 5.9 at. % Ti	97
4-44.	Cross sectional views of vapor deposited $Nb_xAl_yTi_z$ (sample JD300-16) on niobium foil: (a) optical photomicrograph of an etch sample at 500X; (b) SEM photomicrograph	98

LIST OF FIGURES (continued)

Figure		Page
4-45.	Cross sectional views of $Nb_xAl_yTi_z$ (sample JB300-20) deposited on niobium showing porosity in high titanium concentration areas: (a) optical photomicrograph at 1000X; (b) SEM photomicrograph	99
4-46.	SEM photomicrograph of a cross section of $Nb_xAl_yTi_z$ (sample JB300-22) deposited on niobium showing the formation of a porous high titanium content material between the niobium substrate and the outer intermetallic deposit	100
4-47.	SEM photomicrograph of high titanium content $Nb_xAl_yTi_z$ (sample JB300-24) deposited on niobium without porous and multiple $Nb_xAl_yTi_z$ layers previously observed in equivalent experimental trials	101
5-1.	SEM photomicrographs of niobium aluminide infiltrated 3M alumina tow as processed in experiment JB300-4	105
5-2.	SEM photomicrographs of niobium aluminide infiltrated 3M alumina tow as processed in experiment JB300-6	106
5-3.	Schematic diagram of the experimental setup used for vapor infiltration of alumina tow	107
5-4.	Examples of porous niobium aluminide deposits on 3M alumina from experiments (a) JB300-8, (b) JB300-10-1	108
5-5.	Metallographic photomicrographs at 500X of chemical vapor infiltrated 3M alumina tow from experiments (a) JB300-10-1 and (b) JB300-12-1 showing partial infiltration and nonuniform deposition of the exterior of the fiber tow	109
6-1.	Single filament tensile tester used for Nb_xAl_y foil tensile tests	112
6-2.	Nb_xAl_y foil sample epoxy bonded to a paper template .	113
6-3.	Test sample epoxy bonded to a paper template and mounted in the test fixture	114

LIST OF TABLES

Table		Page
3-1.	High Temperature Al Coating Reactions	9
3-2.	AlX_3 Properties	10
3-3.	High Temperature Nb Coating Reaction	11
3-4.	NbX_5 Properties	11
3-5.	Aluminum Chloride Equilibria (Pressures in atm)	12
3-6.	High Temperature Coating Reactions	14
3-7.	High Temperature Combined Nb-Al Coating Reactions	15
3-8.	Thermodynamics of $AlCl_3(g)$ Reduction to $Al(\ell)$ by H_2	21
4-1.	Process Parameters for Nb_xAl_y Deposition at Atmospheric Pressures from the AlCl Reduction of $NbCl_5$ with Hydrogen	34
4-2.	Process Parameters for Nb_xAl_y Deposition at Atmospheric Pressures from the AlCl Reduction of $NbCl_5$ without Hydrogen	35
4-3.	Evaluation Results of Selected Nb_xAl_y Deposition Experiments	36
4-4.	Process Parameters for the CVD of Nb_xAl_y Foil by the Molten Aluminum - AlCl Process	52
4-5.	Results of Nb_xAl_y Deposition from the Molten Aluminum - AlCl Process	54
4-6.	Process Parameters for Nb_xAl_y Deposited from the H_2 Reduction of $AlCl_3$ and $NbCl_5$ on Double Supported Substrates	71
4-7.	Process Parameters for the CVD of Nb_xAl_y Foil from the Hydrogen Reduction of $AlCl_3$ and $NbCl_5$ on Singly Supported Niobium Substrates	76
4-8.	Evaluation Results of Nb_xAl_y Deposition from the H_2 Reduction of $NbCl_5$ and $AlCl_3$ on Singly Supported Substrates	84
4-9.	Process Parameters for CVD Nb_xSi_y Foil Deposition	86
4-10.	Results of Nb_xSi_y Deposition Experiments	87
4-11.	Ternary Alloy Deposition	96

LIST OF TABLES (continued)

Table		Page
4-12.	Results of $Nb_xAl_yTi_z$ Deposition Experiments	102
5-1.	Process Parameters for Chemical Vapor Infiltration of 3M Alumina Tow	104
5-2.	Composition of Nb_xAl_y Deposits on 3M Alumina Tow . .	104

CHEMICAL VAPOR SYNTHESIS OF NIOBIUM ALUMINIDES

1. PROGRAM OVERVIEW

The objective of this Phase II project was to develop and evaluate chemical vapor deposition (CVD) processes for producing foils which might potentially be used in the preparation of intermetallic matrix composites. All process and material development efforts were supported by thermochemical modeling of the deposition reactions. Two processes for the formation of niobium aluminide were examined: (1) AlCl reduction of $NbCl_5$ by AlCl disproportionation and (2) H_2 reduction of $AlCl_3$ and $NbCl_5$. AlCl was formed in situ by passing gaseous $AlCl_3$ through molten aluminum. Deposition temperatures in the AlCl reduction process were typically 400° to 600°C cooler than those in the H_2 reduction process owing to the greater stability of $AlCl_3$ relative to HCl. The AlCl process was found to be strongly influenced by both the process parameters and the geometry of the system. The reactions between the precursor gases are apparently very rapid. Deposits from this process were porous, which is typical of deposits found in gas phase nucleated processes. The high temperature of the H_2 reduction process for niobium aluminide formation made reactivity between the deposit and substrate unavoidable. The deposition process was, however, more readily controlled than with the AlCl process.

CVD processes for the deposition of Nb_xSi_y were also evaluated. The hydrogen reduction of the halides of niobium and silicon was used in the CVD of niobium silicides. While this deposition process was more easily controlled than those used in the formation of niobium aluminides, interdiffusion of silicon between the deposit and substrate was unavoidable.

Nb-Al-Ti ternary alloys were successfully deposited by both the AlCl and H_2 reductions of the metal halides. Compositional control of these deposits by this process is unknown.

Chemical vapor infiltration of Nb_xAl_y matrices into thermochemically compatible ceramic fiber tow was attempted. Filaments of the tow were coated but chemical vapor infiltration was not demonstrated.

The deposits tested were primarily characterized by optical microscopy, scanning electron microscopy (SEM), and energy dispersive x-ray (EDAX). Limited attempts to tensile test samples of the product intermetallic foils failed because of the porosity of the deposits.

2. TASK DESCRIPTIONS

The project consisted of the following tasks:

1. Process Modeling
2. Process Optimization
3. Deposition of Nb-Si Compositions
4. Deposition of Ternary Intermetallic Compositions
5. Deposition of Intermetallic Compounds Containing Dispersed Metallic Phases
6. Chemical Vapor Infiltration of Ceramic Fiber Tow
7. Material Characterization

3. MODELING STUDIES

The starting point for each experimental investigation was a thermodynamic evaluation of potential gas precursors. In this section the equilibrium conditions for the deposition of desired products are described as a function of gas composition and temperature. These descriptions should aid in selecting process parameters to generate deposits with the desired composition.

Two basic chemical approaches were considered. In the first approach, AlCl(g) prepared by the reaction of $AlCl_3$(g) with Al(l) served as the Al source and as the reducing agent for the preparation of $NbAl_x$ from $NbCl_5$. In the second approach, $AlCl_3$ served as the Al source and H_2 served as the reducing agent for both Al and Nb.

3.1 AlCl(g) AS AN Al SOURCE FOR $NbAl_x$ DEPOSITION

3.1.1 Basic Thermochemistry

The Nb-Al phases expected to be encountered during this study and their chemical stabilities in terms of chemical activities of the basic components were the subject of a literature search and evaluation. There appears to be agreement among several authors regarding the phase diagram for the Nb-Al system, which is shown in Figure 3-1 as reported by Lundin and Yamamoto (Ref. 1). This diagram shows Nb_3Al and Nb_2Al as extended compounds and an $NbAl_3$ line compound, all stable up to temperatures greater than 1500°C. The composition NbAl falls in the two-phase region $Nb_{2-x}Al$-$NbAl_3$ and is not a known compound. The diagram does not indicate the solubility of Nb in Al but does indicate considerable solubility of Al in Nb. Thus, the thermodynamically stable phases for the compositions to be synthesized were Nb, Al, Nb_3Al, $Nb_{2-x}Al$-$NbAl_3$, and $NbAl_3$ (and perhaps two-phase systems in the immediate vicinity of $NbAl_3$).

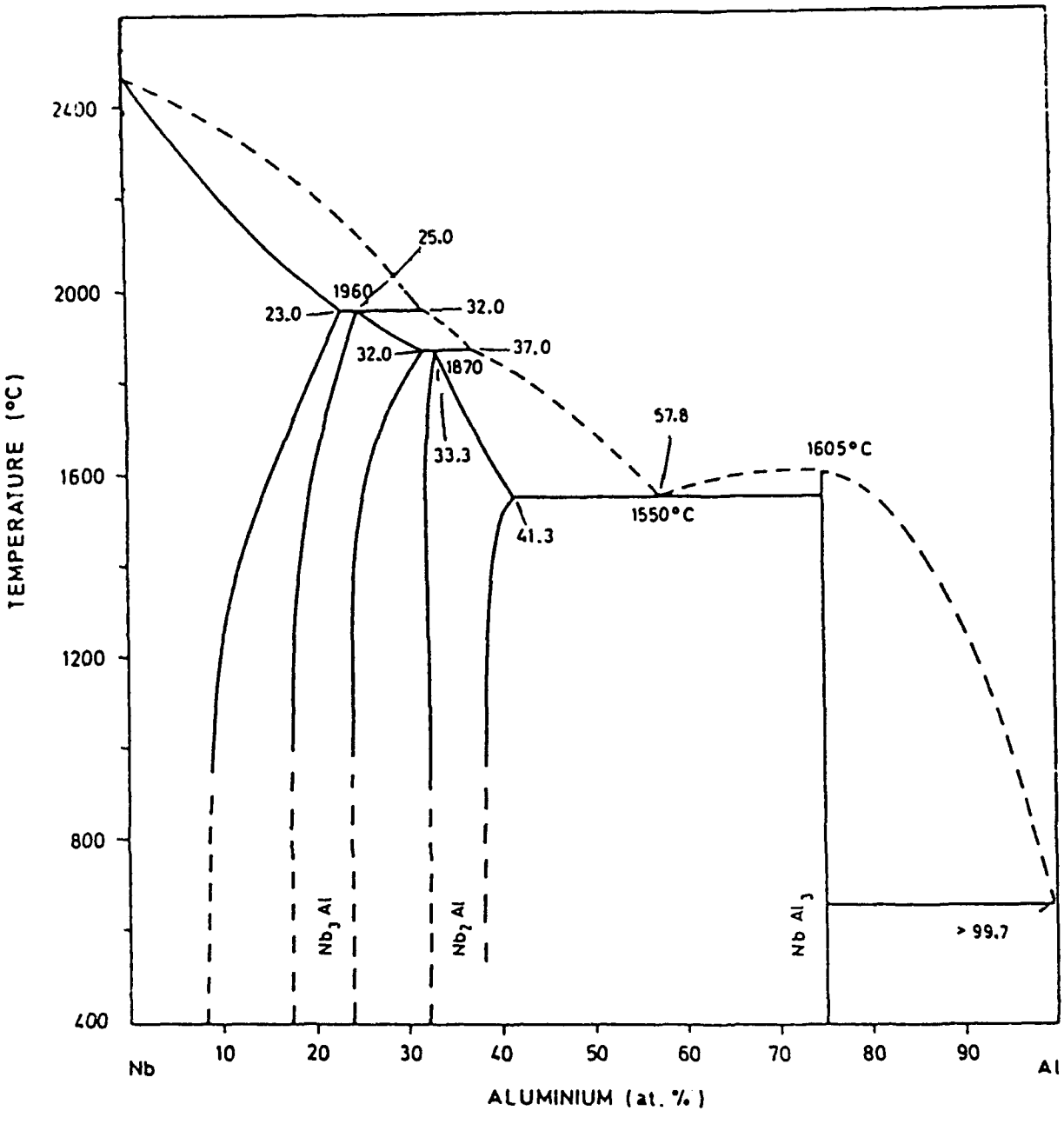

Figure 3-1. Phase diagram of the Nb-Al system.

The thermodynamics of these phases have been described by Malets (Ref. 2), who studied this system electrochemically. A table in his report describes important thermodynamic quantities, both measured and estimated. What have been measured are the voltages of a concentration cell comparing Nb-Al alloys with Al(s) near 900 K. Here the 900 K data of Malets have been reduced to Al activities and, additionally, to Nb activities at this temperature using Gibbs-Duhem techniques. Figure 3-2, which is an activity diagram at 900 K, has been constructed from Malets' values (Ref. 2) where the data allow. The dotted lines, used to fill in this diagram, represent interpolated and extrapolated values and are expected to be qualitatively correct if not quantitatively. The points worthy of note are the low Al activity in Nb-Al solutions as compared with the Nb activity on the high Al side. Al thus appears to be bound more tightly in the intermetallic compounds than Nb. It is also suggested that the $NbAl_3$ compound will exist over a wider range of Al activities than either the Nb_3Al or Nb_2Al compound even though it is basically a line compound. This is also probably true for Nb activities. High temperature synthesis around $NbAl_3$ may indeed lead to $NbAl_{3\pm x}$ phase, and it may be difficult to contaminate this phase with Al or $Nb_{2-x}Al$ in small amounts due to this high stability if one is using near-equilibrium methods of film deposition.

Figure 3-2 can also be used to predict alloys deposited under various, close to equilibrium, coating conditions. For instance, $Nb_{0.96}Al_{0.04}$ would be deposited with an Nb activity near unity and an Al activity of 10^{-11} at 900 K. For a system $pAlCl_3 = 0.01$, $pH_2 = 0.1$, $pHCl = 0.01$, the Al activity is 4×10^{-12}. Thus, Al will be codeposited while depositing Nb (from $NbCl_5$ reduction by H_2) at a concentration around 4%, but its activity would be far below that necessary to make Nb_3Al (Al activity = 10^{-6}). Therefore, the temperature must be considerably increased or the Al activity increased using techniques other than H_2 reduction for successful codeposition.

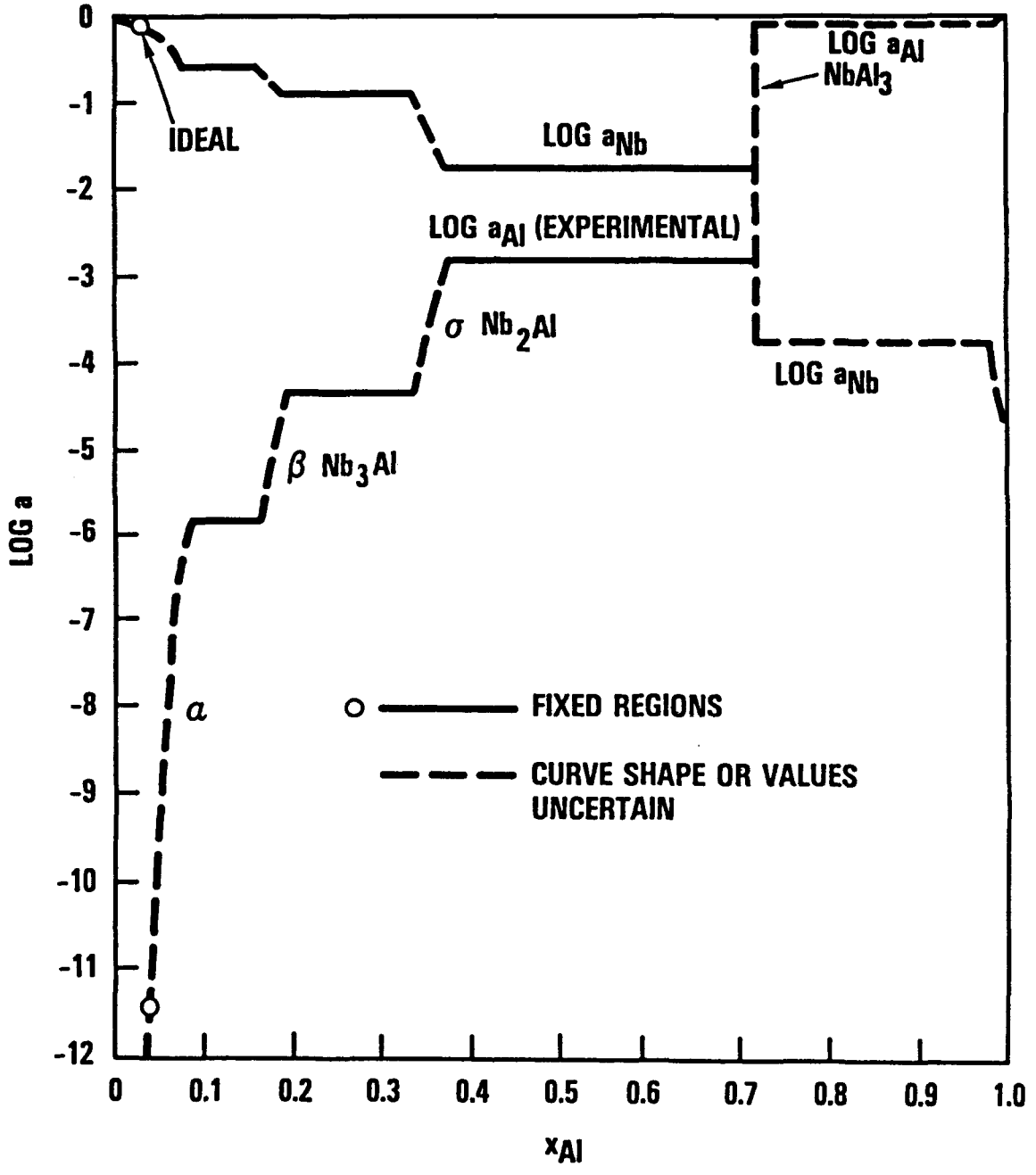

Figure 3-2. Al-Nb activity diagram according to Malets' data (900 K).

High temperature Al deposition has usually been performed by a sequence similar to that occurring in a pack cementation process where $AlCl_3(g)$ is reduced to AlCl(g) by Al(s). This reaction then reverses in the presence of an Al sink or upon lowering of the temperature. The extended equations which govern this process are shown in Table 3-1. Physical properties of various AlX_3 halides are shown in Table 3-2 for aiding the selection of the proper halide for the coating process. Note the 3HCl energies listed and compared with the $AlX_3(g)$ energies. This comparison indicates that it is difficult (at lower temperature at least) to reduce an aluminum halide with H_2. This process will work, but only at rather high temperatures.

In contrast, for chlorides the reaction shown in Table 3-3 and the data shown in Table 3-4 for Nb are more encouraging since they are 20 kcal lower for $NbCl_5$ reduction than $AlCl_3$ reduction. The liberation of 5HCl instead of 3HCl formed also helps the reduction. The $NbCl_5$ reduction proceeds readily at about 1000 K in H_2.

Calculations of equilibrium pressures of HCl, AlCl, $AlCl_2$, $AlCl_3$, and Al_2Cl_6 have been made under conditions representative of a coating process. These demonstrate the Al deposition capability of $AlCl/AlCl_3$ gas mixtures having high effective Al activity. The calculations were performed for species in equilibrium with Al(s,1) at various temperatures. The data, developed from the JANAF Thermochemical Tables (Ref. 3), are shown in Table 3-5. The last portion of this table is the most revealing. It shows that high capacities for depositing Al are attained by about 1200 K where the AlCl pressure exceeds 10^{-2} atm (e.g., two thirds of the AlCl may be transformed into metallic Al) and where $AlCl_3$ is approaching 10^{-1} atm $AlCl_3$. Note that under these conditions Al_2Cl_6 is largely dissociated and does not enter into the considerations. Coating temperatures in the vicinity of 900°C plus are required for efficient Al deposition.

Table 3-1. High Temperature Al Coating Reactions.

$$3\ AlX(g) \rightleftarrows 2\ Al(s) + AlX_3(g)$$

$$6\ AlX(g) \rightleftarrows 4\ Al(s) + Al_2X_6(g)$$

$$3\ AlX_2(g) \rightleftarrows Al(s) + 2\ AlX_3(g)$$

$$3\ AlX_2(g) \rightleftarrows 2\ Al(s) + Al_2X_6(g)$$

where X = halide

Table 3-2. AlX_3 Properties.

[$AlX_3(g) + 3/2\ H_2 \rightarrow Al(s) + 3HX$]

X	MP (°C)	BP (°C)	ΔH_f (298)(s) (kcal/mole)	ΔH_f (298)(g) (kcal/mole)	3HX(g) ΔH_f (298) (kcal/3 mole)	AlX_3(g) - 3HX ΔH_f (298)(g) (kcal/mole)
F	-	1276	-361.0	-289.0	-195.4	-93.4
Cl	190*	181	-168.3	-139.7	-66.2	-73.5
Br	98	256	-126.0	-101.1	-26.0	-75.1
I	191	385	-73.9	-49.0	+18.9	-67.9

*2.5 atmospheres

Table 3-3. High Temperature Nb Coating Reaction.

$$NbX_5(g)^* + 5/2\ H_2 \rightarrow Nb(s) + 5\ HX$$

where X = halide

*Lower halides, e.g., NbX_4, are also known.

Table 3-4. NbX_5 Properties.

X	MP (°C)	BP (°C)	ΔH_f (kcal/mole)	5HX(g) ΔH_f (kcal/5 mole)
F	79.0	234.0	-433.5	-325.7
Cl	203.4	242.4	-190.5	-110.3
Br	254.0	365.0	-133.0	-43.3
I	-	-	-64.6	+31.5

Table 3-5. Aluminum Chloride Equilibria (Pressures in atm).

$AlCl_3 + 2Al(s,l) \rightleftarrows 3AlCl \qquad K_1 = pAlCl^3/pAlCl_3$

$2AlCl_3 + Al(s,l) \rightleftarrows 3AlCl_2 \qquad K_2 = pAlCl_2{}^3/pAlCl_3{}^2$

$2AlCl_3 \rightleftarrows Al_2Cl_6 \qquad K_3 = pAl_2Cl_6/pAlCl_3{}^2$

	Al_2Cl_6	$AlCl_3$	$AlCl$	$AlCl_2$			
T(K)	log K	log K	log K	log K	log K_1	log K_2	log K_3
600	99.822	48.338	9.005	26.319	-21.323	-17.707	3.146
800	71.708	35.589	7.813	20.152	-12.150	-10.722	0.530
1000	54.774	27.885	7.025	16.383	-6.810	-6.6621	-0.996
1200	43.358	22.671	6.410	13.782	-3.441	-3.996	-1.984
1400	35.208	18.939	5.954	11.910	-1.077	-2.148	-2.67

	For $pAlCl_3 = 0.1$			For $pAlCl_3 = 0.01$		
T (K)	log pAl_2Cl_6	log $pAlCl$	log $pAlCl_2$	log pAl_2Cl_6	log $pAlCl$	log $pAlCl_2$
600	1.146	-7.441	-6.569	-0.854	-7.774	-7.236
800	-1.470	-4.383	-4.241	-3.470	-4.717	-4.907
1000	-2.996	-2.603	-2.874	-4.996	-2.937	-3.540
1200	-3.984	-1.480	-1.999	-5.984	-1.814	-2.665
1400	-4.670	-0.692	-1.382	-6.670	-1.026	-2.049

This analysis suggests the most likely way to deposit high purity Nb-Al alloys. If H_2 is used to reduce $NbCl_5$, the resultant product HCl is expected to react with Al, AlCl, or $AlCl_2$, producing H_2 and forming stable $AlCl_3$, which will reduce the Al deposition rate. These two coating reactions and the interfering HCl reaction are shown in Table 3-6. Also shown is the reaction producing intermetallics which will aid the deposition of Al as governed by the activities shown in Figure 3-2. At temperatures around 1200 K, it appears better to avoid H_2 reduction systems and consider AlCl(g) as the reductant for $NbCl_5$(g). Significant amounts of AlCl(g) will be used in a coating process to reduce $NbCl_5$(g) to the metal. Since codeposition of Al with Nb is desired, an excess of AlCl will have to be present.

The deposition reactions for the appropriate intermetallic compounds using NbX_5(g) and AlX(g) are shown in Table 3-7. These equations describe the stoichiometry from both AlX and AlX_2 species and clearly demonstrate the large excess of AlX necessary to produce the various intermetallic compounds. Note, for example, the 7/1 ratio of AlX over NbX_5 needed to obtain $NbAl_3$(s). This effect will be quite apparent during the operation of the Al source. One will have to inject about 10 times as much $AlCl_3$ into the Al reactor as $NbCl_5$ to produce $NbAl_3$. This assumes that $pAlCl_3 \approx pAlCl$ at the exit of the Al source and that AlCl is almost absent at the coating chamber exit. When H_2 is suggested as a possible carrier gas, it is to aid in Nb deposition if the AlCl-$NbCl_5$ reaction kinetics are poor. In any case the presence of H_2 is expected to be only catalytic and not as an overall reactant.

3.1.2 Reaction Mechanisms of $NbAl_x$ Deposition

The reaction of $AlCl_3$(g) with Al(s) to produce AlCl(g) is almost certainly a heterogeneous reaction involving (1) the adsorption of $AlCl_3$(g) on the Al surface, (2) the interaction of the $AlCl_3$(ads) with the surface Al, and (3) the desorption of

Table 3-6. High Temperature Coating Reactions.

Nb:

$$NbCl_5 + 1/2H_2 \rightleftarrows NbCl_4 + HCl$$

$$NbCl_4 + 2H_2 \rightleftarrows Nb + 4\ HCl$$

Al:

$$AlCl_3 + 2\ Al \rightleftarrows 3\ AlCl$$

Interference Reactions:

$$2\ HCl + AlCl \rightleftarrows AlCl_3 + H_2$$

$$3\ HCl + Al \rightleftarrows AlCl_3 + 3/2\ H_2$$

Assistance Reactions:

$$Al + 2Nb \rightleftarrows Nb_2Al\ (\text{or } Nb_3Al, \text{ or } NbAl_3)$$

Table 3-7. High Temperature Combined Nb-Al Coating Reactions.

$$4NbX_5(g) + 13AlX(g) \rightleftarrows 2Nb_2Al(s) + 11AlX_3(g)$$

$$2NbX_5(g) + 13AlX_2(g) \rightleftarrows 2Nb_2Al + 12AlX_3(g)$$

$$3NbX_5(g) + 9AlX(g) \rightleftarrows Nb_3Al + 8AlX_3(g)$$

$$3NbX_5 + 18AlX_2(g) \rightleftarrows Nb_3Al + 17AlX_3(g)$$

$$NbX_5(g) + 7AlX(g) \rightleftarrows NbAl_3 + 4AlX_3(g)$$

$$NbX_5 + 14AlX_2(g) \rightleftarrows NbAl_3 + 11AlX_3$$

where X = halide

(Al_2X_6 also a product)

AlCl(ads) from the surface to give gaseous AlCl. The formation of $AlCl_2(g)$ would follow a similar route, and $AlCl_2(ads)$ may be an intermediate. Thus:

$$AlCl_3(g) \rightarrow AlCl_3(ads)$$

$$AlCl_3(ads) + 2Al(s) \rightarrow 3AlCl(ads) \text{ [or Al(ads)]}$$

$$3AlCl(ads) \rightarrow 3AlCl(g)$$

The reverse reactions depositing Al undoubtedly follow a similar course.

While these reactions seem appropriate for AlCl formation and decomposition, reactions involving H_2 may be important, particularly in the case of $NbCl_5$ reduction. Here again, absorbed state reactions are likely to constitute the critical path. An important step on many metal surfaces is the adsorption and dissociation of H_2 on the surface:

$$H_2 \rightarrow H_2(ads)$$

$$H_2(ads) \rightarrow 2H(ads)$$

These absorbed H atoms can approach adsorbed halides and extract halide sequentially:

$$NbCl_n(ads) + H(ads) \rightarrow NbCl_{(n-1)}(ads) + HCl(ads)$$

The adsorbed HCl can then react with adsorbed AlCl:

$$HCl(ads) + AlCl(ads) \rightarrow AlCl_2(ads) + H(ads)$$

$$HCl(ads) + AlCl_2(ads) \rightarrow AlCl_3(ads) + H(ads)$$

and the formed $AlCl_3$ vaporized:

$$AlCl_3(ads) \rightarrow AlCl_3(g)$$

Thus, H_2 may act catalytically to facilitate the reduction of $NbCl_5$ by AlCl. Indeed, what we have observed is a faster rate of coating of Nb-Al alloy (or intermetallics) in the presence of H_2 than when using $NbCl_5(g)$ + AlCl(g) alone. Thus, the use of catalytic H_2 in Nb-Al alloy coating appears useful in aiding the Nb reduction at least.

It should also be noted that the Nb-Al alloys do not appear to be generated as powders by reduction and condensation from the gas states. This is another confirmation of adsorbed state reactions being rate controlling.

3.1.3 $NbAl_x$ from $NbCl_5$ and AlCl Generated from MAl_x

The problems of using molten Al could be circumvented by changing the Al source. A solid Al source to replace Al(l) for this process could be $NbAl_3$. It is a solid, relatively high Al-activity source ($a_{Al} \sim 10^{-2}$) over the range of composition $NbAl_3$ to its neighboring Al-depleted phase Nb_2Al. In a thermodynamic sense, this is a fixed a_{Al} system, and thus the reaction:

$$AlCl_3 + 2Al \rightarrow 3AlCl$$

can be run at $\sim 10^{-2}$ a_{Al}. This situation is governed by the equilibrium constant whose value as a function of temperature is shown in Figure 3-3. One must use higher temperatures with $NbAl_3$ as a source to generate the same concentration of AlCl as produced by

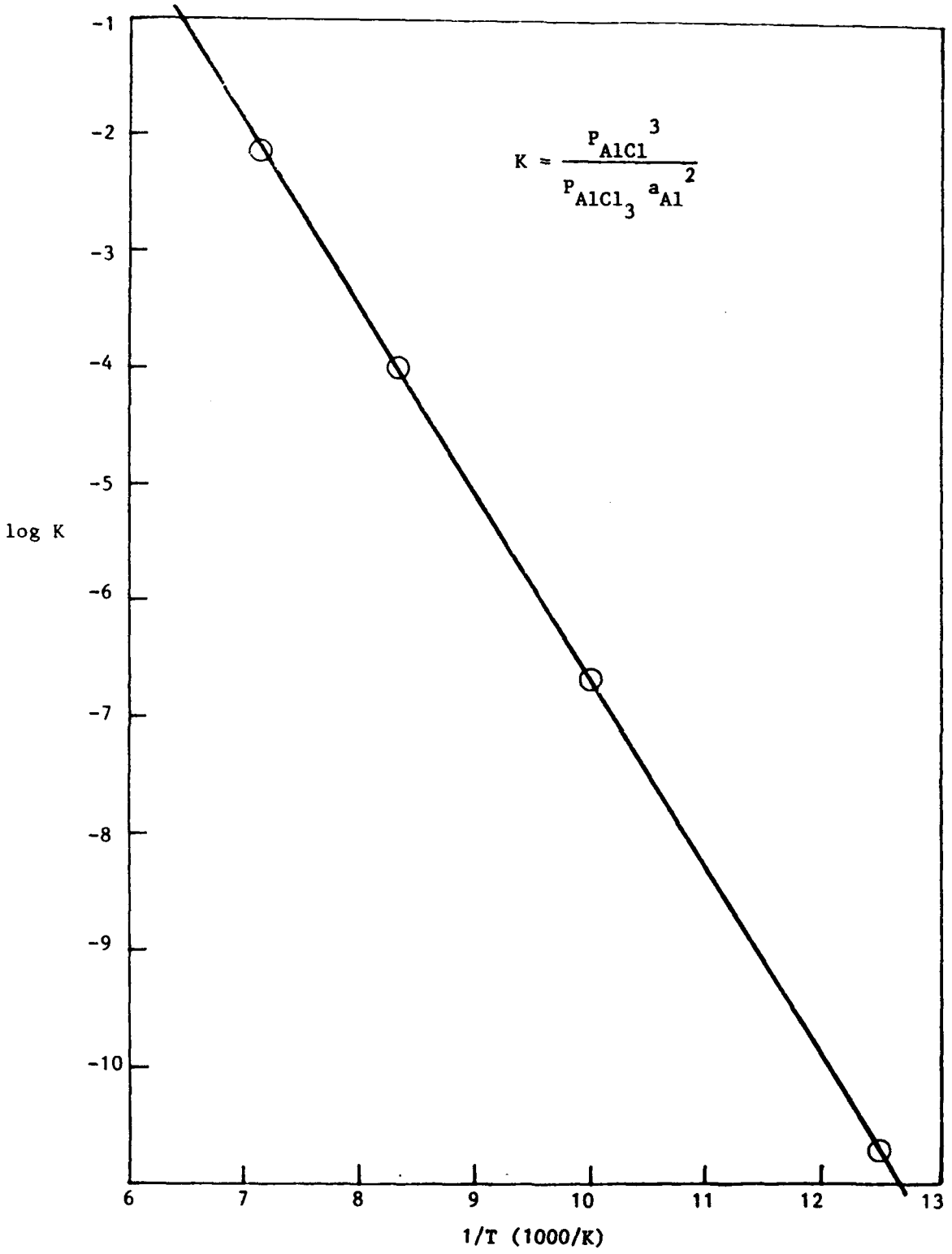

Figure 3-3. Equilibrium constant for AlCl(g) formation from Al(l) + $AlCl_3$(g).

molten Al. An $a_{Al} = 10^{-2}$ source means that these higher temperatures must be used to counteract the 10^{-4} (i.e., a_{Al}^2) factor to give good conversion to AlCl. A temperature increase of ~300°C may be required to effect this conversion using an $NbAl_3$ source. Once the AlCl is made, temperatures of the conversion gases can be reduced to do the planned $NbAl_x$ CVD without plating out Al, but the Al source bed can remain solid. Nb should not be transferred by this process. However, if it is transferred in minor amounts, the overall CVD process will not be affected appreciably.

$FeAl_3$, Al_4C_3, or certain other aluminides could also serve as alternatives to the use of $NbAl_3$. Some of these sources could have a higher Al activity than $NbAl_3$, and thus deposition temperatures for some of these alternative aluminides may be lower than that needed for $NbAl_3$. Contamination from the Fe-containing alternative source might not be a problem. $FeAl_3$ should not transfer Fe because of the higher stability of the $AlCl$-$AlCl_3$ system.

3.2 HYDROGEN REDUCTION OF ALUMINUM AND NIOBIUM CHLORIDES TO PRODUCE INTERMETALLIC COMPOUNDS

In the discussion of AlCl reduction it was noted that if H_2 were used to reduce $NbCl_5$, the product HCl would inhibit the hydrogen reduction of Al. However, it is possible to identify a high temperature regime in which H_2 can serve as the reductant for both $NbCl_5$ and $AlCl_3$.

Hydrogen will readily reduce $NbCl_5(g)$ to Nb(s) at moderate temperatures and will reduce $AlCl_3(g)$ to Al(l) at extreme conditions of system temperature and species pressures as compared with $NbCl_5(g)$ reduction conditions. Thus, the problem of creating Nb-Al intermetallics by hydrogen reduction can be ascertained by deciding what conditions will be necessary to deposit Al at the desired activity as defined by the intermetallic compound.

This problem can be approached by making equilibrium calculations of the limiting reaction in the intermetallic compound function. It appears that the most efficient way to carry out this analysis is to consider the reaction:

$$AlCl_3(g) + 3/2\ H_2 \rightarrow Al(l) + 3HCl$$

We will consider that this reaction is in equilibrium at the site where the intermetallic compound is being deposited.

Two pieces of thermodynamic data are required for this analysis:

1. The free energies (or their equivalents, such as equilibrium constants) of the reduction reaction.
2. The activities of Al in the various Nb-Al intermetallic compounds and alloys.

The former data are found in the JANAF tables (Ref. 3), and we have previously reported the Malets data (Ref. 2) on the metal activities, as shown in Figure 3-2. Table 3-8 presents the reduction reaction equilibrium constants from the JANAF data. These data are plotted in Figure 3-4 as the solid line labeled K_p. The Malets data have been extended to higher temperature according to the assumption that the partial molar entropy of Al in the alloy is zero. This extension of single phase regions is given by the areas between the dotted lines from the Malets data. This assumption has no valid basis, but the trend of the activity data toward zero at increased temperatures seems correct.

Figure 3-4 is a plot of the maximum (i.e., equilibrium) Al activity that could be achieved by reducing $AlCl_3$ with H_2 versus temperature. The K_p line corresponds to 1 atm $AlCl_3$, 1 atm H_2, and 1 atm HCl at the reacting surface. Note that there are many equivalent pressure conditions that would be described by the K_p line.

Table 3-8. Thermodynamics of $AlCl_3(g)$ Reduction to $Al(\ell)$ by H_2

(Reduction Reaction Constants)

Temperature (K)	Log Equilibrium Constant ($atm^{1/2}$)
1000	-12.090
1200	-9.345
1400	-7.383
1600	-5.934
1800	-4.762

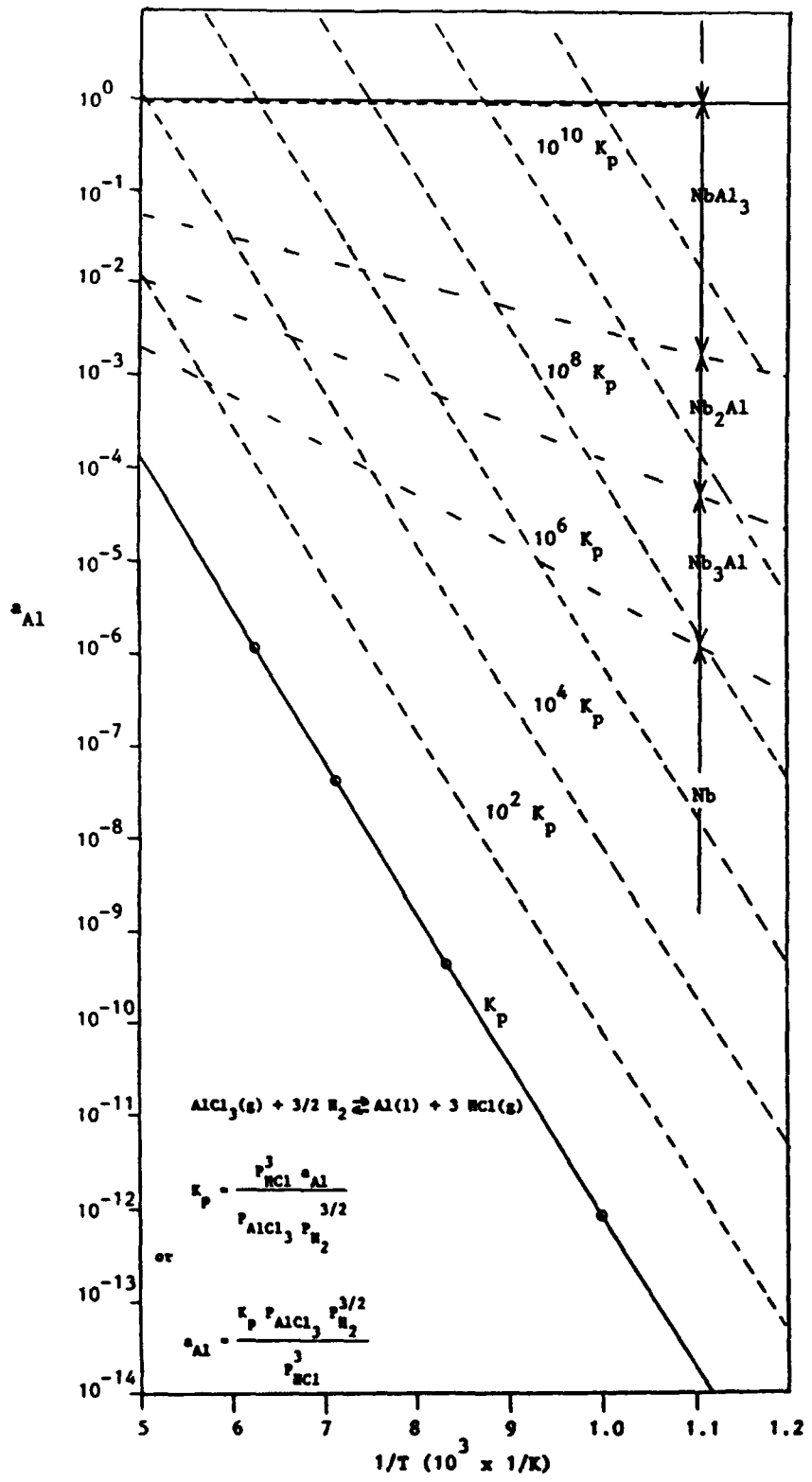

Figure 3-4. Derivable Al activities from $AlCl_3$, $NbCl_3$, H_2 mixtures as compared with Nb-Al activities.

Those are pressure ratios where $P_{AlCl_3}P_{H_2}^{3/2}/P_{HCl}^3 = 1$. For instance, other than the 1:1:1 case described, 1:0.01:0.1 or 0.001:1:0.01 will also result in the K_p line. However, to make higher activity Al at a given temperature, one must increase the value of $P_{AlCl_3}P_{H_2}^{3/2}/P_{HCl}^3$ (i.e., a_{Al}). This is obviously done by operating at high P_{AlCl_3} and P_{H_2} values and low P_{HCl} values, with P_{HCl} the most sensitive factor because it is cubed. Dotted lines parallel to the K_p line are included in Figure 3-4 to demonstrate this potential for increasing the achievable Al activities.

The intersections of the K_p $P_{AlCl_3}P_{H_2}^{3/2}/P_{HCl}^3$ lines with the Malets lines describe regions where the particular niobium aluminides could be expected to form if equilibrium conditions exist at the deposition interface. Note that the values of P_{AlCl_3}, P_{H_2}, and P_{HCl} should be those at the deposition surface and not those in the bulk gas which is separated from the surface by a reaction boundary layer.

The general aspect of Figure 3-4 shows that, since the heat of the reduction reaction greatly exceeds the partial molar heat of Al in the Nb-Al intermetallics, higher temperatures are favored. Making Nb_3Al can be approached by using a H_2 atmosphere, low $AlCl_3$ pressures (10^{-2} to 10^{-3}), and low conversions (i.e., P_{HCl} values of 10^{-3} atm) at temperatures around 800°C. For Nb_2Al the temperature needs to be increased to 900°C, and for $NbAl_3$ temperatures of 1000°C are needed. However, the effective HCl pressure is the most important feature. The change from 10^{-3} atm HCl to 10^{-2} atm HCl is equivalent to a required temperature change from 800°C to nearly 1200°C.

Low conversions of Al indicate that the conditions for H_2 reduction of $AlCl_3$ and $NbCl_5$ to intermetallic compounds is best done in an atmosphere with relatively high $AlCl_3$ pressures and an order of magnitude or more lower $NbCl_5$ pressures. Low $AlCl_3$ conversions (atom percent) thus can be expected for the intermetallics at

moderate temperatures. If one tries to run at high conversion rates and high deposition rates, it would appear to be difficult to produce intermetallic compounds of Al and Nb.

Complications arise when $AlCl_3(g)$ is not the major Al gaseous species at the deposition surface. At higher temperatures AlCl(g) will become dominant. The appearance of this labile gaseous Al species will actually work against further gains in coating by providing another sink for $AlCl_3(g)$; that is, by lowering the P_{AlCl_3} put into the reduction reaction, the ultimate achievable Al activity is thereby also lowered.

The conclusions of this investigation are that $AlCl_3$, $NbCl_5$, and H_2 mixtures can be used to deposit Nb-Al intermetallics, but it would appear, at best, to be a low efficiency Al conversion process. Perhaps this situation can be improved by working at still higher temperatures.

3.3 CONCLUSIONS

Deposition of $NbAl_x$ compounds should be achievable at temperatures around 900 K by using AlCl(g) from the $AlCl_3$+Al(ℓ) reaction. When AlCl(g) is put in the presence of $NbCl_5(g)$, thermodynamics indicate that $NbAl_x(s)$ materials will result. The system deposits these aluminides at lower, the same, and even somewhat hotter temperatures than those at which the AlCl(g) was generated. This results in a requirement for controlling deposition on a given surface by means of space, temperature, flow pattern, and residence time. It is not a hot wire technique.

Al sources other than Al(ℓ) were considered. While possible, none are particularly attractive because of the lowered Al activity in the alternative Al sources.

The H_2 reduction of $AlCl_3$ and $NbCl_5$ can be projected as a very high temperature hot wire technique (~1400°C) with appropriate control of $NbCl_5$, $AlCl_3$, and H_2 pressures. This appears to be a slow, difficult process because of the difficult conditions indicated by the calculations.

4. DEPOSITION STUDIES

As discussed in the modeling section, two distinct chemical processes for depositing $NbAl_x$ were examined. Both processes use $NbCl_5$ and $AlCl_3$ as the precursor gases for the metallic components of the deposit. One process involves the formation of AlCl as an intermediate by the reaction:

$$AlCl_3(g) + 2\ Al(l) = 3\ AlCl(g) \qquad (4\text{-}1)$$

with $NbAl_x$ deposition via the reaction:

$$(3x + 5)/2\ AlCl(g) + NbCl_5 = NbAl_x(s) + (5 + x)/2\ AlCl_3 \qquad (4\text{-}2)$$

Since this deposition process runs at low temperatures, thermal degradation of the mechanical properties of the substrate material was not of much concern. A greater concern was the possible encapsulation of contaminants such as chlorine in the deposits.

A second experimental procedure for controlling the composition and properties of $NbAl_x$ is the direct CVD of $NbAl_x$ from the hydrogen reduction of $AlCl_3$ and $NbCl_5$ described by the overall reaction:

$$xAlCl_3(g) + NbCl_5(g) + (3x + 5)/2\ H_2 \rightarrow NbAl_x + (3x + 5)HCl \qquad (4\text{-}3)$$

While conceptually simple, the process has several drawbacks. First, it requires temperatures above 1200°C, which restricts the choice of substrates. Second, even when substrates can tolerate the high temperatures, even small differential thermal expansions between the substrate and the deposit can impose unacceptably high stresses at the substrate-deposit interface.

In both of the chemical approaches, initial investigations employed substrates supported between two electrodes. This

configuration provided the option of independently controlling the temperature of the substrate by electrical resistance heating. Flexing of the substrate during heating and cooling was found to cause samples to spall off. For this reason procedures were modified to provide for operation with singly suspended samples.

All of the intermetallics have coefficients of thermal expansion (CTE's) that are incompatible with those of the substrates used in these experiments. These differential thermal expansions caused some of the cracking and spalling noted in the deposits. However, the main reason for cracks and spalling in the resistance heated samples was bowing of the substrate due to CTE mismatch during heating and cooling. Deposits made on substrates held at one end could frequently be separated from the substrates with gentle prying of a knife blade. The deposition of intermetallics on substrates which do not react with the intermetallics and are easily separated from the substrates during cooldown from the elevated temperature deposition process is thus a viable technique for preparing small samples of intermetallic foils.

Three methods of directly producing foils were considered. The first is the deposition of the intermetallic on a substrate which does not react with the intermetallic and is easily separated from the intermetallic during cooldown from the elevated temperature deposition process. Most of the deposits produced fit into this category. However, these deposits were nearly always fragmented.

The second method of forming foils is to form an adherent deposit from which the substrate can be selectively removed by chemically dissolving it or mechanically stripping it away. Substrates which will not react with the deposit precursor at the deposition temperatures, have CTE's close to that of the intermetallic, and are more readily dissolved than the intermetallic or can be mechanically removed from it have not been found. The

deposited foil is too thin and brittle to make machining or other mechanical means of removing the substrate very attractive.

Partial conversion of the substrate, the third method of foil formation, may be more promising. This process involves the interdiffusion of a component of the intermetallic being deposited into a substrate foil that is made of another component of the intermetallic. Section 4.2 describes the use of this process for the formation of aluminides by the direct reduction of halides by hydrogen at high temperatures. The low substrate temperatures at which potential significant interdiffusion processes are operative were not known. Therefore, evaluation was performed of substrates made from Nb, Mo, Ta and C.

In addition to the primary efforts directed to the deposition of $NbAl_x$, limited investigations were carried out on the deposition of niobium silicides, Nb_xSi_y, and ternary alloys in the Nb-Al-Ti system.

4.1 $NbAl_x$ DEPOSITION WITH AlCl AS Al SOURCE

Phase I studies of the CVD $NbAl_x$ compounds showed that these compounds could be deposited from a gas stream in which AlCl was a major component and which also initially included $NbCl_5$ and some $AlCl_3$. Hydrogen as a component of this stream was also found to affect the process. The various $NbAl_x$ intermetallic compounds ($NbAl_3$, $NbAl_2$, and Nb_3Al) could be deposited by control of gas feed and temperature. The system employed for this work passed an $AlCl_3$-H_2 mixture over Al(l) in an Al_2O_3 boat contained in a quartz reactor producing AlCl(g). $NbCl_5$ was admitted downstream in an argon carrier gas. Just after the entry of $NbCl_5$, the mixed gases were exposed to Mo foil surfaces where the $NbAl_x$ compounds were deposited.

The initial Phase II reactor was also built of quartz. This apparatus did produce solid Nb-Al films. However, the films were found to be contaminated with Si, apparently originating with the quartz reactor walls. Also, there was clearly attack and devitrification of the quartz walls containing the molten Al source and exposed to AlCl. While an attack on the SiO_2 was not discovered in Phase I, it clearly occurred to some degree in every experiment. In order to produce high purity $NbAl_x$ solids, an alumina containment system was selected. A system was designed that could be assembled using Al_2O_3 container materials in the hot zones where they should tolerate the highly reducing atmosphere that Al (condensed) and AlCl(g) represent. The molten aluminum system chamber is shown in Figure 4-1. The alumina system was housed in a stainless steel can for easy installation/removal of the aluminum metal and safe operation.

Gaseous aluminum chloride passed through alumina tubes into the molten aluminum. All saturators were built to include an inert carrier gas. The condensed halides were placed in heated reservoirs, which increased their vapor pressure and allowed a controlled amount of reactant to reach the deposition chamber. Gas lines downstream of the heated reservoir were warmed to temperatures slightly above the reservoir temperature to prevent condensation of reactant in these lines. Temperature controls on all saturators (reactors) were much improved over the Phase I apparatus. The primary containment for the molten alumina was high purity alumina. Secondary containment was provided by a stainless steel chamber. The stainless steel also provided a safety catch basin for inadvertent loss of molten aluminum.

The system shown in Figure 4-1 was designed for deposition on doubly suspended substrates with resistance heating. Suspension was from the two heavy copper electrodes shown. The completed assembly is shown in Figure 4-2.

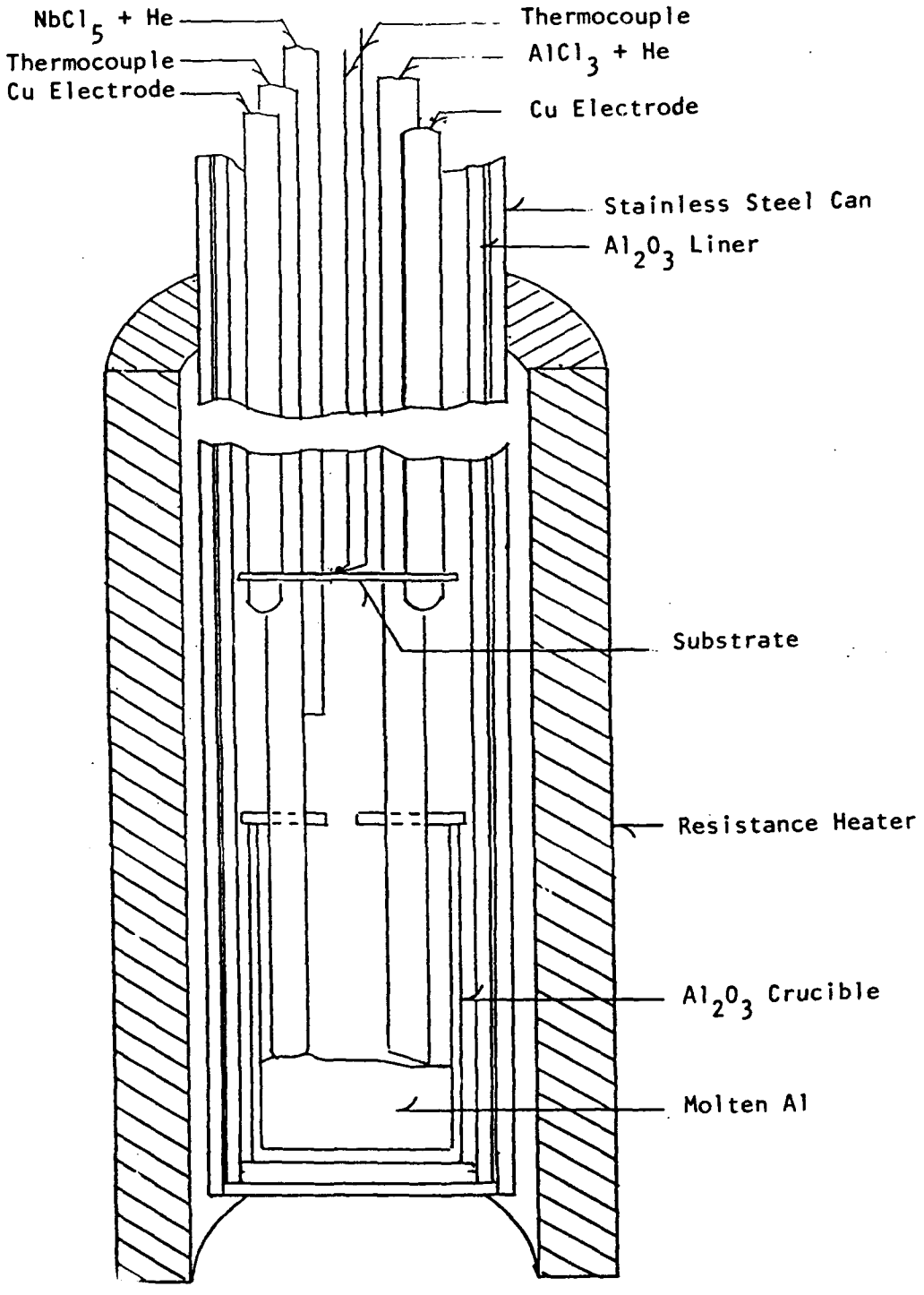

Figure 4-1. Schematic diagram of the molten aluminum system chamber.

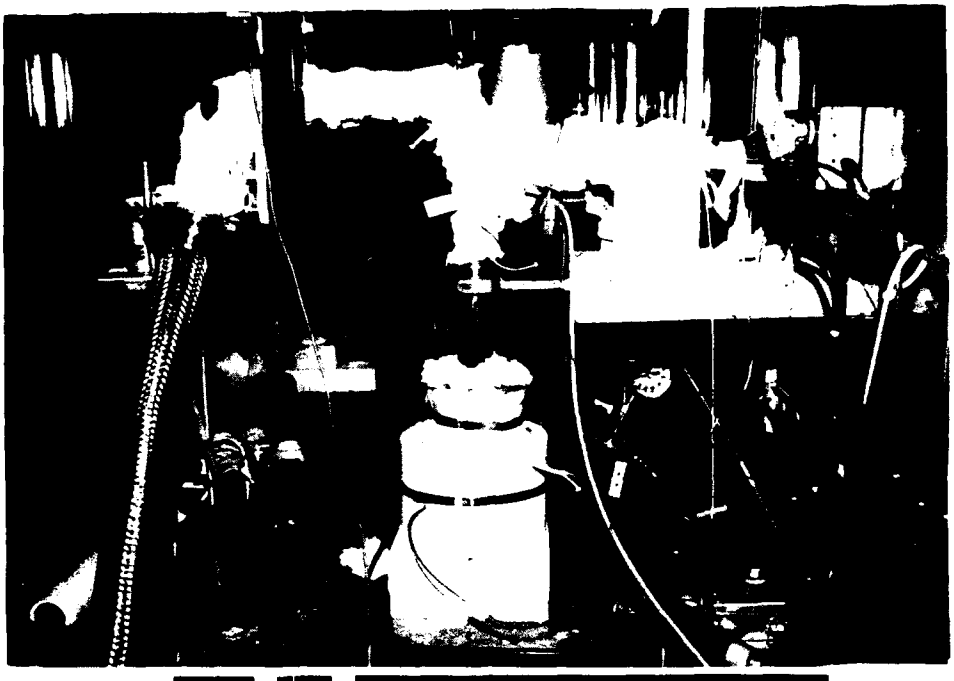

(a)

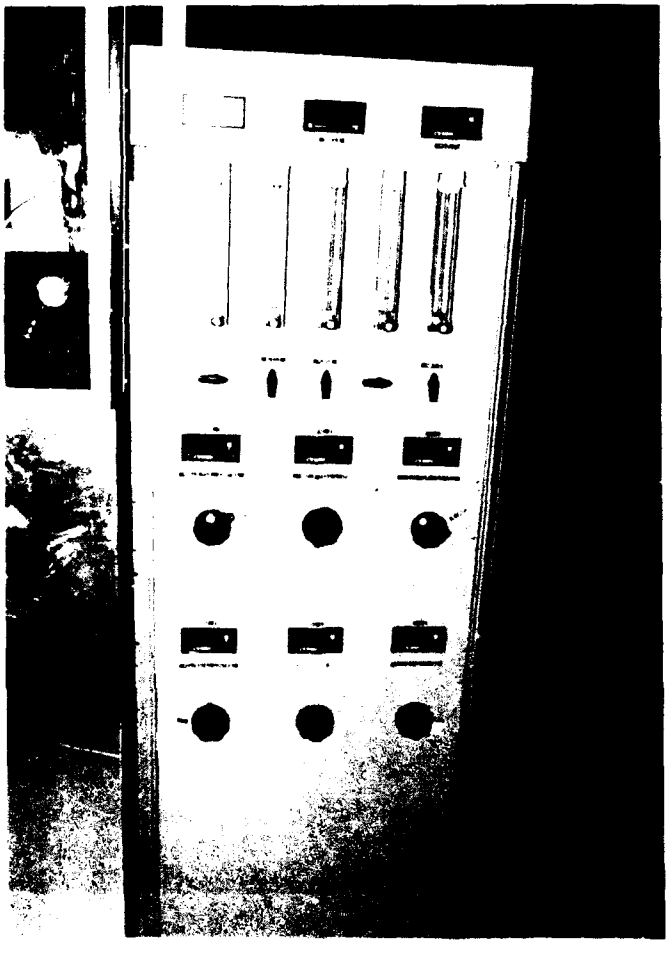

(b)

Figure 4-2. The molten aluminum deposition system showing (a) the assembled deposition chamber, heated chloride sources, and vacuum system and (b) the gas flow control panel and temperature monitors.

4.1.1 Deposition on Doubly Supported Substrates

It was anticipated that a molten aluminum temperature of above 725°C would be needed to obtain appreciable conversion of $AlCl_3$ to AlCl. Initial deposits were made on 1- x 0.25- x 0.004-inch molybdenum or tantalum or 1- x 0.25- x 0.001-inch niobium substrates suspended between two copper electrodes. Substrate temperatures were monitored with Chromel-Alumel thermocouples tack welded to the center of the substrate. A high current, low voltage DC power supply was used to heat the substrate. Gaseous aluminum chloride with added hydrogen or helium was passed through alumina tubes and bubbled through the molten aluminum to form AlCl(g). Temperature profiles of various zones within the deposition chamber such as that shown in Figure 4-3 were taken before the deposition experiments to suppress cold wall condensation of precursor reactant gases, which distorts the expected gas phase chemistry above the substrate. In these experiments $NbCl_5$ with added argon or helium was injected above, at, or below the substrate, but generally 0.25 inch below.

Coated substrates were examined optically and in some samples by SEM. EDAX was used for determining chemical composition and residual chlorine analyses.

Process parameters for these experiments leading to foil deposition are given in Tables 4-1 and 4-2. Temperatures recorded in these and other process parameter tables are mean values that ignore temporary transient temperatures which occur when reactant gases are introduced into the deposition chamber and during stabilization of substrate temperature fluctuations. Molten aluminum temperatures of 725° to 955°C were used for these conversions of $AlCl_3$ to AlCl.

Experimental results are summarized in Table 4-3 and Figures 4-4 through 4-13. Deposits made from $NbCl_5$, $AlCl_3$, H_2, He, and Ar

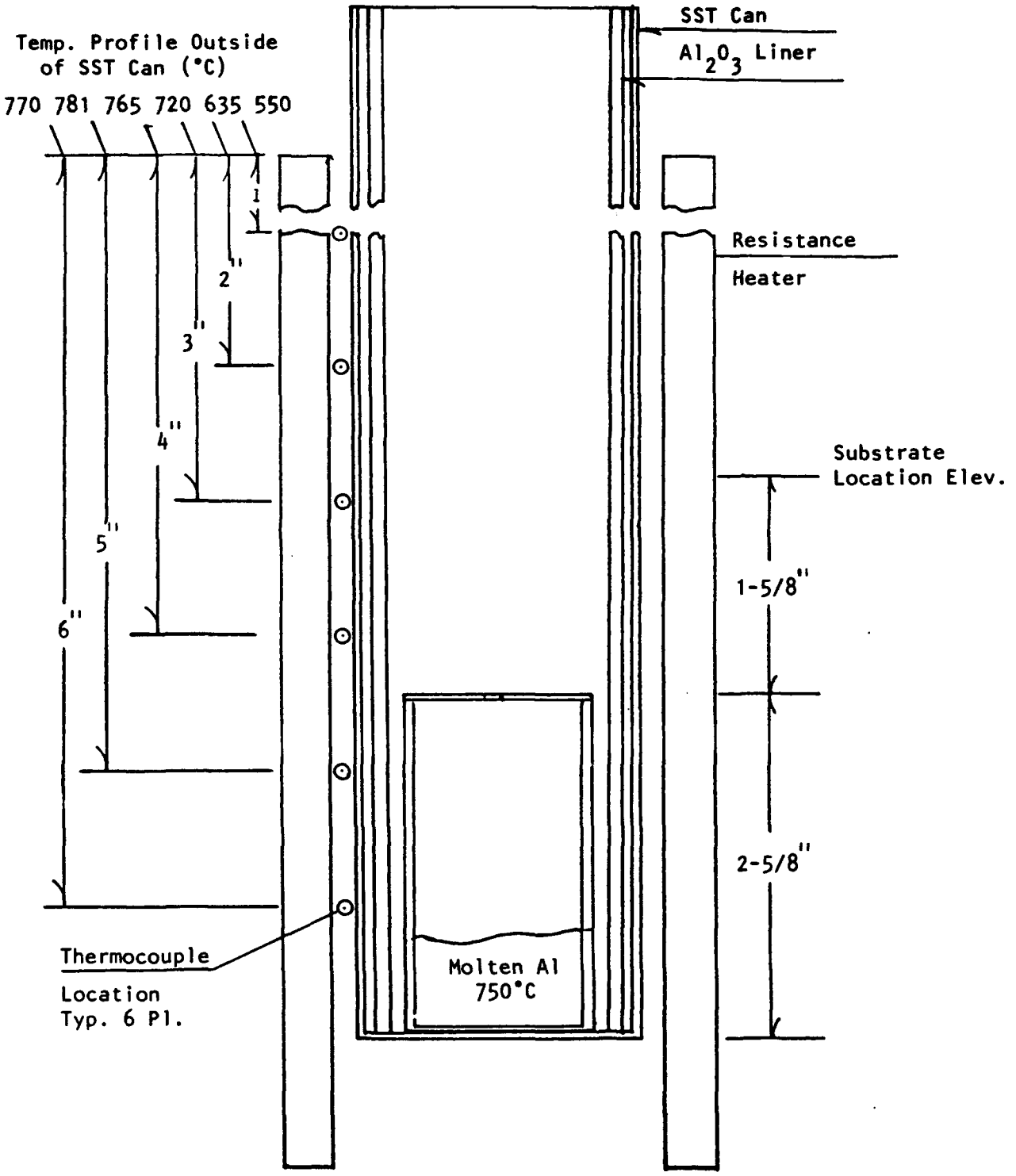

Figure 4-3. Typical temperature distribution in the molten aluminum system deposition chamber.

Table 4-1. Process Parameters for Nb_xAl_y Deposition at Atmospheric Pressures from the AlCl Reduction of $NbCl_5$ with Hydrogen

Sample Number	Substrate	Temperature (°C)				Gas Flow (cc/min)					Time (min)
		Al	$AlCl_3$	$NbCl_5$	Substrate	H_2 in $AlCl_3$	$AlCl_3$	Ar in $NbCl_5$	$NbCl_5$	H_2 Purge	
JB200-84	Mo	730	120	128	910	100	1.3	60	0.66	50	68
-86	Mo	750	120	145	895	100	1.3	30	1.45	50	45
-88	Mo	750	125	142	900	100	2.0	60	1.23	50	60
-90	Mo	740	127	133	~1000	50	1.2	60	0.41	100	130
-92	Ta	760	125	131	925	50	1.0	60	0.39	100	85
-94	Ta	750	126	134	890	50	1.1	60	0.43	100	120
-96	Nb	730	122	130	905	50	0.3	60	0.34	100	123
-98	Ta	830	127	111	705	100	2.4	100	0.30		156
-100	Ta	830	131	106	820	100	3.0	100	0.24		120

Table 4-2. Process Parameters for Nb_xAl_y Deposition at Atmospheric Pressures from the AlCl Reduction of $NbCl_5$ without Hydrogen

Sample Number	Substrate	Temperature (°C)				Gas Flow (cc/min)					Time (min)
		Al	$AlCl_3$	$NbCl_5$	Substrate	He in $AlCl_3$	$AlCl_3$	He in $NbCl_5$	$NbCl_5$	He Purge	
JB200-102	Ta	825	133	115	800	100	3.3	100	0.37	100	158
-104	Ta	820	131	113	815	200	6.1	200	0.66	200	140
-106	Ta	815	126	112	805	200	3.9	200	0.63	200	122
-108	Ta	820	121	107	810	200	2.9	200	0.47	200	288
-110	Nb	820	127	105	805	200	4.5	200	0.46	200	542
-112	Ta	810	126	106	795	200	3.9	200	0.47	200	430
-114	Ta	805	128	111	805	150	3.2	200	0.61	200	420
-116	Ta	810	132	106	810	150	4.3	200	0.47	200	152
-118	Ta	815	132	112	815	150	4.3	200	0.63	200	475
-120	Ta	825	131	105	805	50	1.4	200	0.46	200	270
-122	Ta	805	133	109	805	150	4.9	200	0.55		480
-124	Ta	960	133	105	820	150	4.9	200	0.46		137
-126	Ta	945	134	106	885	150	2.6	200	0.47	380	365

Table 4-3. Evaluation Results of Selected Nb_xAl_y Deposition Experiments

Sample No.	Composition (at.%)			Thickness (μm)	Remarks
	Nb	Al	Cl		
JB200- 84					$NbCl_5$ in 1 inch above substrate.
200- 86					$NbCl_5$ line plugged.
200- 90					Thermocouple lost.
200- 92					$NbCl_5$ in 1/2 inch above substrate.
200- 94				1.0	$NbCl_5$ in at substrate.
200- 96				1.0	
200- 98	38.42	58.99	2.59		$NbCl_5$ in 1/4 inch below substrate.
200-100				1.0	$AlCl_3$ plugged.
200-102				9.0	
200-104					Lid blew, sample loss.
200-106				1.0-3.0	Repeat of JB200-104.
200-108				2.3-3.0	
200-110	67.27	32.73		1.0-1.1	
200-112L	11.43	82.42	6.15		
200-112M	29.58	67.37	3.05	< 1.0	Excess $AlCl_3$ in chamber.
200-112R	38.58	52.92	8.50		
200-114	91.90	8.10		1.0-3.0	
200-118	99.20	0.80		5.0	
200-120 Surface	99.38	0.62			
200-120 Below Surface	56.38	43.62			
200-122				< 1.0	Substrate DPH[a] 216
200-124	12.49 9.26 2.86 49.06 35.63	87.51 90.74 97.14 50.94 64.37		5-20	Substrate DPH[a] 342, Coating 462
200-126				2.0	Substrate DPH[a] 146

[a]Microhardness

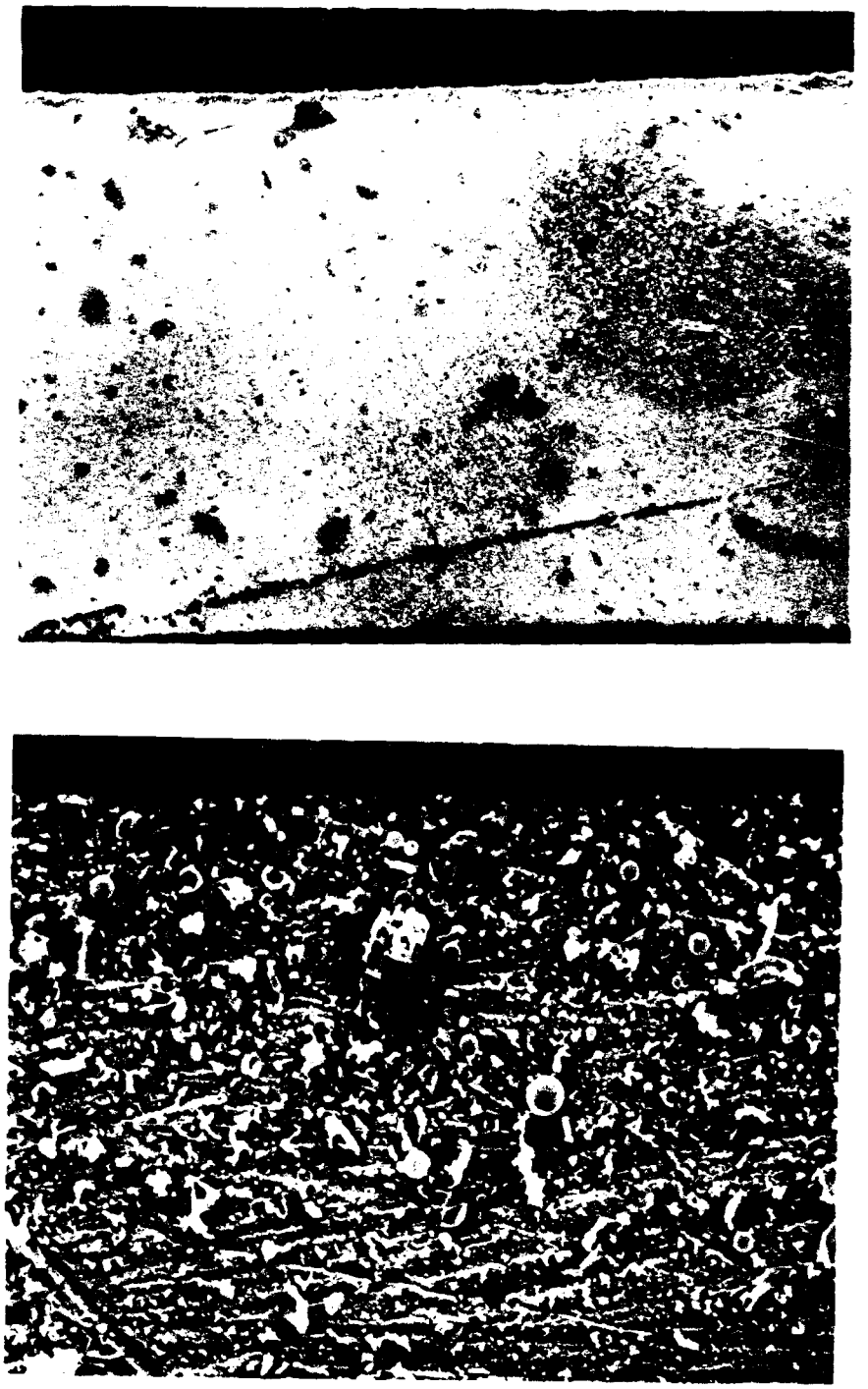

Figure 4-4. Surface features of porous, discontinuous Nb_xAl_y which are typical of gas phase nucleated deposits from AlCl, $NbCl_5$, and H_2 (sample JB200-86).

Figure 4-5. Optical photomicrograph of the cross section of a porous, discontinuous Nb_xAl_y deposit from AlCl, $NbCl_5$, and H_2 (sample JB200-94).

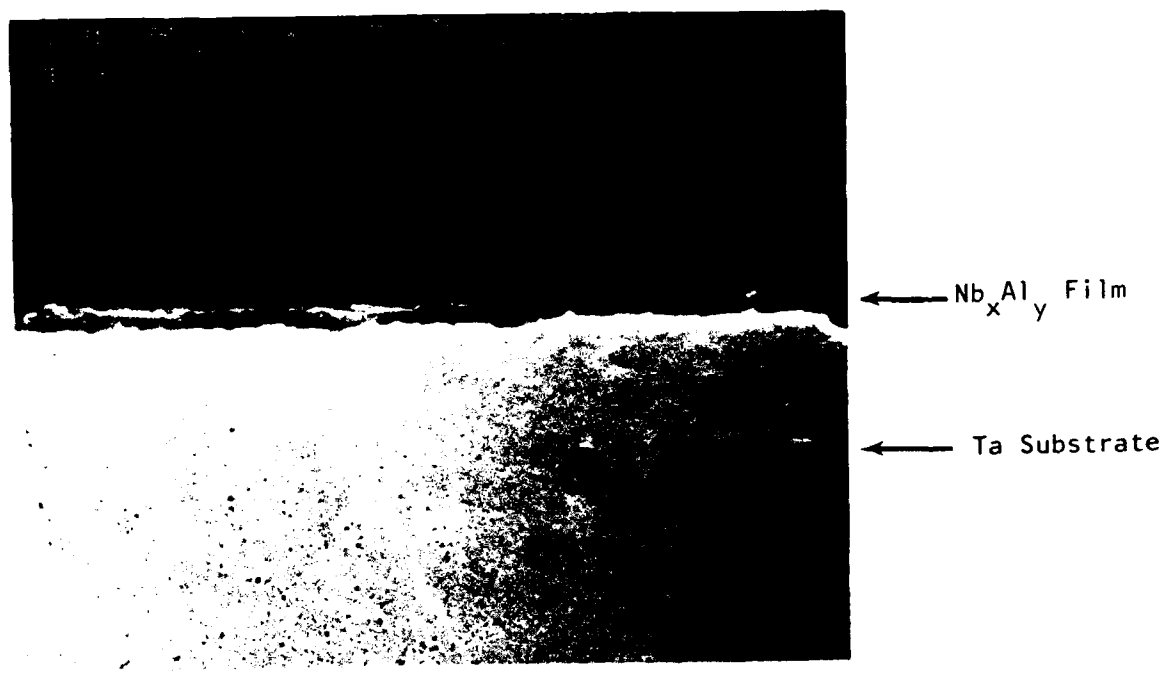

Figure 4-6. A continuous film of Nb_xAl_y deposited from the AlCl reduction of $NbCl_5$ without hydrogen (sample JB200-98).

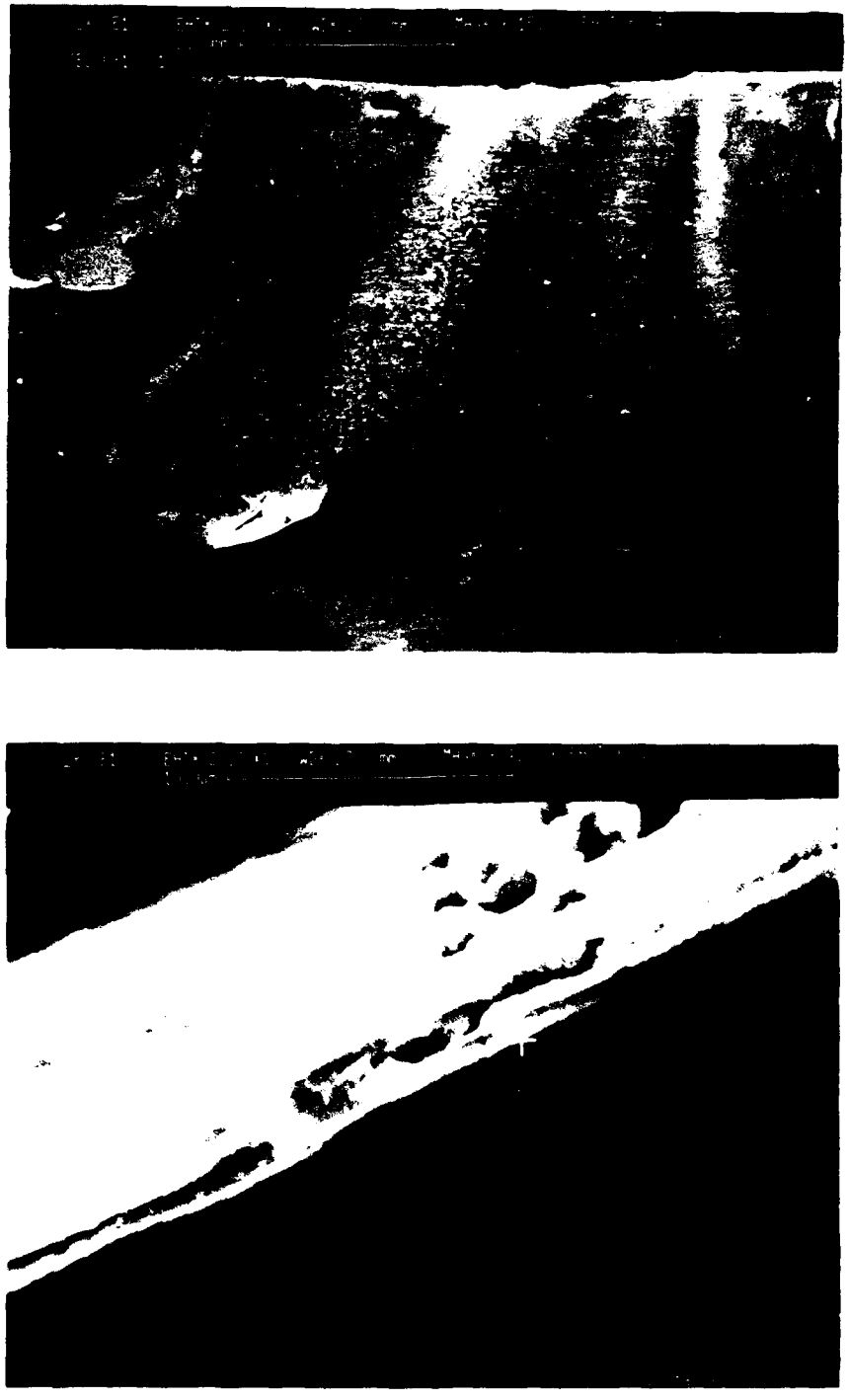

Figure 4-7. Niobium aluminide deposited from a moderate increase in the flow rates of $NbCl_5$, AlCl, and He over samples JB300-84 to JB300-96 (sample JB200-108).

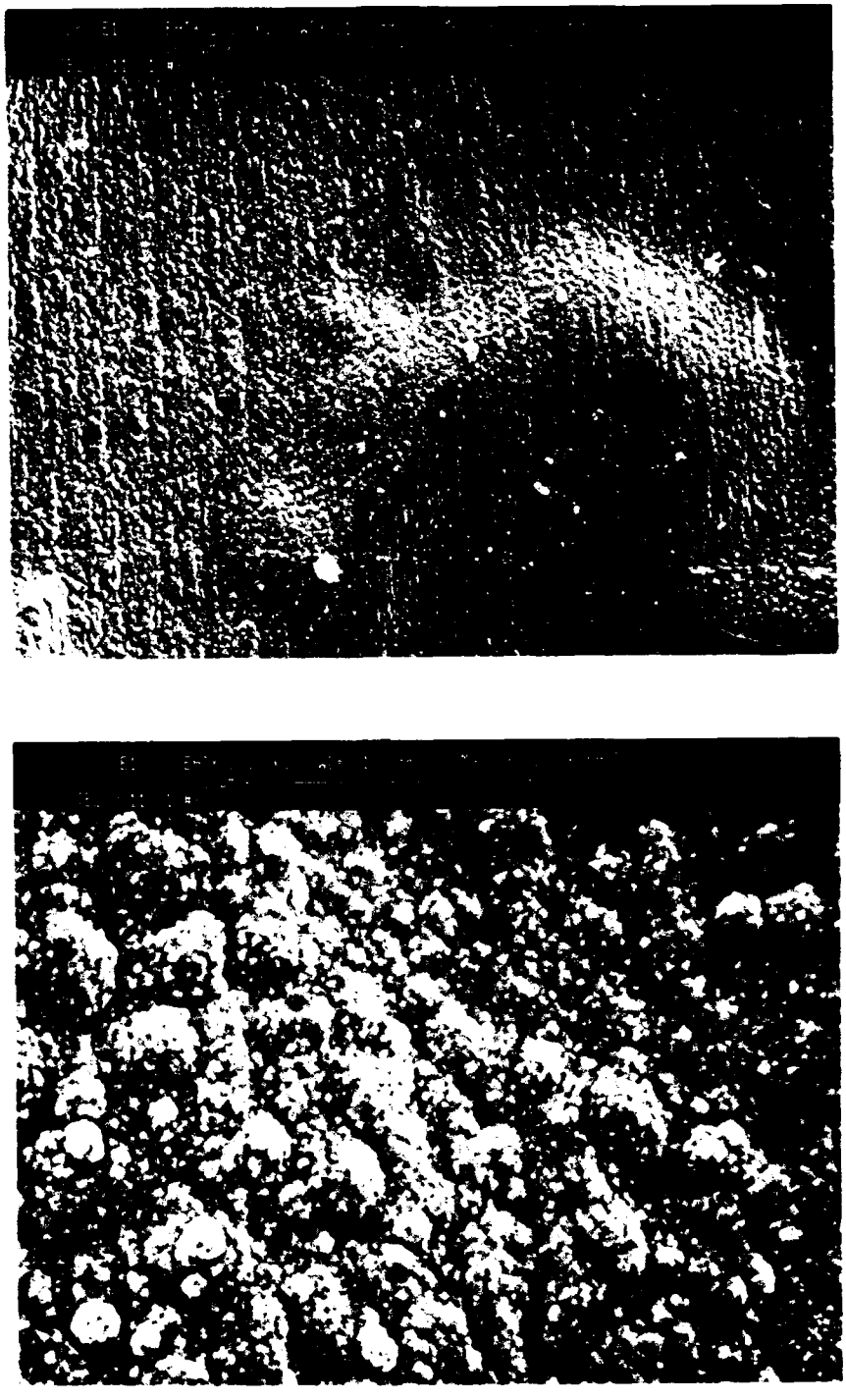

Figure 4-8. Surface morphology of niobium aluminide deposited on niobium from moderate flow rates of $NbCl_5$, AlCl, and He (sample JB200-110).

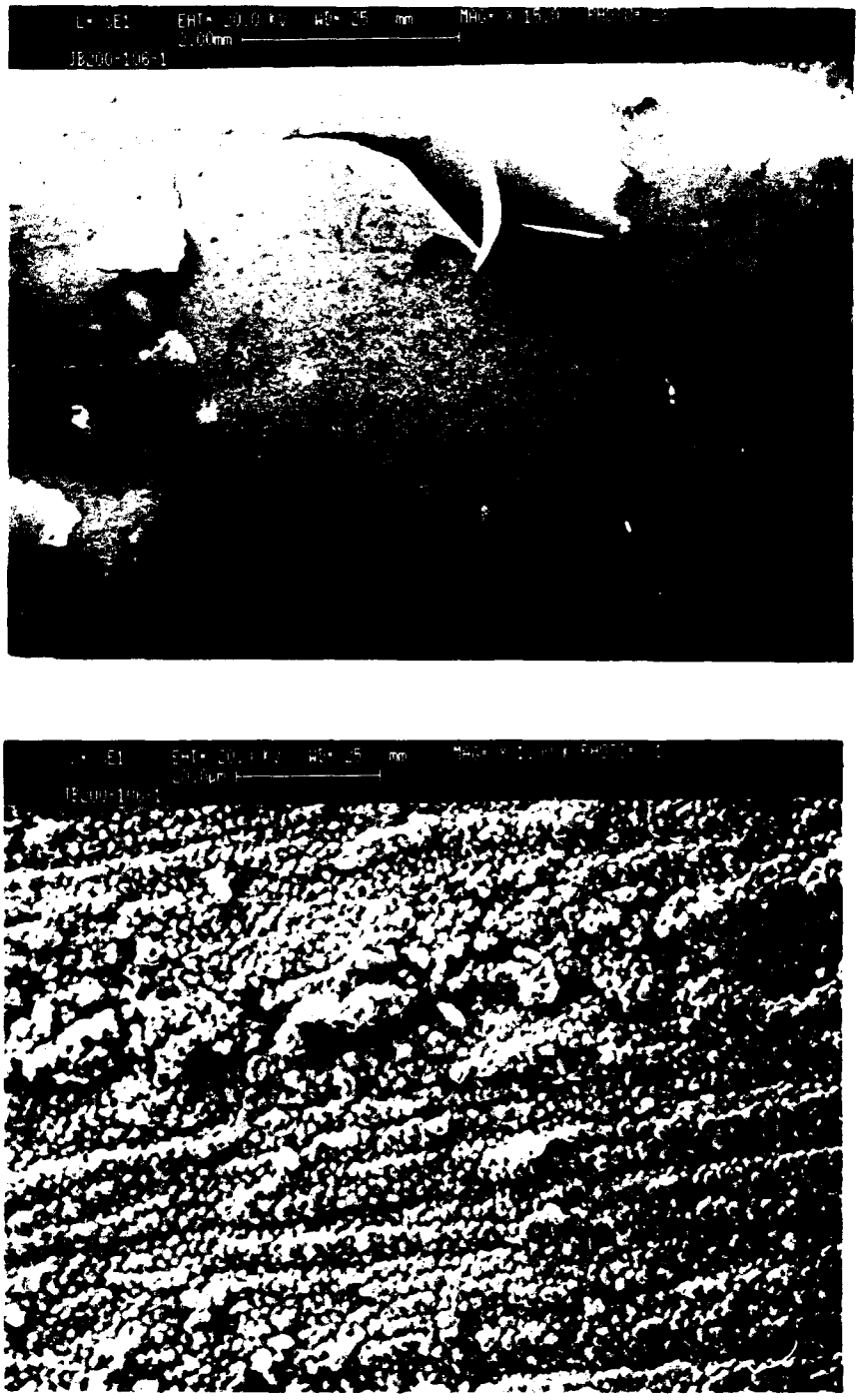

Figure 4-9. Film fractures due to CTE mismatch between CVD niobium aluminide and the tantalum substrate (sample JB200-106).

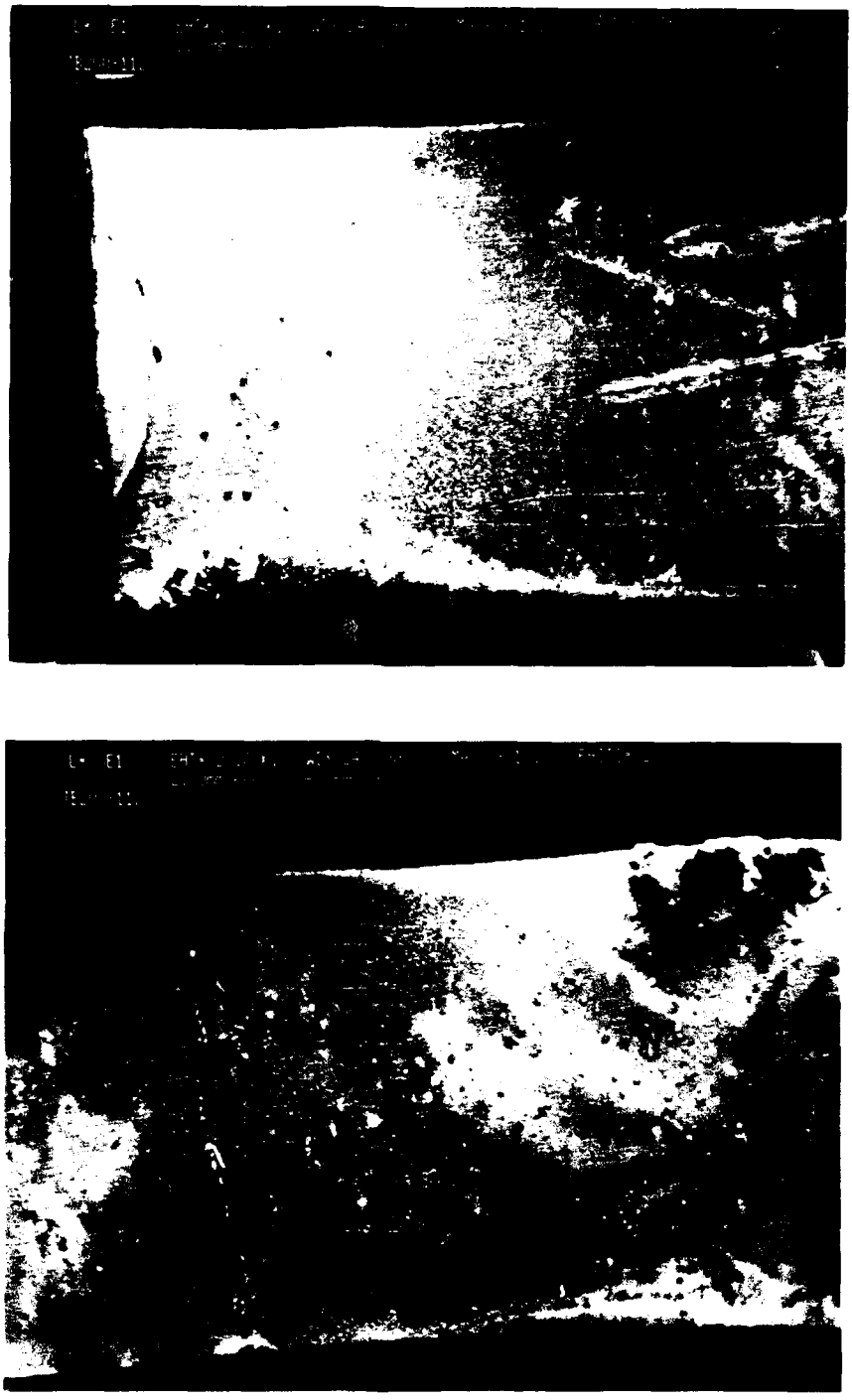

Figure 4-10. Overview of a CVD Nb_xAl_y film on tantalum with variable niobium and aluminum contents end to end (sample JB200-112).

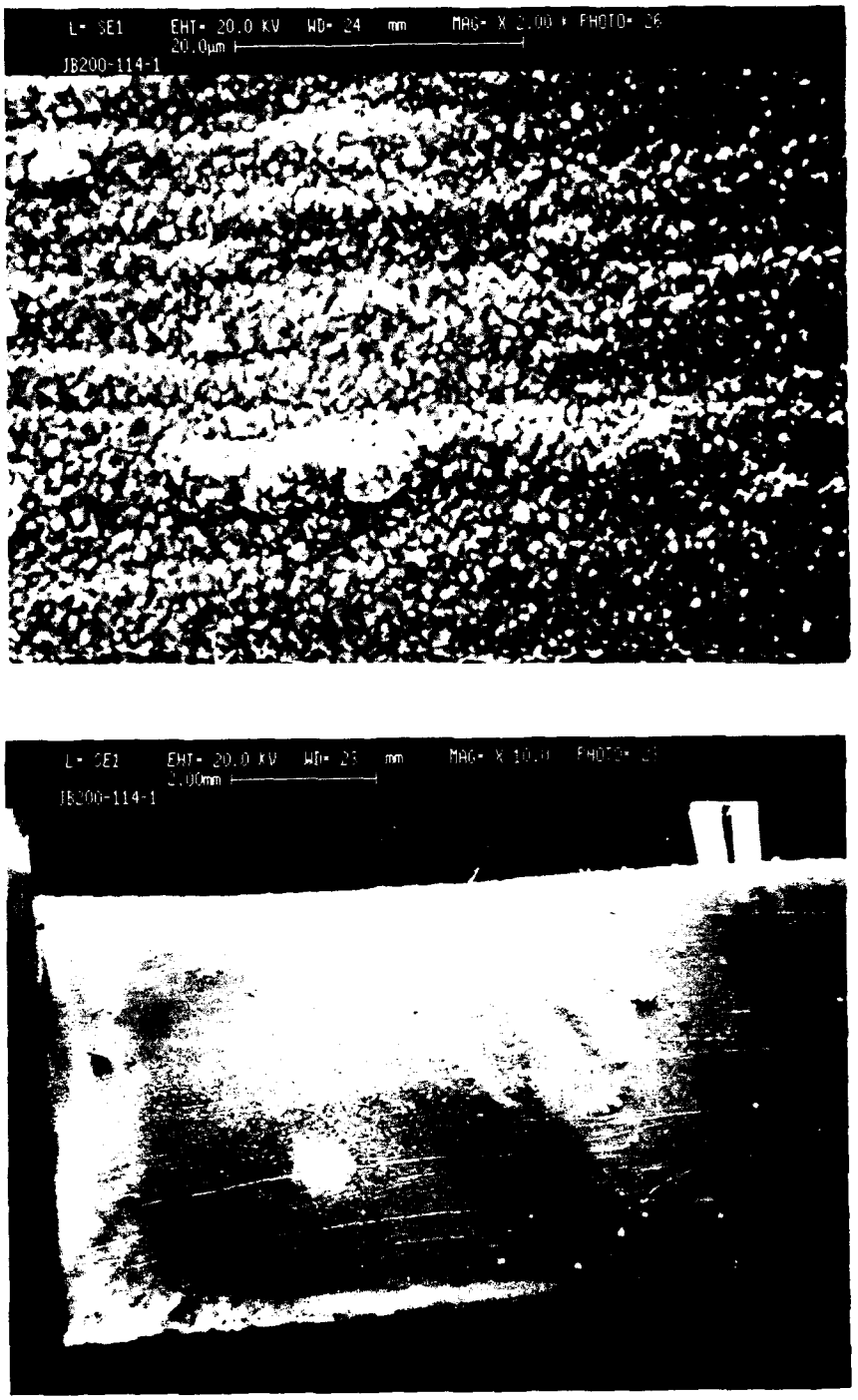

Figure 4-11. High niobium content, nearly crack-free Nb-$NbAl_x$ films deposited on tantalum by the AlCl reduction process (sample JB200-114).

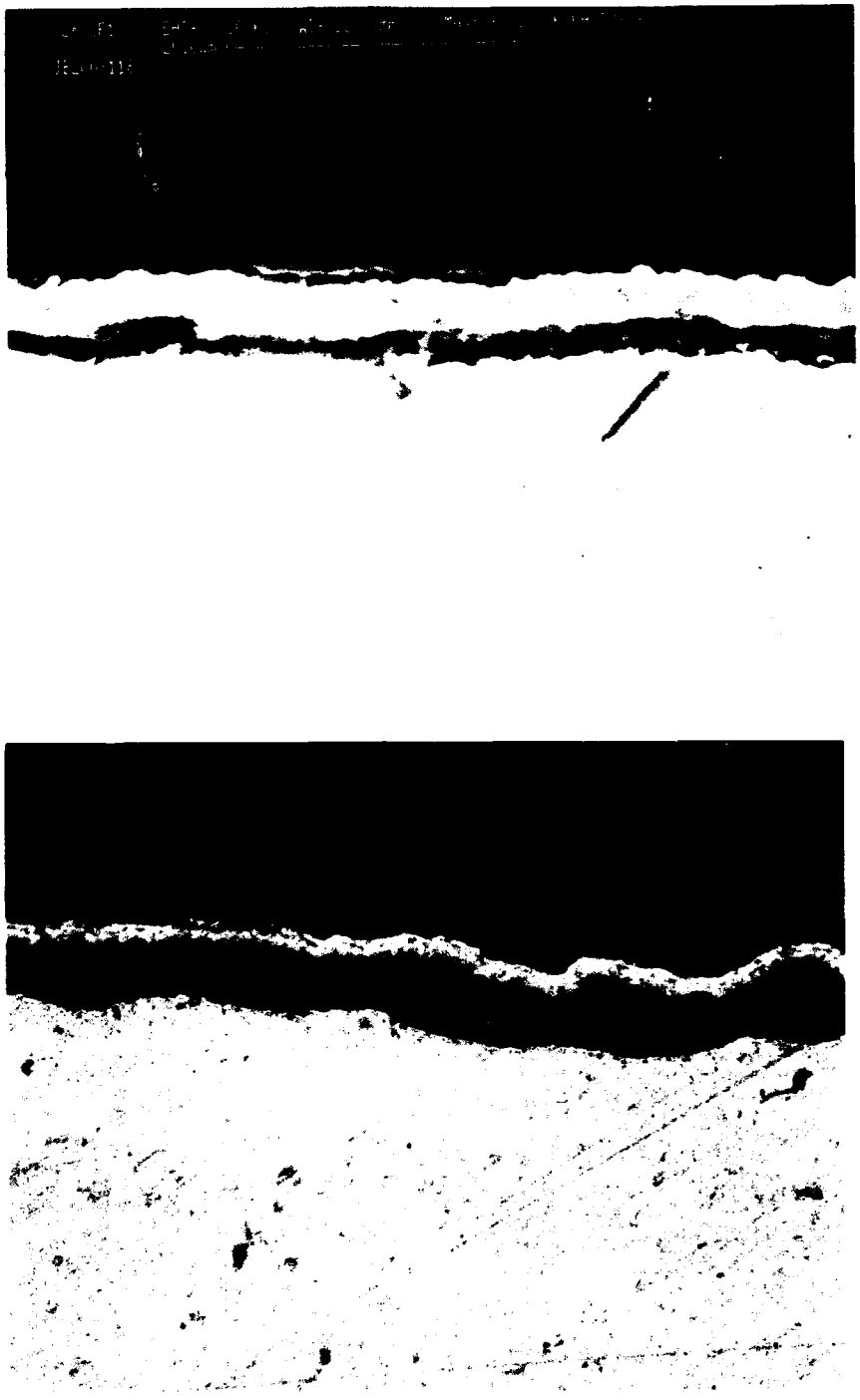

Figure 4-12. High niobium content, nearly crack-free Nb-$NbAl_x$ films deposited by the AlCl reduction process (sample JB200-118).

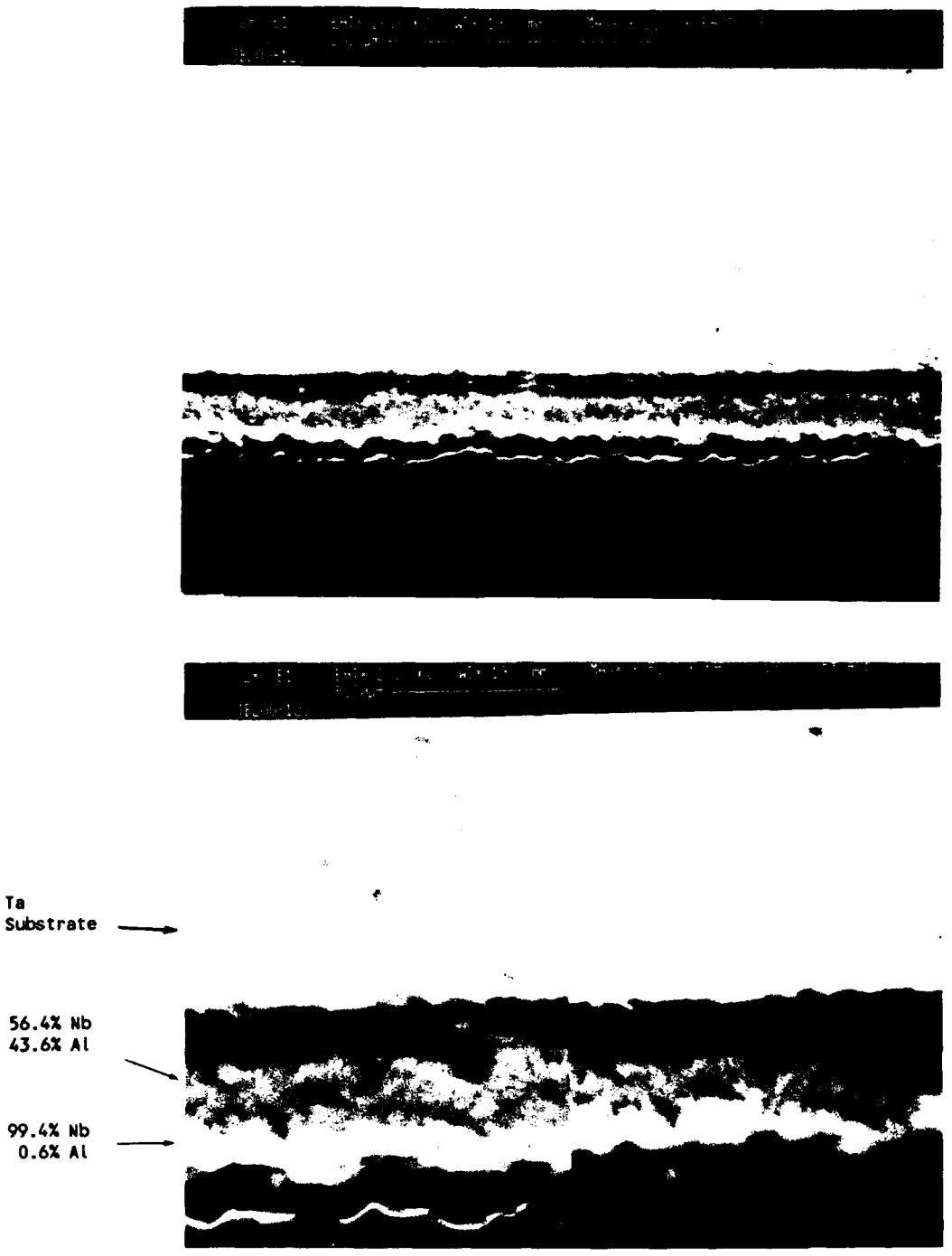

Figure 4-13. SEM photomicrograph of a Nb_xAl_y deposit on tantalum with a high niobium content surface and lower niobium content deposit/substrate interface (sample JB200-120).

gas mixtures with 725° to 760°C aluminum pot temperatures were thin, porous, and discontinuous. Examples of these deposits are shown in Figures 4-4 and 4-5 (samples JB200-86 and JB200-94, respectively).

Eliminating the hydrogen and increasing the temperature of the molten aluminum to above 810°C densified the deposits and made them continuous.

When the substrate was not heated and allowed to thermally float, its temperature was 700°C when the molten aluminum temperature was 830°C. A deposit made under these conditions (JB300-98, Figure 4-6) was porous and contained trapped chlorine. Raising the substrate temperature improved the apparent density of the deposit but did not eliminate the trapped chlorine. Switching from argon to helium in the gas passing through $NbCl_5$ and doubling the precursor gas flows improved the SEM appearance of the deposit in some cases (Figures 4-7 and 4-8) but not always (Figure 4-9).

Chemical compositions of the deposits were very process dependent. The aluminum content of the niobium aluminide deposits varied from 0.80 to 82.42 at. % as determined by SEM/EDAX examinations. Measurements taken across sample JB200-112 (Figure 4-10) show nonuniform distribution of niobium and aluminum in the sample. This nonuniformity was also visually evident when the experiment was disassembled. There was more chlorine entrapped in the deposits on the cooler parts of the substrate near the rectangular substrate support electrodes than in the warmer sample center. Substrates were changed back to a "dog bone" shape to minimize temperature gradients across the length of the sample. Higher gas flows were investigated as a means of reducing thermal gradients in the sample.

Crack-free deposit samples, such as JB200-114 and JB200-118 (Figures 4-11 and 4-12) were almost all niobium.

There was a higher niobium content on the surface of sample JB200-120 (Figure 4-13) than just below the surface. The measured niobium contents were 99.38 and 56.38 at. % on the surface and 2 μm below the surface, respectively. This may be due to residue gas compositions during shutdown. Attempts were made to minimize this possibility by shutting off the $NbCl_5$ first.

Overall, deposition rates were erratic and lower than desired.

4.1.2 Deposition on Singly Supported Substrates

As discussed previously, resistance heating of the substrates was found to contribute to spallation of the deposits. Resistance heating of the substrate was discontinued in experiments JB200-128 to JB200-150. The substrates were supported at one end and hung vertically in the system. Substrate temperatures in experiments JB200-124 and JB200-128 to JB200-138 were allowed to thermally float, with heat supplied by the proximity of the molten aluminum furnace to the substrate.

Starting with experiment JB200-140, the substrate was heated with a separate tube furnace mounted over the exterior of the stainless steel deposition chamber as shown in Figure 4-14. Additional helium was injected into the deposition chamber as a gas mixing aid and directed at the molten aluminum, at the substrate as shown in Figure 4-15, or at right angles to the substrate as shown in Figure 4-16.

Substrate temperatures were monitored with Chromel-Alumel thermocouples tack welded to the center of the substrate in all experimental setups. Details of the process parameters for these attempts at foil deposition are given in Table 4-4. Deposits and substrates were examined optically, with metallography, and in some samples by SEM. EDAX was used to determine the aluminum and niobium contents of the deposits.

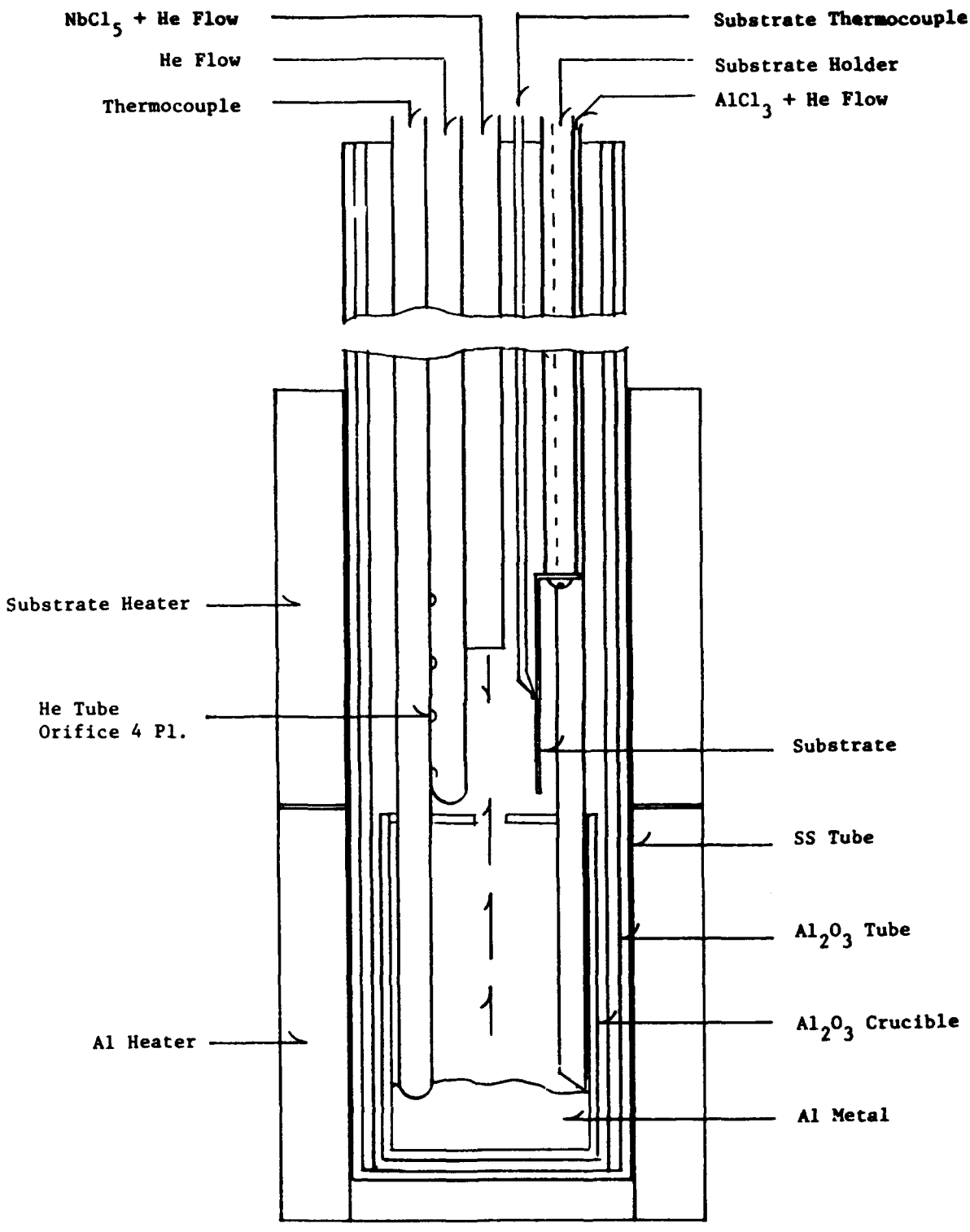

Figure 4-14. Schematic diagram of the molten aluminum system deposition chamber with a tube furnace heated substrate.

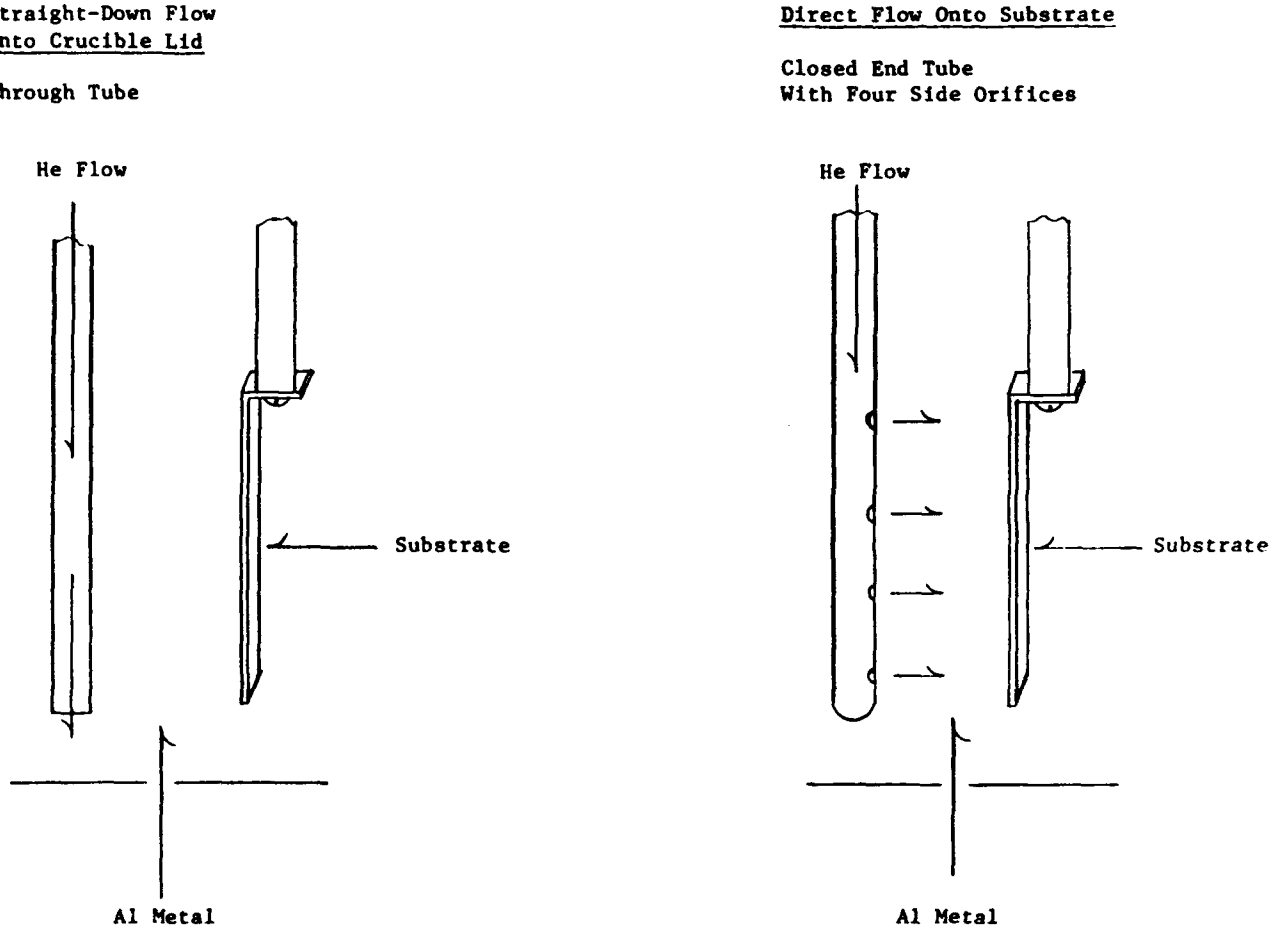

Figure 4-15. Schematic diagram of the inert gas injection system showing the added helium inlets directed at the molten aluminum or at the substrate.

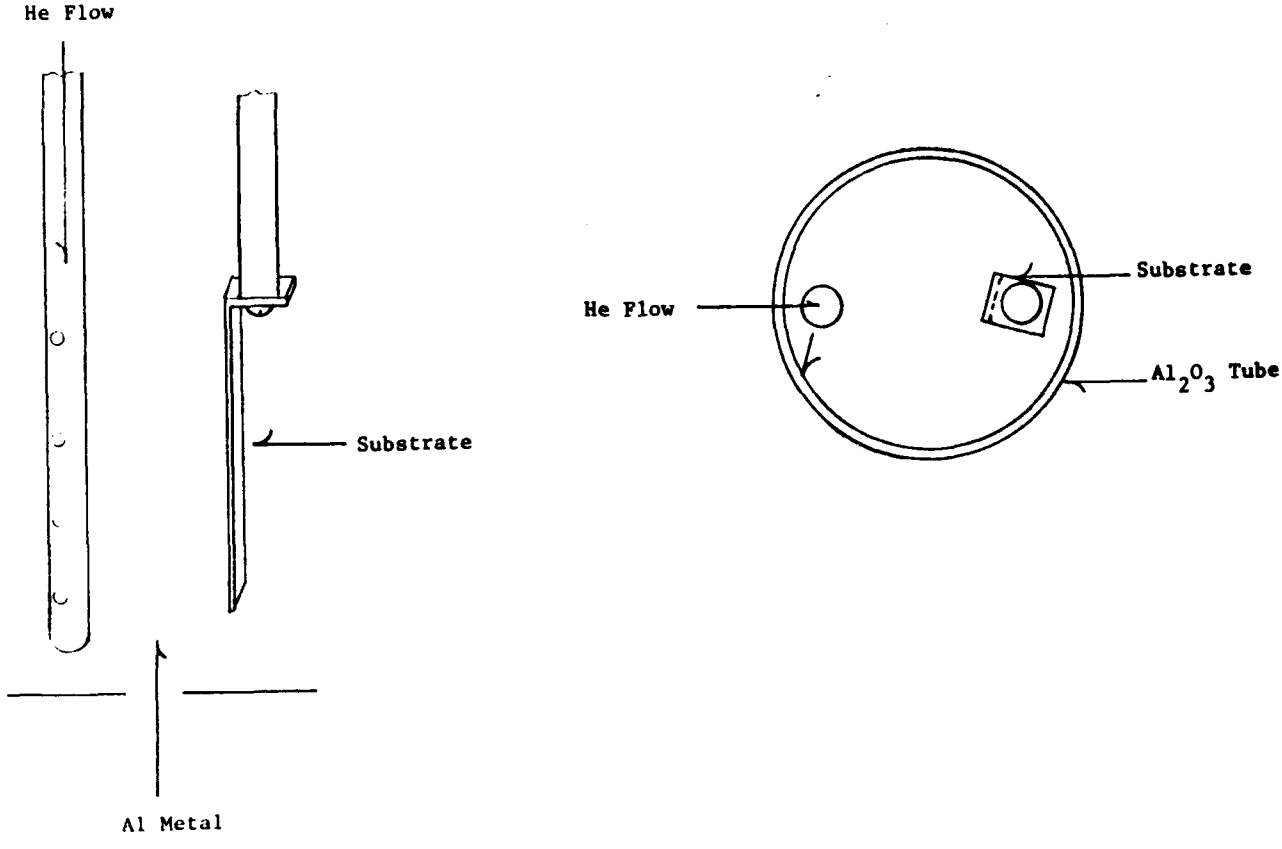

Figure 4-16. Schematic diagram of the added helium gas injection system, directed at right angles to the substrate, showing its relationship to the deposition chamber.

Table 4-4. Process Parameters for the CVD of Nb_xAl_y Foil by the Molten Aluminum - AlCl Process

Sample Number	Substrate	Temperature (°C)				Gas Flow (cc/min)					Time (min)	Pressure (torr)
		Substrate	$AlCl_3$	$NbCl_5$	Al	He + $AlCl_3$	$AlCl_3$	He in $NbCl_5$	$NbCl_5$	He		
JB200-128	Ta	840	135	106	946	150	5.9	200	0.47	380[a]	420	760
JB200-130	Ta	890	134	105	956	150	5.3	200	0.45	1200[a]	420	760
JB200-132	Ta	870	133	105	955	150	4.9	200	0.45	1600[a]	228	760
JB200-134	Nb	870	135	107	973	150	5.9	200	0.50	1600[a]	240	760
JB200-136	Nb	865	133	106	962	150	4.9	200	0.47	2000[a]	330	760
JB200-138	Nb	825	136	107	945	150-35	6.3-1.5	200-70	0.50-0.18	2000-355[a]	135	14-51
JB200-140	Nb	930	135	106	960	150	5.9	200	0.47	2000[a]	242	8
JB200-142	Nb	920	133	112	960	150	4.9	200	0.63	2000[a]	243	7-8
JB200-144	Nb	900	132	112	955	100	3.2	100	0.32	2000[b]	253	5-6
JB200-146	Nb	920	128	106	960	100	2.4	100	0.24	2000[b]	50	7-13
JB200-148	Nb	920	135	106	950	100	4.0	100	0.24	2000[b]	248	6-7
JB200-150	Nb	975	132	108	955	100	3.2	100	0.26	2000[c]	245	6
JB300-2	Nb	1000	134	108	970	100	3.6	100	0.26	2000[c]	240	6-7

[a]Helium purge gas input just above $NbCl_5$ + He input pointed at Al source.

[b]Helium purge gas input from four holes directed at the substrate surface.

[c]Helium purge gas input from four holes directed at right angles to the substrate.

Experimental results for these singly supported isothermally heated substrates are summarized in Table 4-5. Deposits made with 800° to 995°C aluminum pot temperatures and added helium varied from porous to dense. Most were porous. Examples of these deposits are seen in Figures 4-17 through 4-27. Increasing the temperature of the molten aluminum to above 940°C provided an adequate aluminum flux for reasonable deposition rates of the niobium aluminide intermetallic deposits and made them continuous. When the substrate was not heated and allowed to float, its thermocouple monitored temperature varied from 800° to 890°C when the molten aluminum was 935° to 975°C. Based on previous thermocouple measurements, temperatures were expected to be as much as 50°C cooler on the supported end of the sample than on the lower end of the substrate, just above the molten aluminum-containing crucible. To minimize the influence of this temperature gradient on these deposits, samples were taken within 0.3 inch of the thermocouple. Visually there were still nonuniformities in the deposits.

Chemical compositions of the deposits, as determined by SEM/EDAX examinations, were both process dependent and system geometry dependent. While there was no consistent relationship between the pressure and the sample composition, as the pressure decreased, the composition along the length of the substrate become more uniform.

The geometrical arrangements of the gas inlets, the substrate location, and the thermal patterns within the system apparently have great effect on the chemical composition of these deposited films. The aluminum content of the niobium aluminide deposits varied from 3 to 89 at. %, and the niobium contents varied from 11 to 97 at. %. Measurements taken at different positions across sample JB200-124 (Figure 4-26) show nonuniform distribution of niobium and aluminum in the sample. This nonuniformity was also visually evident when the experiment was disassembled. The introduction and orientation of additional helium as a mixing aid to the

Table 4-5. Results of Nb_xAl_y Deposition from the Molten Aluminum - AlCl Process

Sample Number	Composition[a] (at %)		Microhardness (DPH)		Thickness (μm)	Deposition Rate (μm/min)	Remarks
	Nb	Al	Substrate	Coating			
JB200-128			158		5	0.012	
JB200-130	50.16 48.91	33.00 24.34	105		5	0.012	
JB200-132	10.96 57.01	89.04 42.99	137		10	0.044	Isolated columnar grains
JB200-134	22.04 69.90	77.96 30.10	251		3-20	0.012-0.083	Porous deposit
JB200-136	22.86	77.14	223		300	0.91	Porous deposit
JB200-138			139	831	65	0.48	A 10 μm second phase on substrate
JB200-140	96.97	3.03	87	568	15	0.062	Isolated columnar grains
JB200-142			138	945	100-175	0.41-0.72	Porous deposit
JB200-144	36.83	63.17	128		10-25	0.04-0.099	Thin side denser than thick side
JB200-146	55.86 59.46 44.79 62.50 49.71	44.14 40.54 55.21 37.50 50.29	269	456	5-10	0.10-0.20	Thin side denser than thick side; both sides still porous
JB200-148	70.13 59.04 62.84 86.00	29.87 40.96 37.16 14.00	267		25	0.10	Thick deposit on chamber wall; deposit density dependent on its position in the system
JB200-148 (Chunk)	58.12[b] 61.20 71.39	41.88[b] 38.80 28.61			275	1.11	Sample taken from alumina liner near $NbCl_5$ inlet
JB200-150	26.70 33.12 30.64 31.31 27.78	73.30 66.88 69.36 68.69 72.22	90				Deposit morphology dependent on its position in the system
JB300-2	60.06 59.89 60.65 60.99	39.94 40.11 39.35 38.80					Porous deposit

[a] Measurements taken at uniform intervals from the top to the bottom of the niobium foil substrate.
[b] Measurements taken at uniform intervals from near the substrate interface to the surface of the deposit.

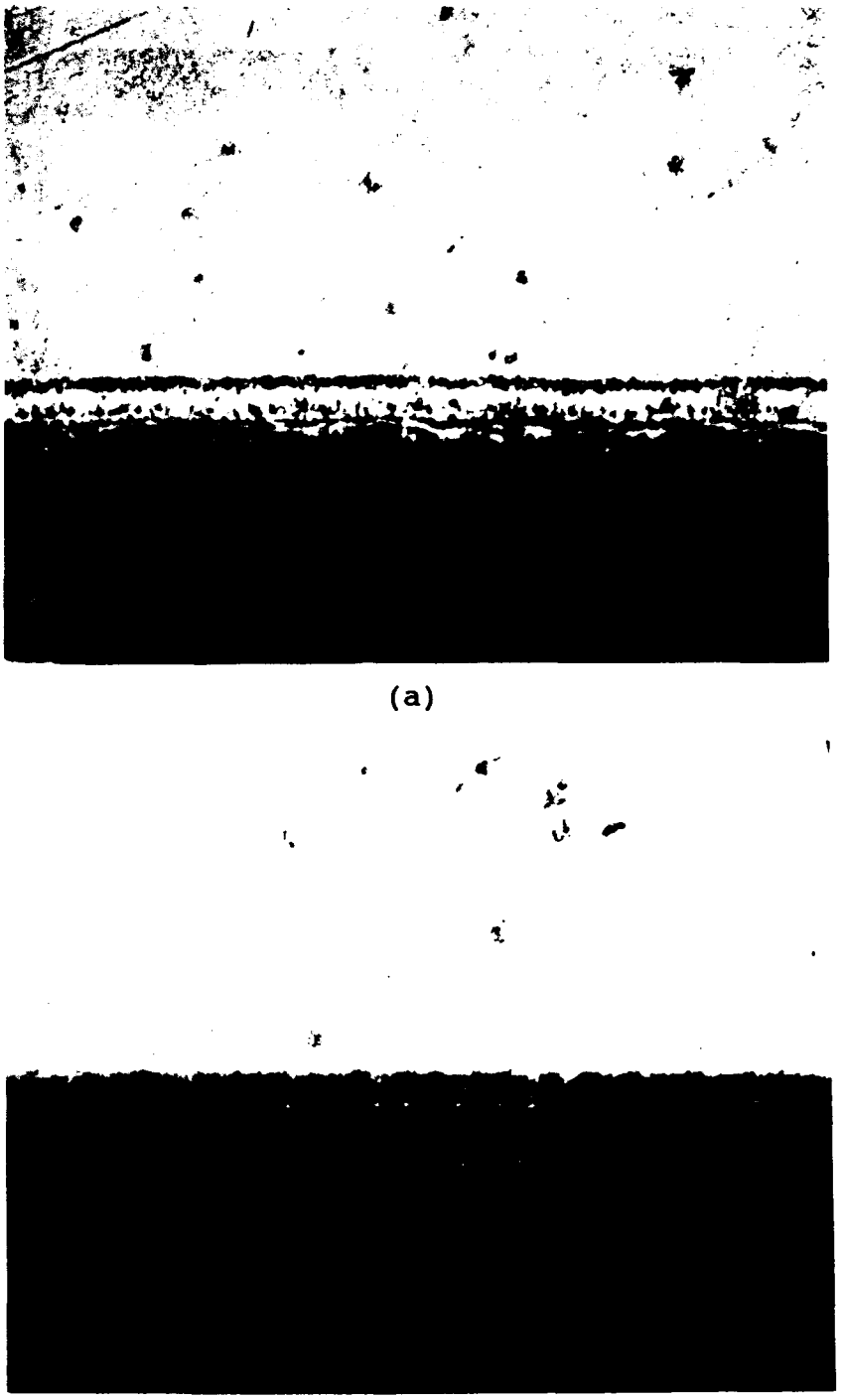

(a)

(b)

Figure 4-17. Optical photomicrographs at 1000X of deposit samples (a) JB200-128 and (b) JB200-130 on tantalum.

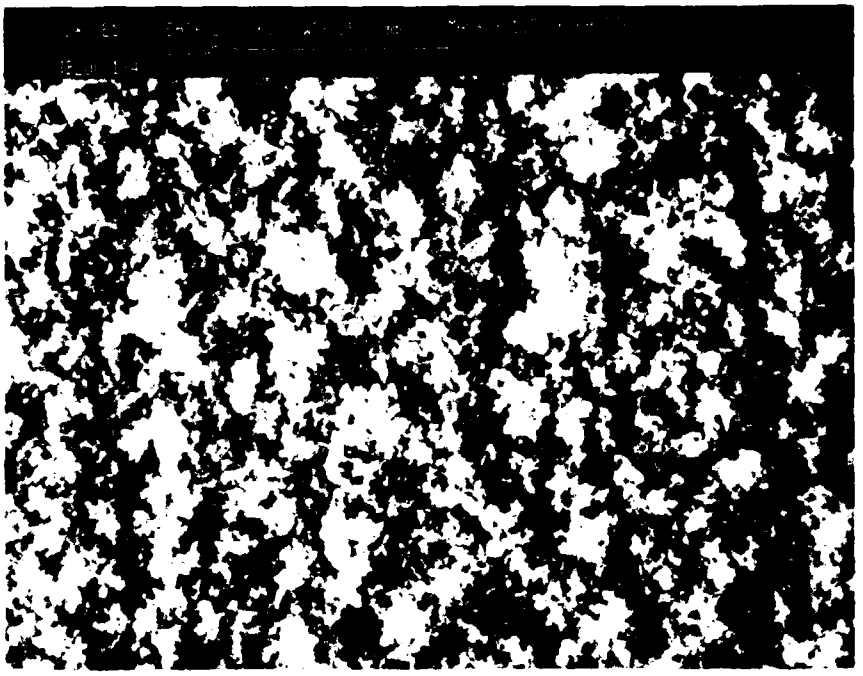

(a)

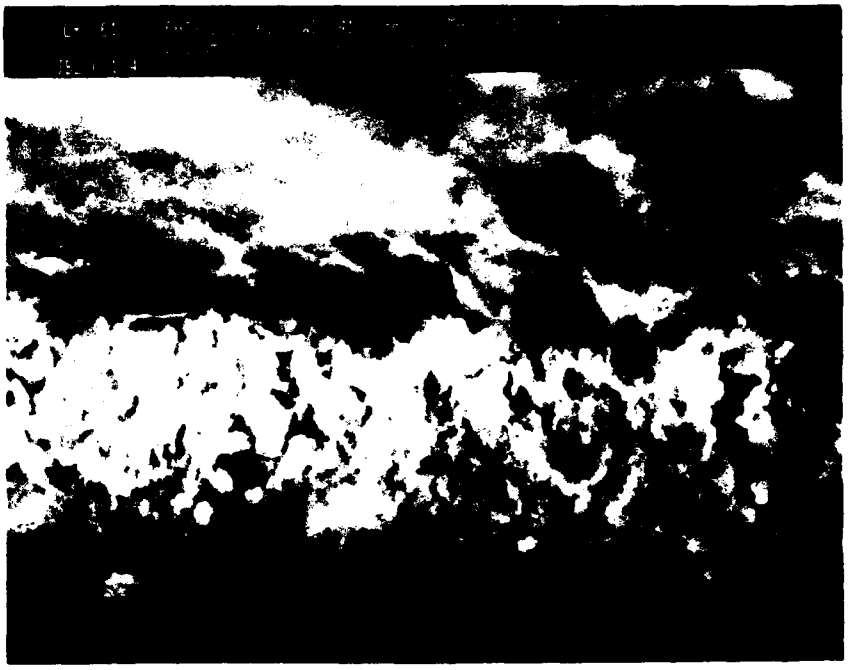

(b)

Figure 4-18. SEM photomicrographs of (a) a typical porous niobium-aluminum deposit (JB200-134) as viewed normal to the substrate and (b) a fractured cross section of the deposit.

Figure 4-19. SEM photomicrograph of a fractured cross section of deposit JB200-136 on a 25-μm thick niobium foil substrate.

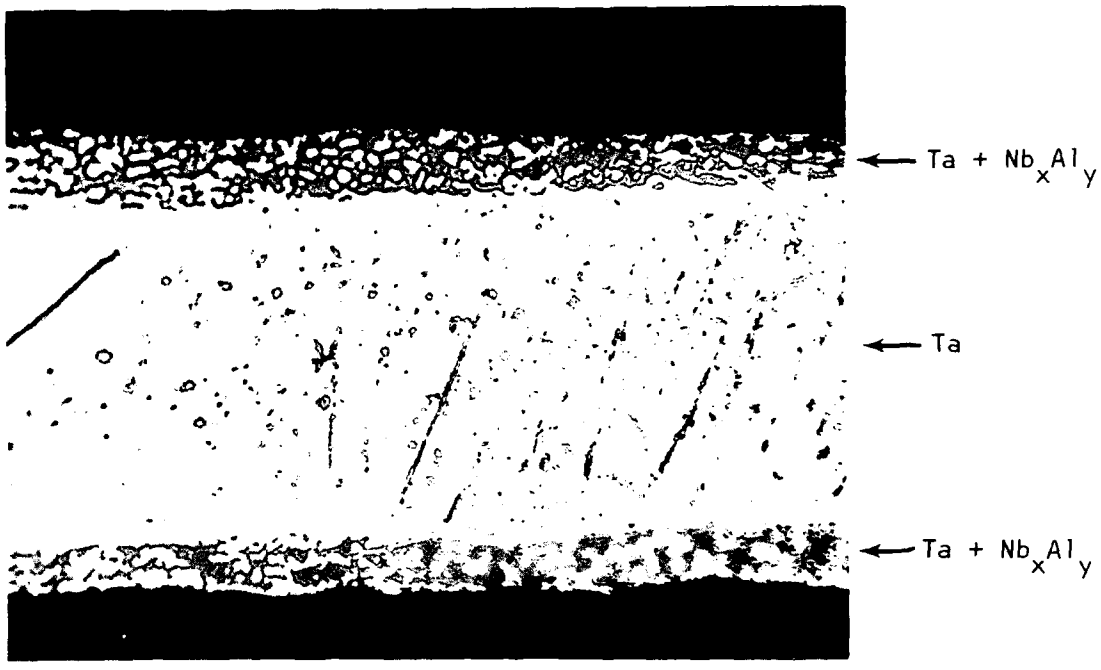

(a)

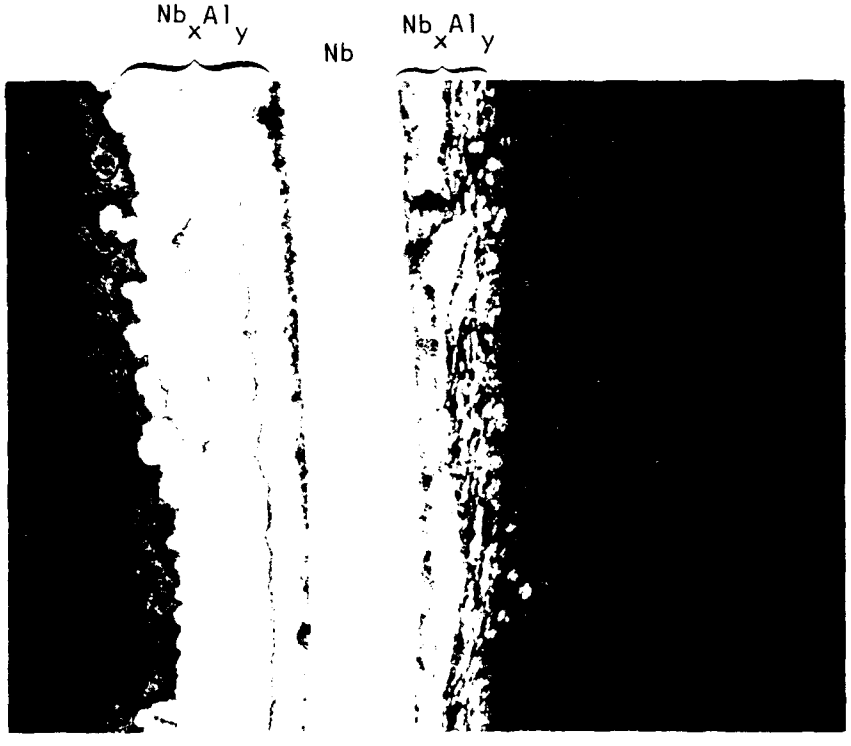

(b)

Figure 4-20. Optical photomicrographs of niobium-aluminum deposits showing (a) reactivity with a tantalum substrate at 960°C (sample JB200-124, 500X) and (b) no reactivity with a niobium substrate at 950°C (sample JB200-138, 200X).

(a)

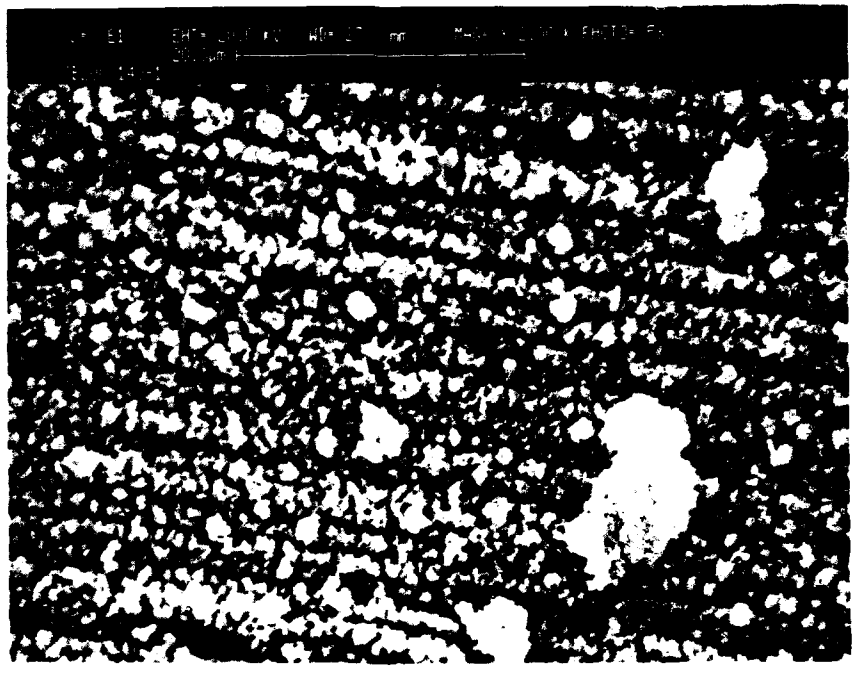

(b)

Figure 4-21. SEM photomicrographs of sample JB200-140, an isolated grain columnar deposit of niobium-aluminum on niobium.

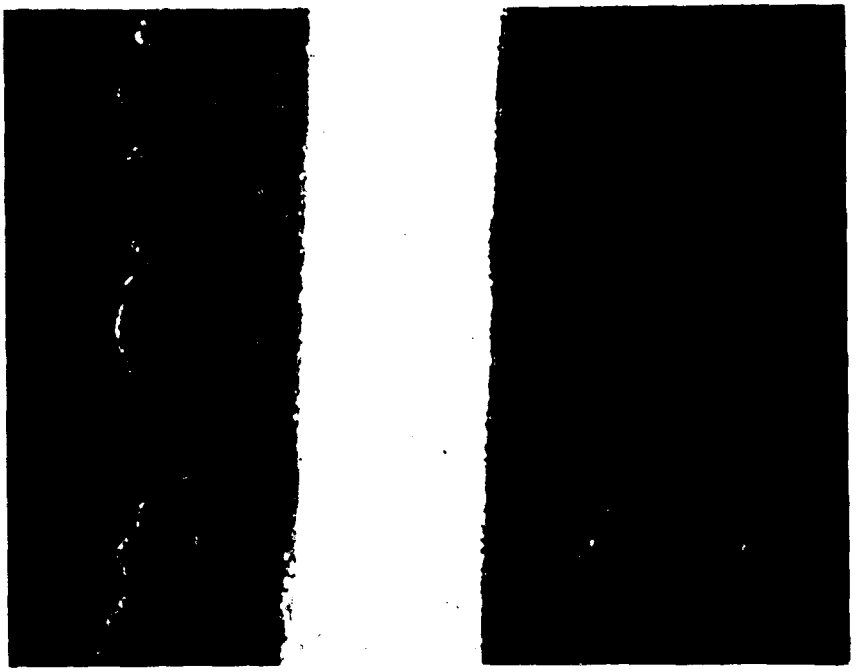

(a)

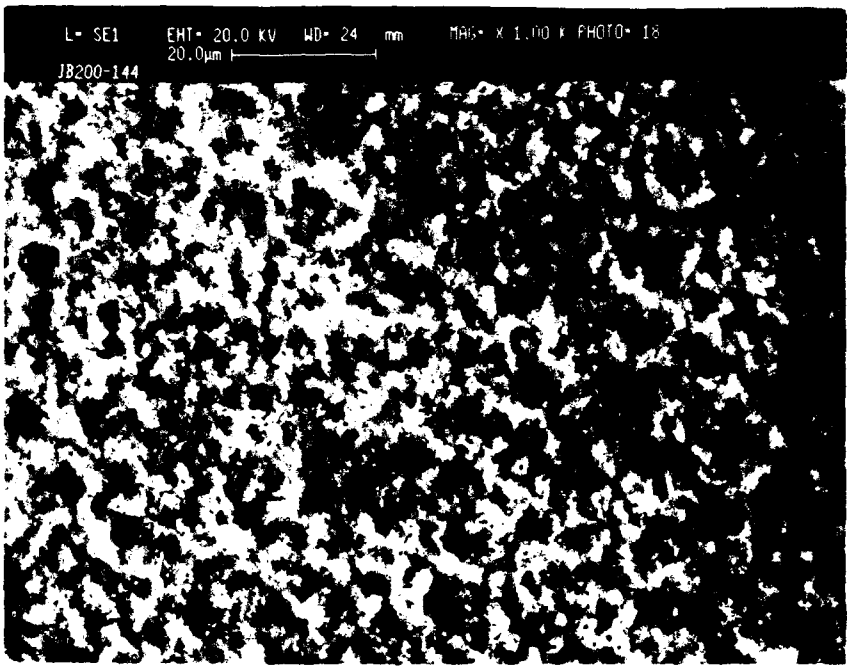

(b)

Figure 4-22. Porous niobium-aluminum sample JB200-144 deposited on niobium at 7 torr.

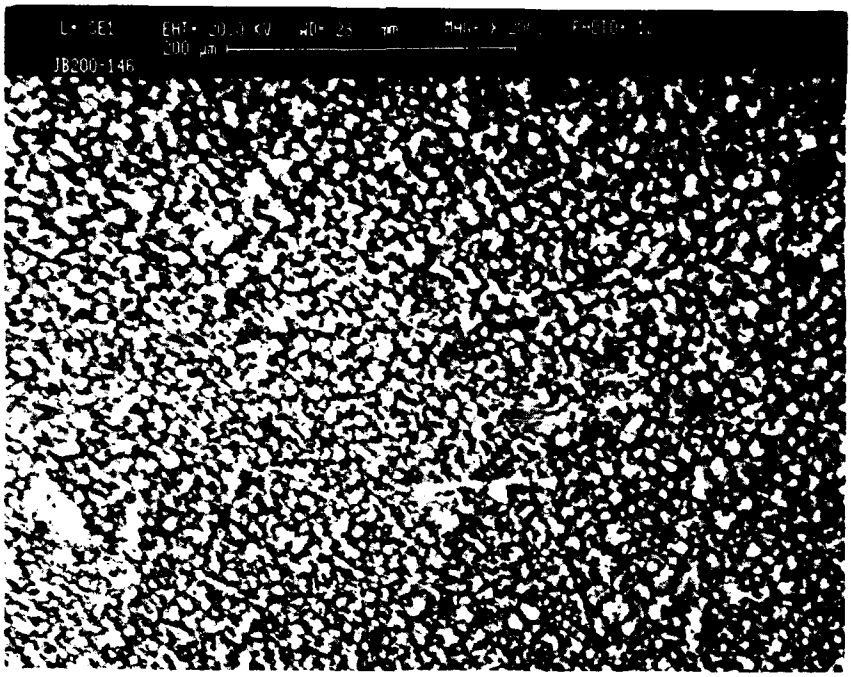

(a)

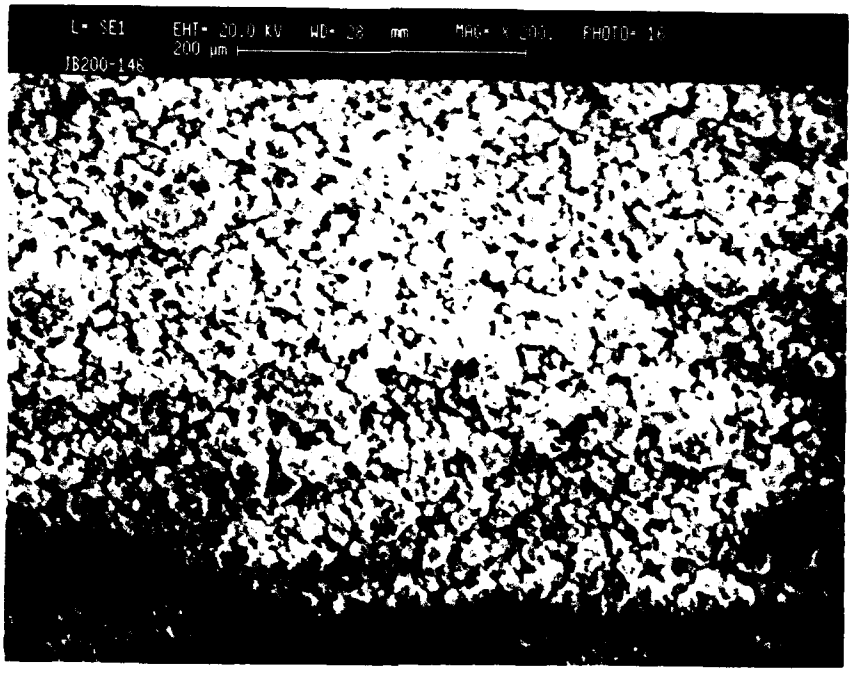

(b)

Figure 4-23. Variation in the morphology of deposit JB200-146 across the length of the niobium foil substrate.

(c)

Figure 4-23. (Continued) Variation in the morphology of deposit JB200-146 across the length of the niobium foil substrate.

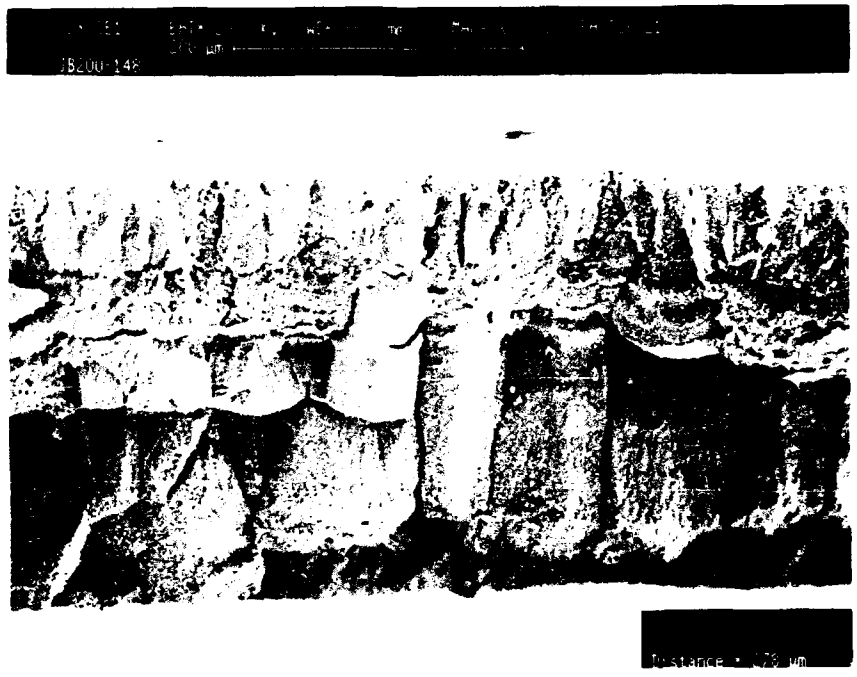

(a)

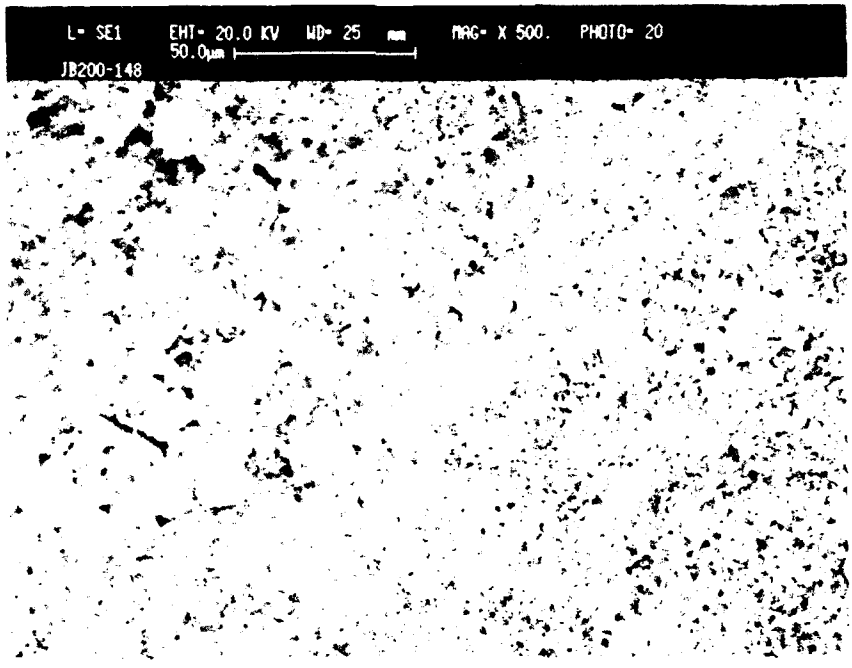

(b)

Figure 4-24. SEM photomicrographs of a thick niobium-aluminum deposit (JB200-148) formed with auxiliary helium impinging on the substrate.

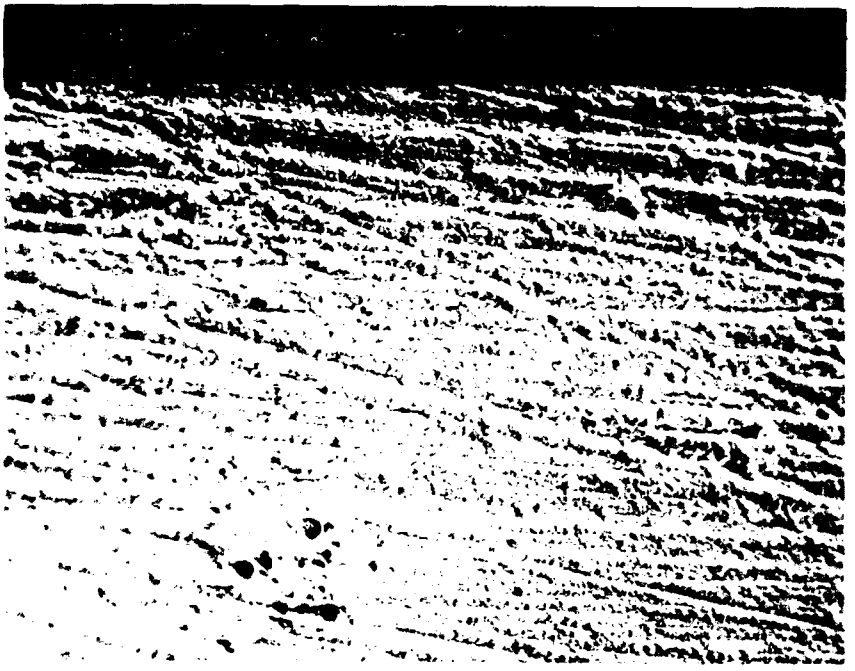

(a)

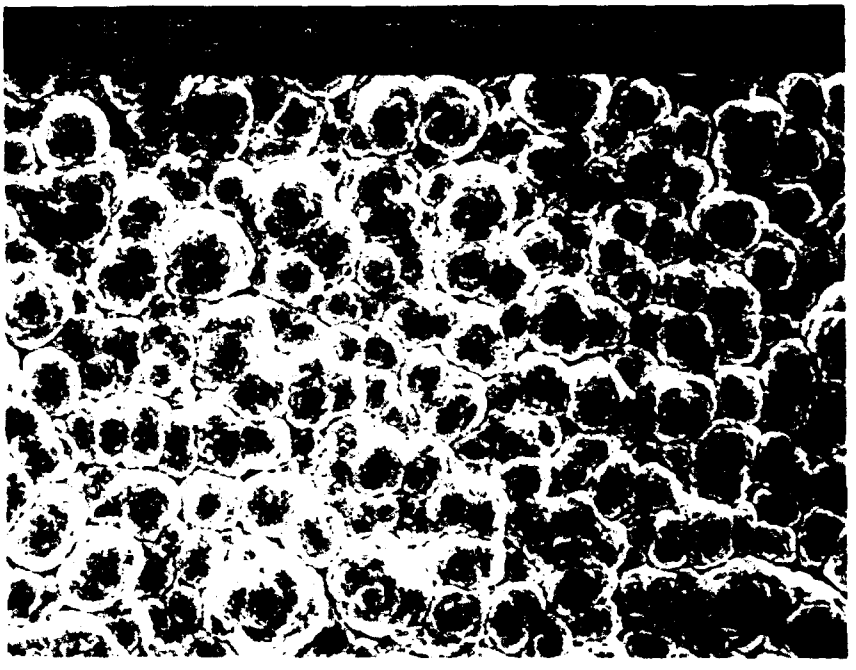

(b)

Figure 4-25. SEM photomicrographs of niobium-aluminum sample JB200-150 deposited with auxiliary helium flow parallel to the substrate surface.

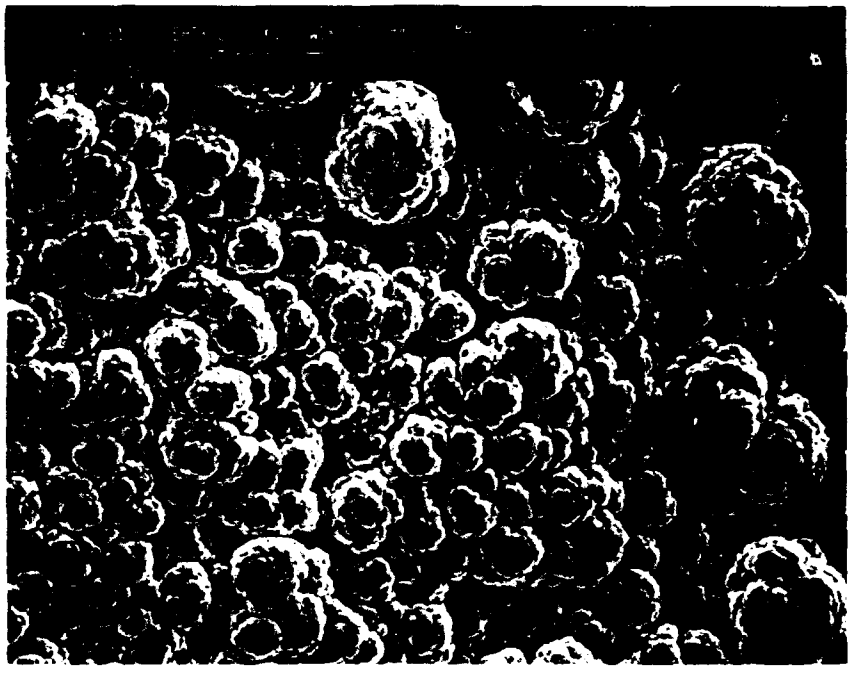

(c)

Figure 4-25. (Continued) SEM photomicrographs of niobium-aluminum sample JB200-150 deposited with auxiliary helium flow parallel to the substrate surface.

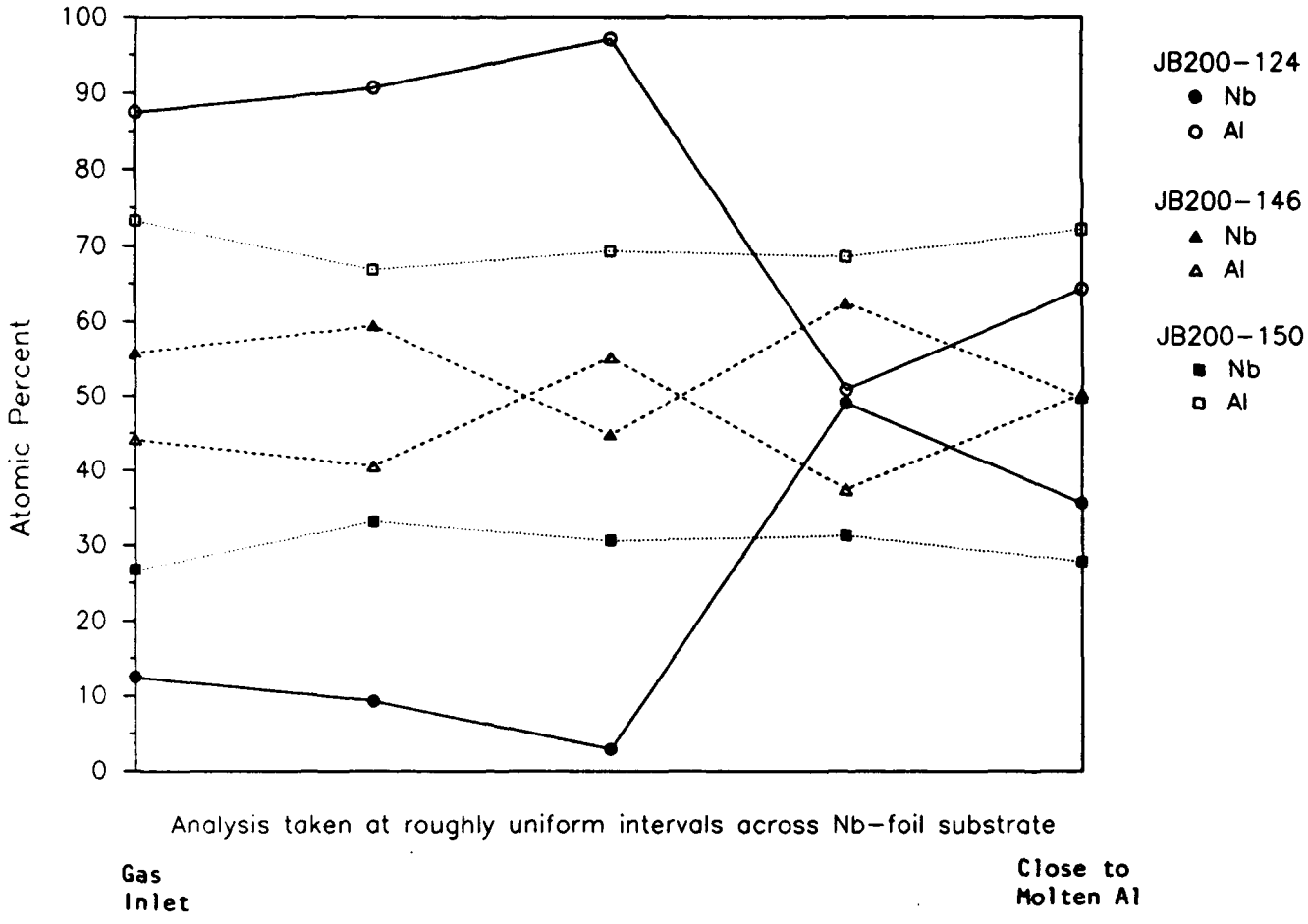

Figure 4-26. Niobium and aluminum contents, end to end, of deposits formed (1) without auxiliary helium in the reactive gas (sample JB200-124), (2) with auxiliary helium directed at the molten aluminum (sample JB200-146), and (3) with auxiliary helium parallel to the substrate (sample JB200-150).

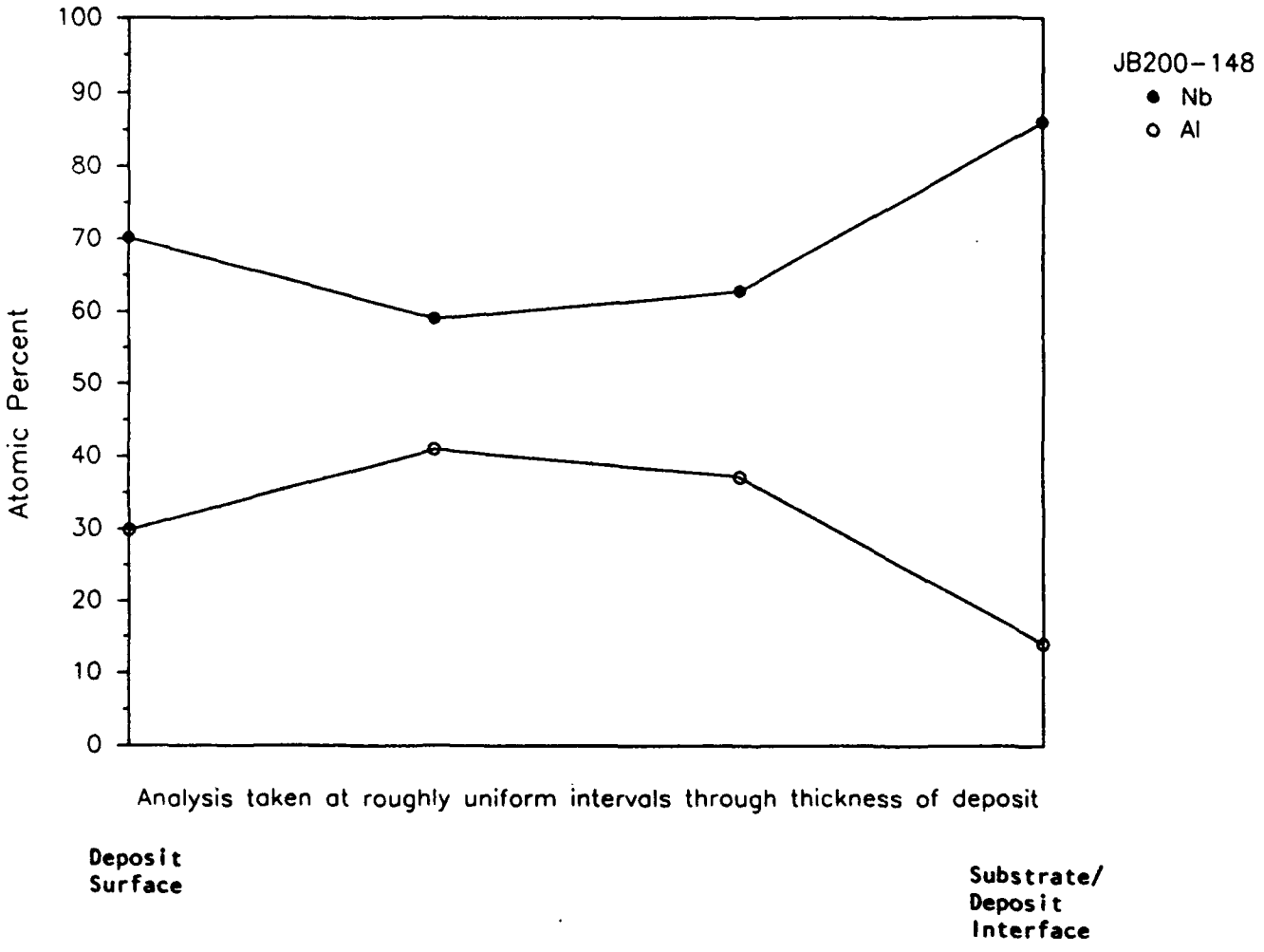

Figure 4-27. Niobium and aluminum contents of deposit JB200-148 taken from the substrate surface to the deposit surface.

deposition chamber improved not only the visual appearance of the deposit but also the uniformity of its chemical composition (Figures 4-23, 4-25).

Installation of the substrate heater improved the visual uniformity of the samples. However, as SEM examinations (Figure 4-25) and EDAX examinations (Figures 4-26, 4-27) show, there were still variations in both the morphology and chemical composition of the deposits. The composition changed both along the length of the substrate and across the depth of the deposit. These variations are probably due to the dynamic gas mixing processes occurring within the deposition chamber.

No chlorine was detected in any of these samples. This is consistent with earlier results which showed no chlorine in samples deposited on substrates hotter than 800°C.

Deposition rates were particularly dependent upon the gas flow dynamics in the system. As the helium flow directed at the molten aluminum was increased from 380 cc/min to 2000 cc/min in 760 torr deposits, the deposition rate increased from 0.012 μm/min to 0.91 μ/min. Lowering the pressure and/or the gas flows through the metal halides reduced the deposition rates. With high helium gas flows at atmospheric pressures, aluminum vapor was distributed widely in the system and gas phase nucleation was a prominent feature of the deposition process. Incorporation of these nucleated particles caused the formation of porous deposits, examples of which can be seen in Figures 4-20 through 4-22. When auxiliary helium was added to the process and focused directly on the substrate, the porous deposit was on the back side of the substrate but not on the side facing the impinging helium. When the added helium was focused parallel to the substrate, porous deposits did not form on the substrate.

High reaction rates and flow sensitivity result in a process that is difficult to control accurately. The present work suggests that this is a major issue in the development of CVD processes based on reduction by AlCL.

4.2 $NbAl_x$ DEPOSITION BY H_2 REDUCTION

This process requires temperatures above 1200°C because of the stability of the aluminum trichloride (see Section 3).

4.2.1 Deposition on Doubly Supported Substrates

The equipment used for the first high temperature depositions of $NbAl_x$ from the hydrogen reduction of $NbCl_5$ and $AlCl_3$ is shown in Figure 4-28. Process parameters used in these experimental trials are given in Table 4-6. First molybdenum wires and then molybdenum foils were used as substrates. In both cases it was difficult to maintain a uniform temperature on the substrate. Graphite rectangular and graphite "dog bone" shaped samples were also used. The dog bone substrates provided uniform temperatures but were inappropriate for chemical compatibility and CTE match reasons. Tantalum foil substrates were tried but were lost when the reactive gases were introduced into the chamber. Molybdenum dog bone samples were made which, when held with relatively massive copper nuts and bolts, finally provided uniformly heated substrates that were moderately compatible with the niobium-aluminide intermetallics.

$AlCl_3$ + H_2 gases were mixed with heated $NbCl_5$ gas over a resistance heated molybdenum substrate to form the reactive gas mixture. Modest adjustments in the $AlCl_3$ and $NbCl_5$ flows were made to determine what degree of control was provided on the resulting composition of the deposited intermetallic. Most of these deposits cracked and spalled off the substrates.

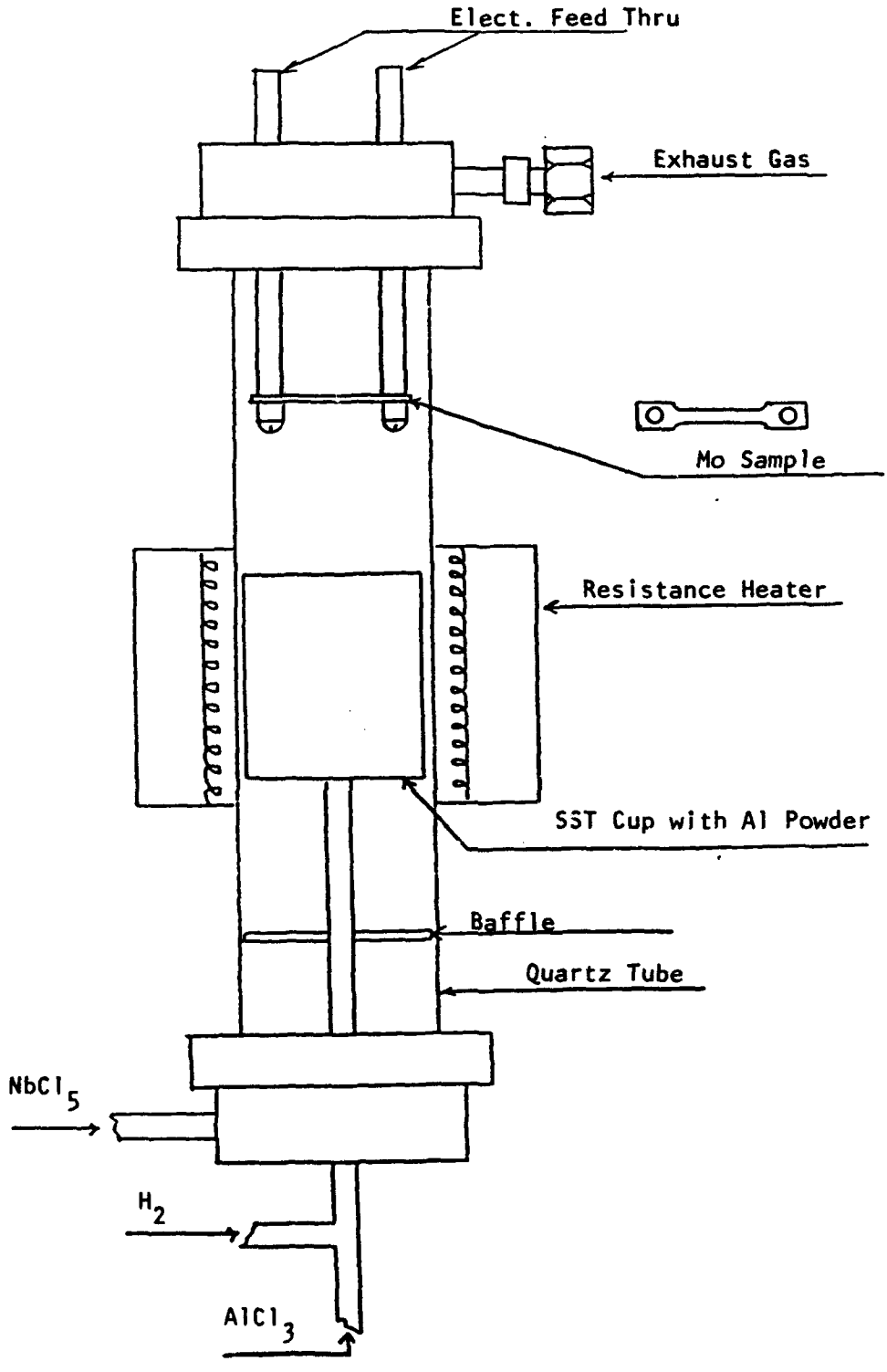

Figure 4-28. Schematic diagram of the resistance heated reactor used for $NbAl_x$ deposition from $NbCl_5$ + $AlCl_3$ + H_2.

Table 4-6. Process Parameters for Nb_xAl_y Deposited from the H_2 Reduction of $AlCl_3$ and $NbCl_5$ on Double Supported Substrates

Sample Number	Substrate	Pressure (torr)	Temperature (°C)				Gas Flow (cm^3/min)					Time (min)
			Substrate	Al	$AlCl_3$	$NbCl_5$	H_2 in $AlCl_3$	$AlCl_3$	Ar in $NbCl_5$	$NbCl_5$	H_2 Purge	
JB200-3	Mo filament	760	1600	540	125	140	110	2.2	50	0.59	60	71
JB200-6	Mo foil	760	1600 1200	480	141	146	108	6.4	50	0.76	60	62
JB200-7	HD graphite	760	1360	480	135	135	200	7.4	80	0.74	100	283
JB200-9	HD graphite	760	1230	480	125	139	200	3.9	80	0.88	100	297
JB200-11	HD graphite	760	1600	480	115	130	200	2.0	80	0.58	100	310
JB200-13	HD graphite	760	1550	480	120	138	200	2.7	80	0.84	100	120
JB200-15	HD graphite	760	1500	480	119	140	109	1.4	53	0.62	100	177
JB200-17	Ta foil	760	1400	Foil loss when reactive gases introduced.								
JB200-18	2020 graphite	760	1400	Graphite loss when reactive gases introduced.								
JB200-19	2020 graphite	760	1400	Graphite loss when reactive gases introduced.								
JB200-21	HD graphite	760	1520	-	140	125	200	10.8	80	0.45	100	172
JB200-22	HD graphite	760	1500	-	125	138	200	3.9	53	0.56	100	263
JB200-24	Mo foil	760	1530	-	135	128	200	3.9	80	0.56	100	225
JB200-25	Mo foil	760	1470	-	117	80	200	2.2	80	0.08	100	196
JB200-26	Mo foil	760	1650	-	130	90	200	5.5	80	0.10	100	211
JB200-44	Mo foil	1	1520	-	134	139	200	7.3	100	1.07	80	120
JB200-46	Mo foil	2	1500	-	130	120	200	5.5	100	0.46	80	120
JB200-50	Mo foil	2	1500	-	127	141	200	4.4	100	1.20	80	118

SEM photomicrographs of deposit fragments on the molybdenum substrate (Figure 4-29) are typical of what would be expected from moderate temperature deposits. The films were columnar grained and continuous. Microcracks along grain boundaries were frequently found in these deposits.

The preparation of aluminum-containing intermetallics by the hydrogen reduction of the mixed metal halides at 1500°C was shown to be feasible, as theory predicts. However, the cold wall deposition of the niobium aluminide on resistance heated substrates did not generate uniform niobium aluminide deposits from which a foil could be made. With the two ends of the substrate fastened to electrodes, the sample flexed during heating and cooling, causing the deposits to crack and spall. The resistance heated substrate process approach to this method was thus abandoned.

4.2.2 Deposition on Singly Supported Niobium Substrates

The preparation of aluminum-containing intermetallics by the hydrogen reduction of the mixed metal halides continued with a modification of the apparatus to permit controlled subatmospheric deposition of the niobium aluminides. The apparatus used in recent hydrogen reduction experiments was an induction-heated, hot-wall, isothermal system shown in Figure 4-30. Niobium foil substrates were attached to a support above the hot zone with a weight attached to them below the hot zone. Temperatures were monitored by sheathed thermocouples buried in the susceptor. Process parameters used in these experimental trials are given in Table 4-7. Thermocouples were used to monitor these temperatures. Optical measurements were used only as guide lines at the beginning of each trial. Attenuation of light passing through the quartz chamber as the deposition process coated the quartz made apparent optically measured temperatures much lower than actual temperatures.

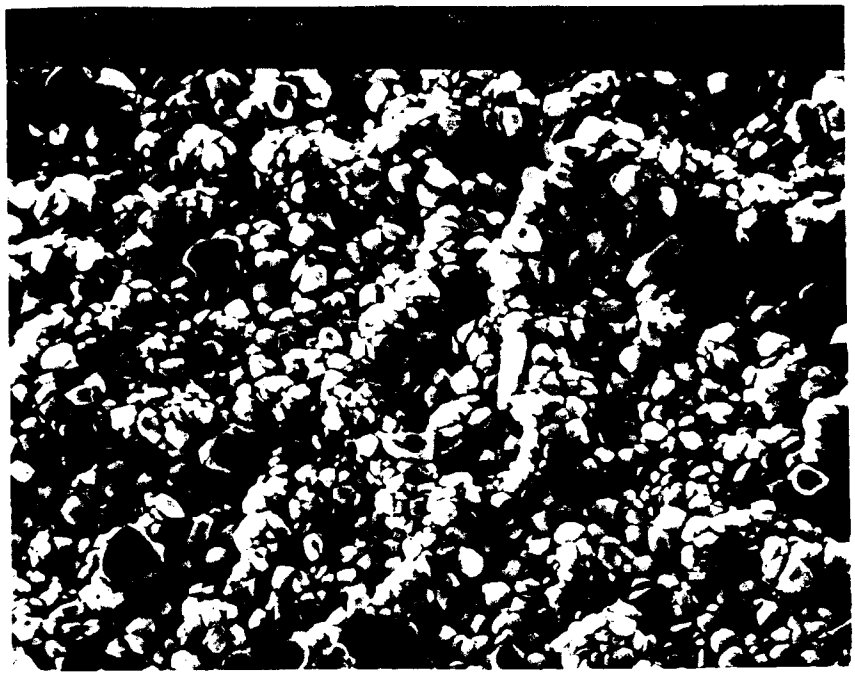

(a)

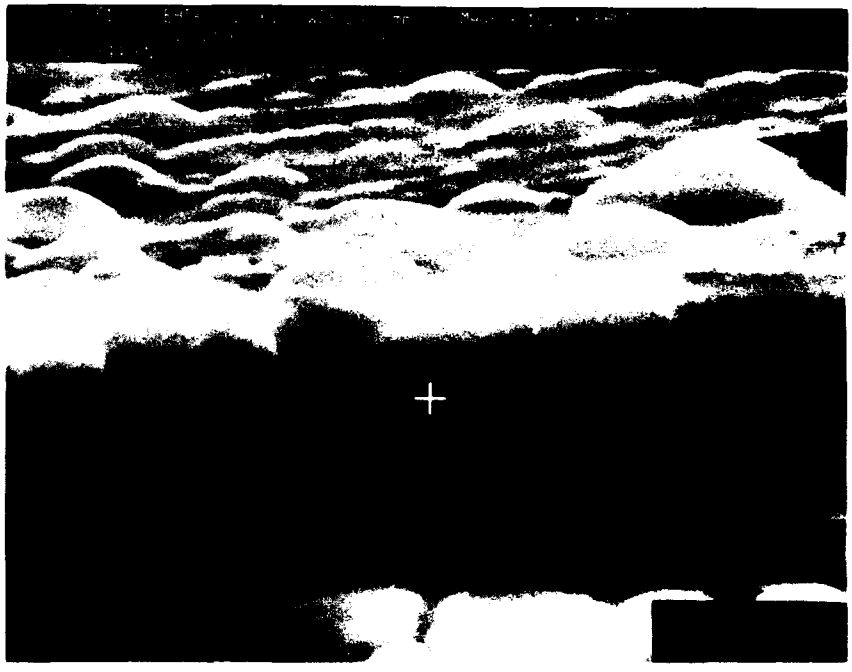

(b)

Figure 4-29. SEM photomicrographs of a subatmospheric 1500°C $NbAl_x$ deposit.

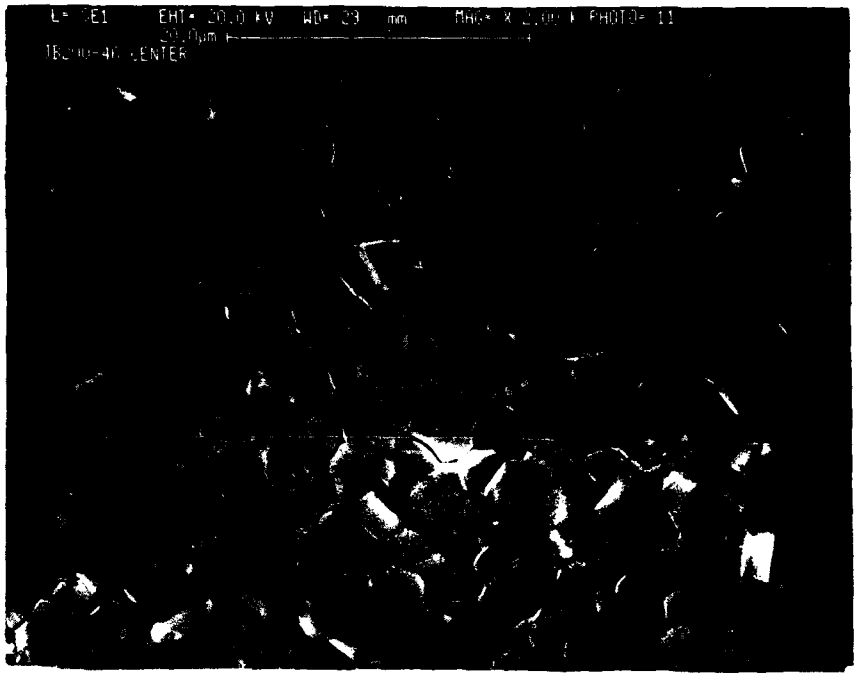

(c)

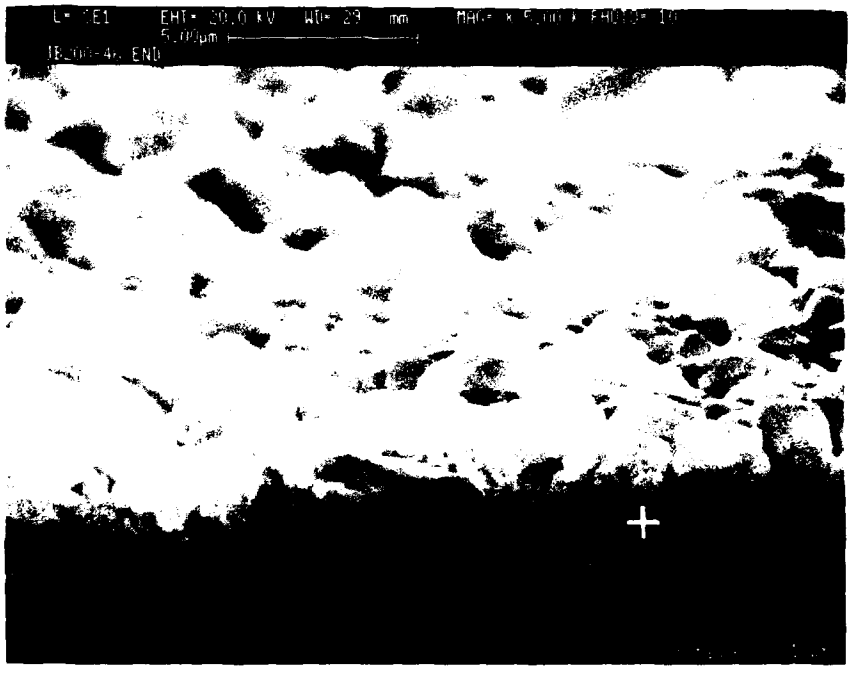

(d)

Figure 4-29. (Continued) SEM photomicrographs of a subatmospheric 1500°C $NbAl_x$ deposit.

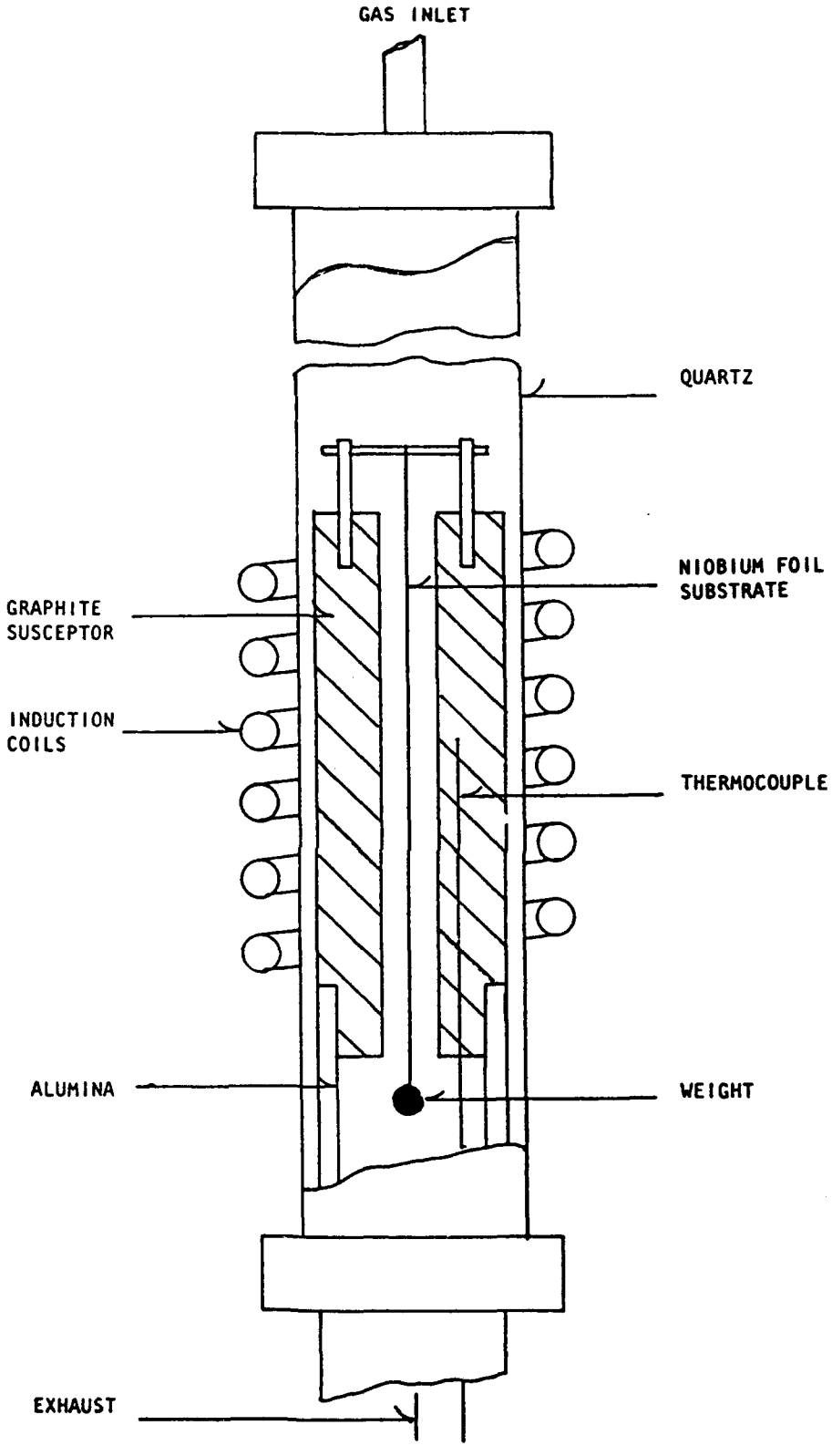

Figure 4-30. Schematic diagram of the isothermal CVD deposition system used for the formation of Nb_xAl_y by the hydrogen reduction of the halides.

Table 4-7. Process Parameters for the CVD of Nb_xAl_y Foil from the Hydrogen Reduction of $AlCl_3$ and $NbCl_5$ on Singly Supported Niobium Substrates

Sample Number	Temperature (°C)			Gas Flow (cc/min)					Time (min)	Pressure (torr)
	Substrate	$AlCl_3$	$NbCl_5$	He in $AlCl_3$	$AlCl_3$	He in $NbCl_5$	$NbCl_5$	H_2		
JD300-40	1600+	135	131	200	7.9	315	2.6	800	14	100
JD300-42	1600	140	129	72-56	3.9-3.0	263-230	1.8-1.6	800	22	45
JD300-43	1550	140	125	200	10.8	400	2.4	800	33	55
JD300-44	1560	145	119	200-14	15.8-1.1	400	1.7	800	14	30
JD300-52	1610	142	118	200	13.2	330	1.3	800	27	23
JD300-53	1555	142	123	200	4.2	300	1.6	800	20	50
JD300-54	1480	126	122	200	4.2	300	1.5	800	12	38
JD300-55	1460	123	119	200	3.4	300	1.3	800	24	45
JD300-56	1460	120	120	100	1.4	300	1.4	800	36	40

Sample JD300-42, deposited at a nominal 1600°C, fragmented and was very brittle. Sample JD300-43, deposited at approximately 1550°C, was thin because of an unplanned shutdown.

Metallographic and SEM examinations of the deposit (Figures 4-31 to 4-36) show that significant interdiffusion of the deposit and substrate occurred at deposition temperatures above 1500°C. When there was unplanned attenuation of the $AlCl_3$ flow, the deposit density increased [Figure 4-35(a), sample JD300-44]. When there was unplanned attenuation of the $NbCl_5$, the deposit porosity increased [Figure 4-35(b), sample JD300-52]. Partial loss of the specimen occurred when the substrate temperature exceeded 1600°C. It is not known whether this was due to the formation of the low melting eutectic or crack formation and sample failure in the brittle intermetallic during process cooldown. Examinations of the subatmospheric deposits were made on a SEM system with an EDAX attachment. EDAX examinations (Table 4-8) show that these deposits have a wide composition range from aluminum-rich to niobium-rich which, as Figure 4-36 shows, changes their microstructure significantly. The diffusion of niobium through the intermetallic and of aluminum through niobium at temperatures between 1450° and 1550°C is apparently slow.

The deposition of niobium aluminides at high temperatures by the hydrogen reduction of $AlCl_3$ and $NbCl_5$ was much easier to control in an isothermal hot wall reactor than either by resistance heating the substrate in a cold wall reactor or reducing the metal halides at lower temperatures with in-situ formed AlCl. Resistance heated deposits crack and spall from specimen flexing during deposition thermal cycling. The aluminum monochloride reduction process is so rapid that it is difficult to mix the reactive gases without gas phase nucleation and the resulting formation of porous, weak deposits of the aluminides.

(a)

(b)

Figure 4-31. Optical photomicrographs at 1000X of cross sections of niobium-aluminum deposited at 1600°C on niobium at (a) moderate $NbCl_5$ flow (sample JD300-40) and (b) low $NbCl_5$ flow (sample JD300-42).

(a)

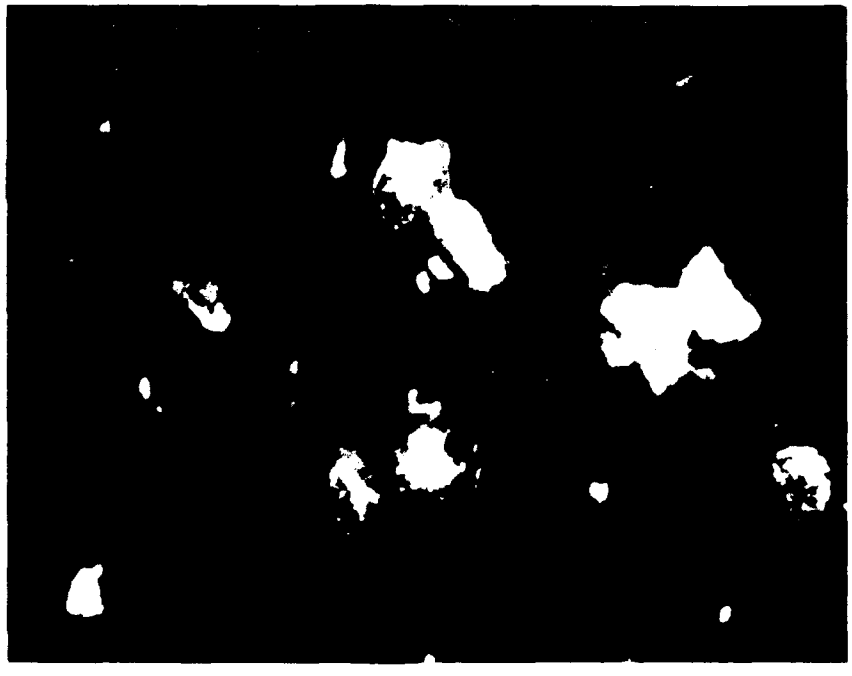

(b)

Figure 4-32. SEM photomicrographs of niobium-aluminum sample JD300-42 showing mud cracking of the deposit due to the differential coefficient of thermal expansion between the substrate and deposit.

(a)

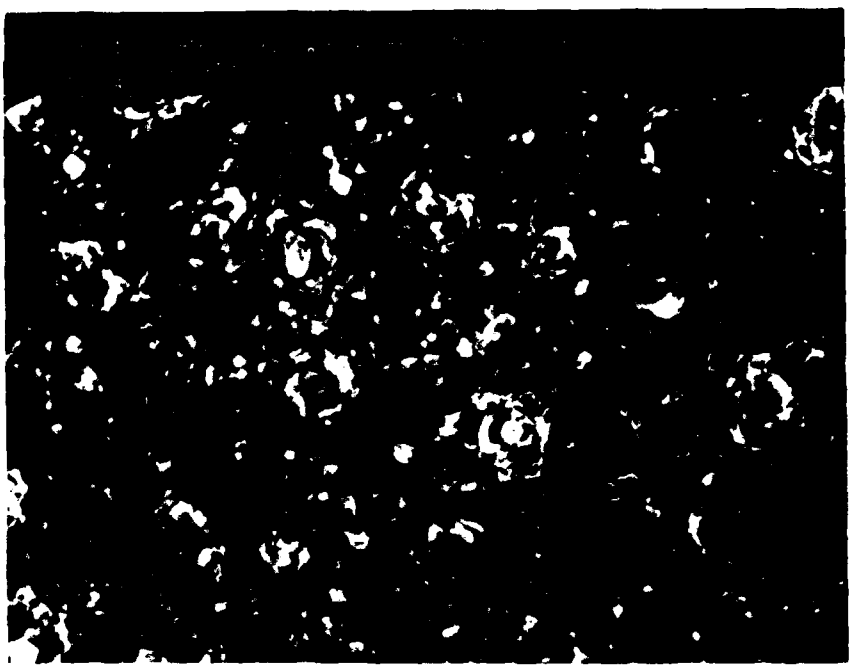

(b)

Figure 4-33. Porous niobium-aluminum deposit (JD300-43) due to excess aluminum in the reactive gas mixture.

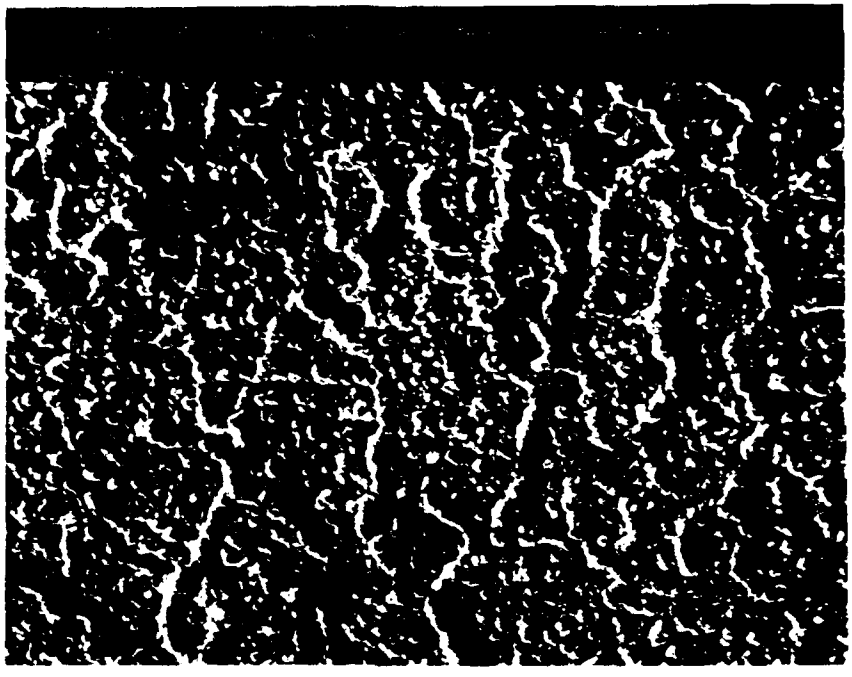

(a)

(b)

Figure 4-34. Dense niobium-aluminum deposit (JD300-44) formed on a niobium substrate.

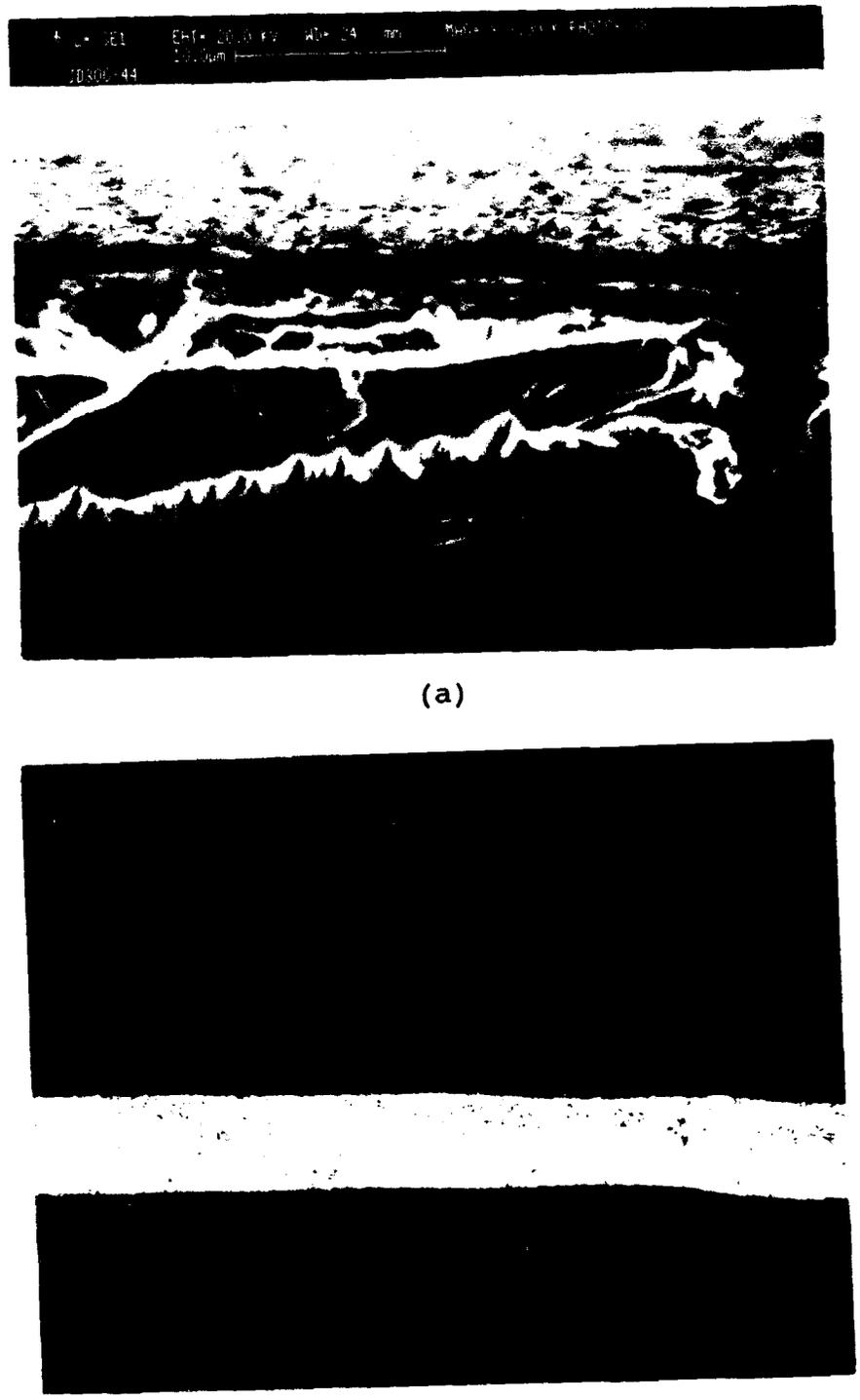

Figure 4-35. Morphology of niobium-aluminum deposited with (a) excess niobium (sample JD300-44) and (b) excess aluminum (sample JD300-52).

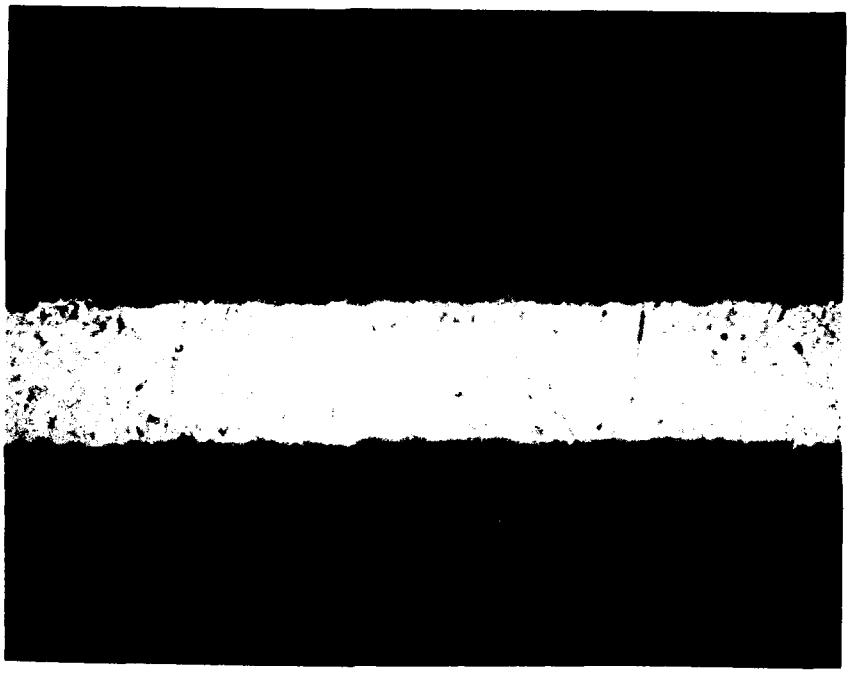

(a)

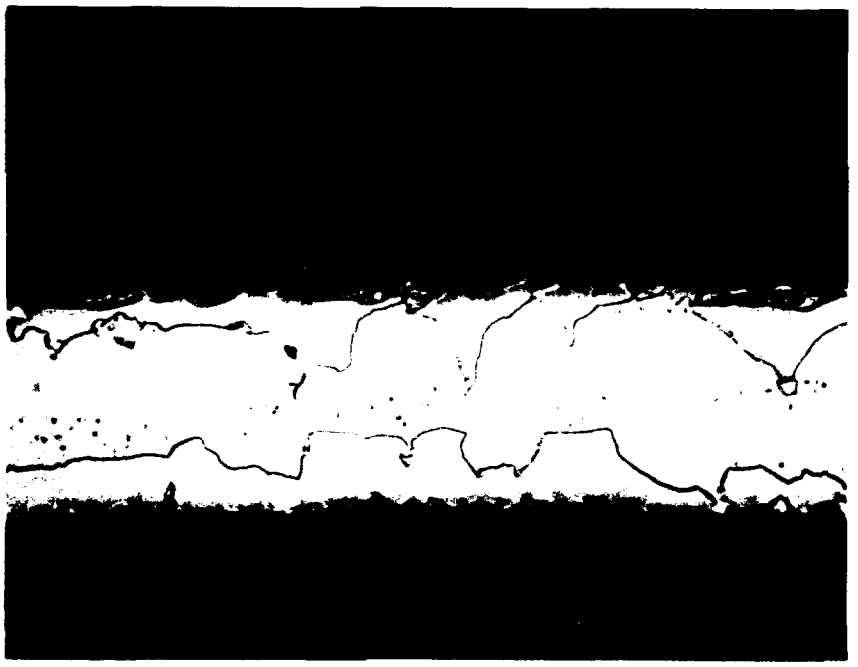

(b)

Figure 4-36. Optical photomicrographs of niobium-aluminum deposited samples: (a) JD300-53, niobium rich; (b) JD300-54, aluminum rich.

Table 4-8. Evaluation Results of Nb_xAl_y Deposition from the H_2 Reduction of $NbCl_5$ and $AlCl_3$ on Singly Supported Substrates

Sample Number	Composition (at. %)		Microhardness (DPH)		Thickness (μm)	Remarks
	Nb	Al	Substrate	Coating		
JD300-40				1517	10	Reaction, substrate - deposit
JD300-42					10-20	Reaction, substrate - deposit
JD300-43	14.98	85.02			18	Porous deposit
JD300-44	42.99	57.01			1-5	Plug developed in $AlCl_3$ inlet
JD300-52			128		30-60	Plug developed in $NbCl_5$ inlet
JD300-53	81.11	18.89	267		7.20	Porous outer layer
JD300-54	12.01	87.99	847		2.5	Irregular second phase
JD300-55			335		<1	
JD300-56	5.81	94.19	185		3	

It is clear from these experiments that reaction of the deposition gases with the substrate at processing temperatures above 1500°C is almost unavoidable. Diffusion and partial conversion will occur when there is a reaction of a component of the intermetallic being deposited with a component of the substrate. This process was expected and found in the deposition of the aluminides on niobium by the hydrogen reduction of the halides at high temperatures. The partial conversion of the niobium substrate plus the deposition of the intermetallic over this partially converted substrate is perhaps the most promising method of fabricating intermetallic Nb_xAl_y foils.

4.3 DEPOSITION OF Nb_xSi_y FROM H_2, $NbCl_5$, AND $SiCl_4$

The deposition of Nb_xSi_y by the direct CVD of Nb_xSi_y from the hydrogen reduction of $SiCl_4$ and $NbCl_5$ is described by the overall reaction:

$$xNbCl_5 + ySiCl_4 + (5x + 4y)/2\ H_2 \rightarrow Nb_xSi_y + (5x + 4y)HCl \qquad (4\text{-}4)$$

The apparatus used for these deposits was again the isothermal CVD apparatus shown in Figure 4-30. Niobium was also used for the substrate in the deposition of the niobium silicides because of its melting point, its CTE, and the fact that it is a component of the intermetallic. Process parameters used in these experiments are given in Table 4-9. Helium was passed through silicon tetrachloride chilled to 0°C in an ice bath. Similarly helium was passed through a temperature controlled niobium pentachloride vapor generator. The carrier gases were assumed to be saturated with the respective halides for the reported flows shown in Table 4-9.

Results of these niobium silicide experimental trials are given in Table 4-10 and Figures 4-37 through 4-41 As can be seen in these figures, thick deposits were formed. The deposition and diffusion reaction between the silicon and niobium substrate caused

Table 4-9. Process Parameters for CVD Nb_xSi_y Foil Deposition

Sample Number	Pressure (torr)	Temperature (°C)		Gas Flow (cc/min)					Time (min)
		Substrate	$NbCl_5$	He in $NbCl_5$	$NbCl_5$	He in $SiCl_4$	$SiCl_4$ (at 0°C)	H_2	
JD300-33	37	1010	128	240-43	1.6-0.29	138-62	10.4-4.6	800	141
JD300-34	54	1030	119	500	2.7	138	10.4	800	130
JD300-35	53	1040	118	450-430	1.9-1.8	75	5.6	800	131
JD300-36	42	1045	120	456-427	2.1-2.0	50	3.8	800	177
JD300-37	52	1070	128	500	3.4	50	3.8	800	124

Table 4-10. Results of Nb_xSi_y Deposition Experiments

Sample No.	Composition (at.%)		Thickness (μm)	Deposition Rate (μm/min)	Remarks
	Nb	Si			
JD300- 33	2.20	97.80	18	0.13	Porous interface material.
300- 34	38.80	61.20	27	0.21	Large voids.
300- 35	33.15	66.85	25	0.19	Large voids.
300- 36	36.02	63.98	28	0.16	Adherent deposit on Nb.
300- 37	36.62	63.38	28	0.22	Adherent deposit on Nb.

(a)

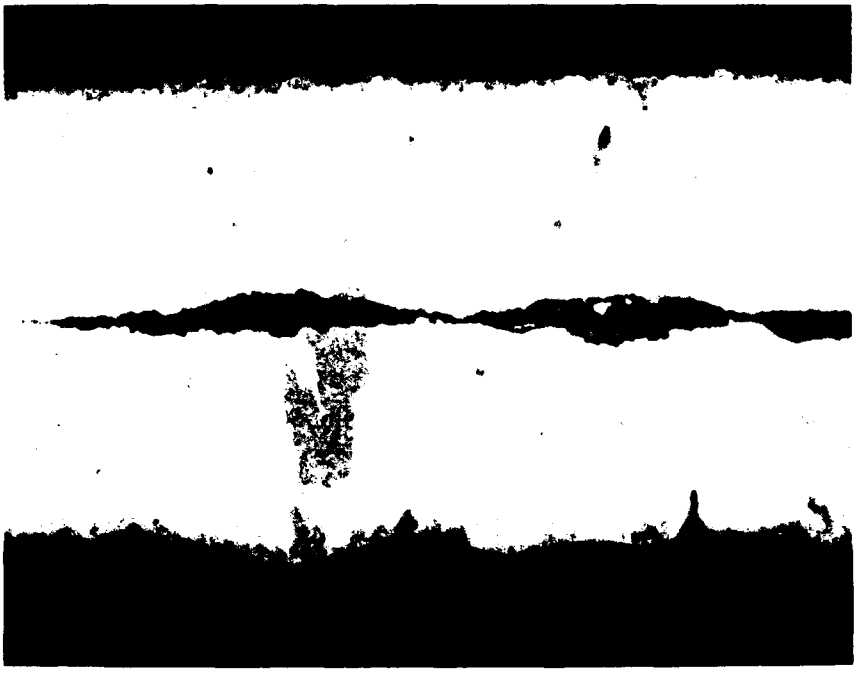

(b)

Figure 4-37. Nb_xSi_y from the hydrogen reduction of the halides showing large void formation (sample JD300-34): (a) SEM photomicrograph; (b) optical photomicrograph (1000X).

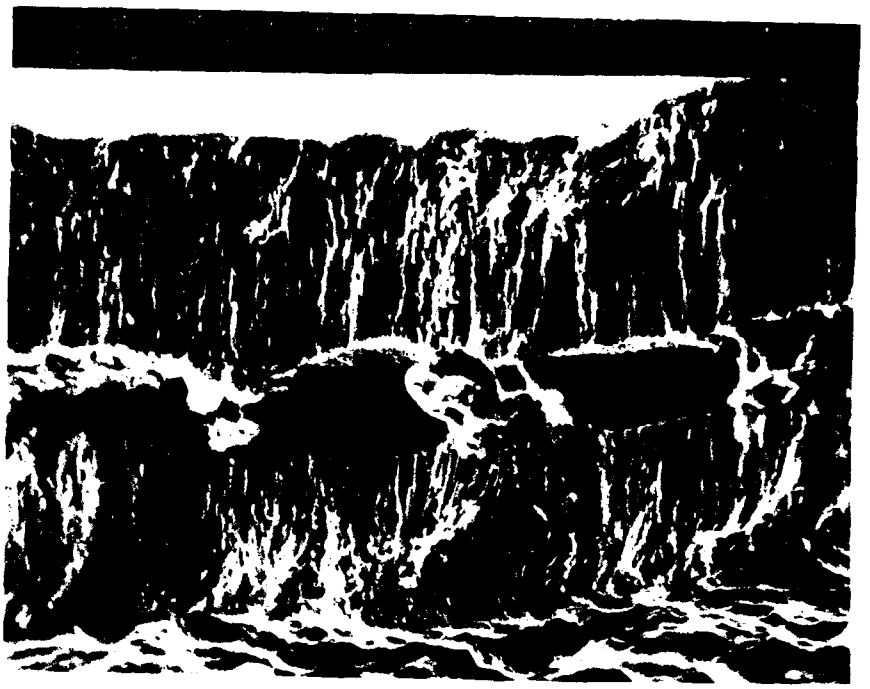

(a)

(b)

Figure 4-38. Nb_xSi_y from the hydrogen reduction of the halides showing large void formation (sample JD300-35): (a) SEM photomicrograph; (b) optical photomicrograph (1000X).

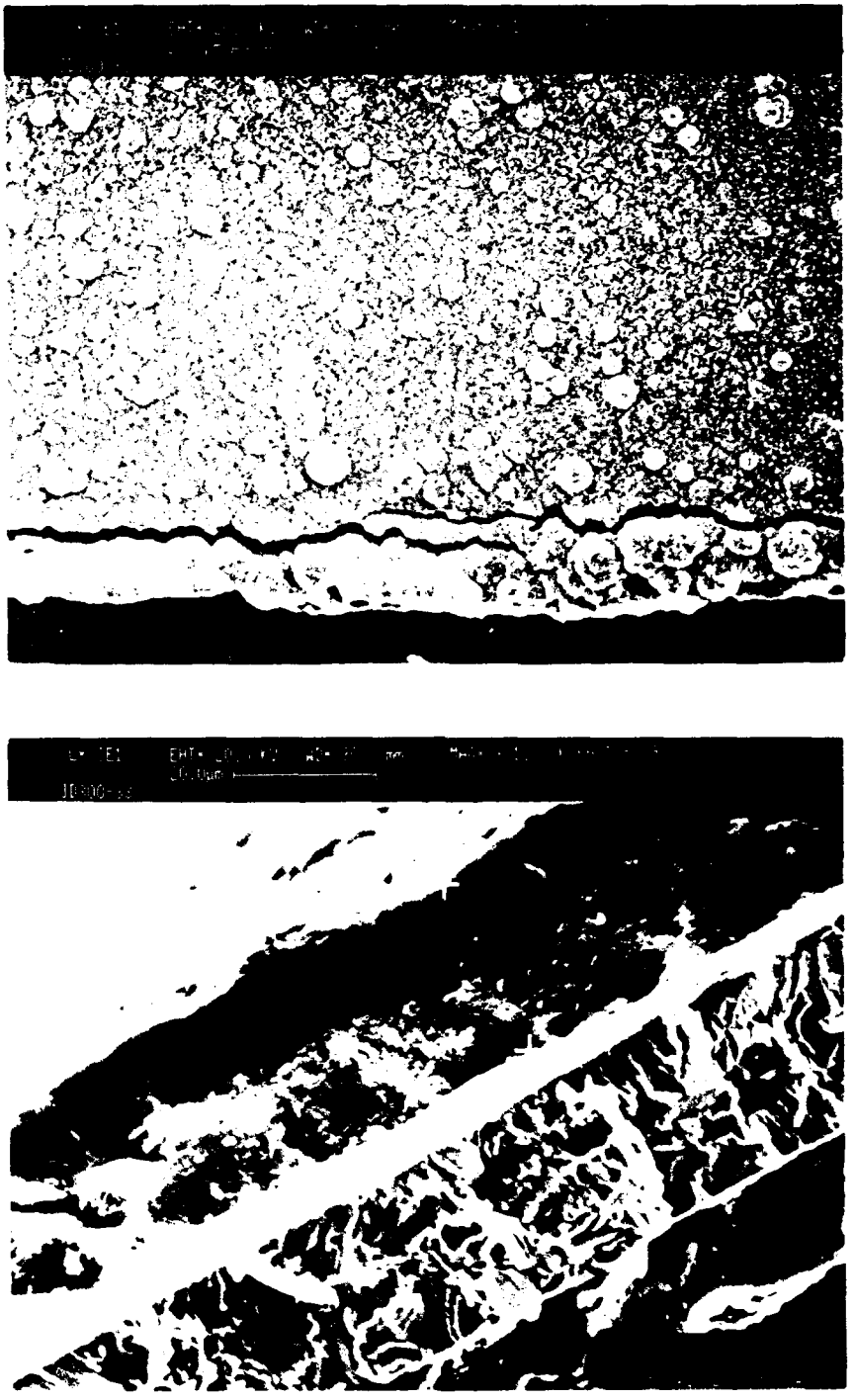

Figure 4-39. SEM photomicrographs of thick Nb_xSi_y films deposited on niobium from the hydrogen reduction of the halides showing minimal void formation (sample JD300-33).

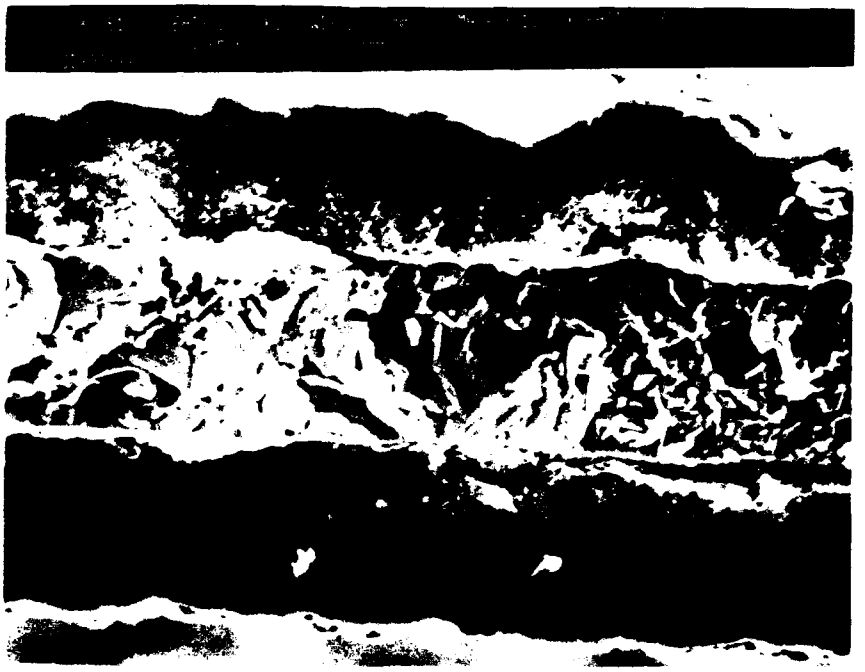

(a)

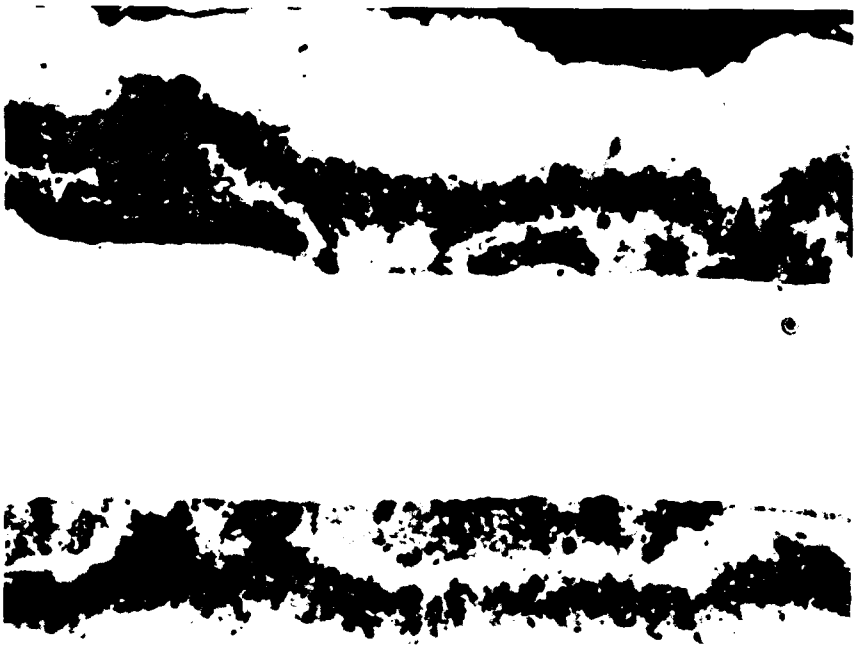

(b)

Figure 4-40. Thick Nb_xSi_y films deposited on niobium from the hydrogen reduction of the halides showing minimal void formation (sample JD300-33): (a) SEM photomicrograph (1000X); (b) optical photomicrograph (1000X).

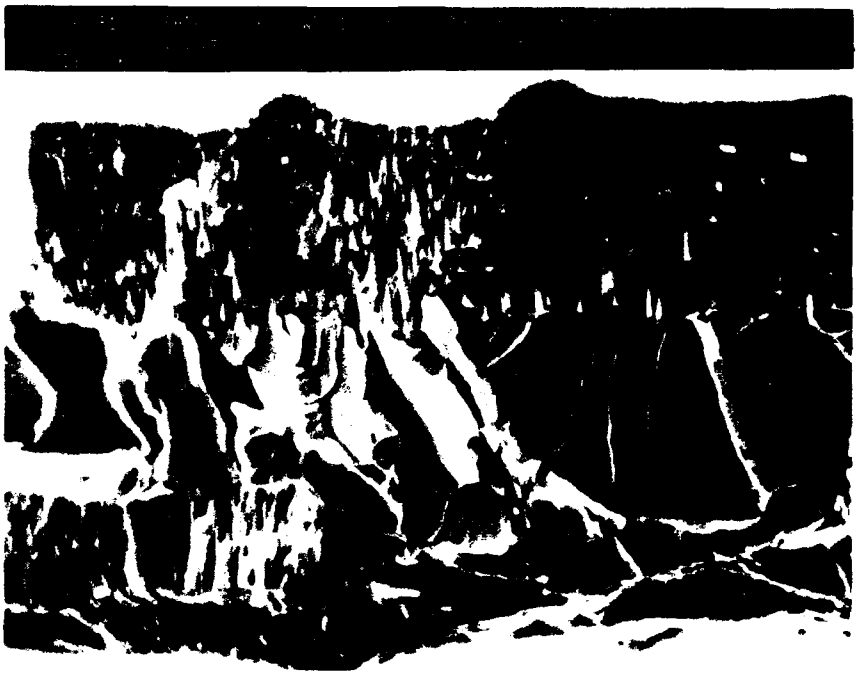

(a)

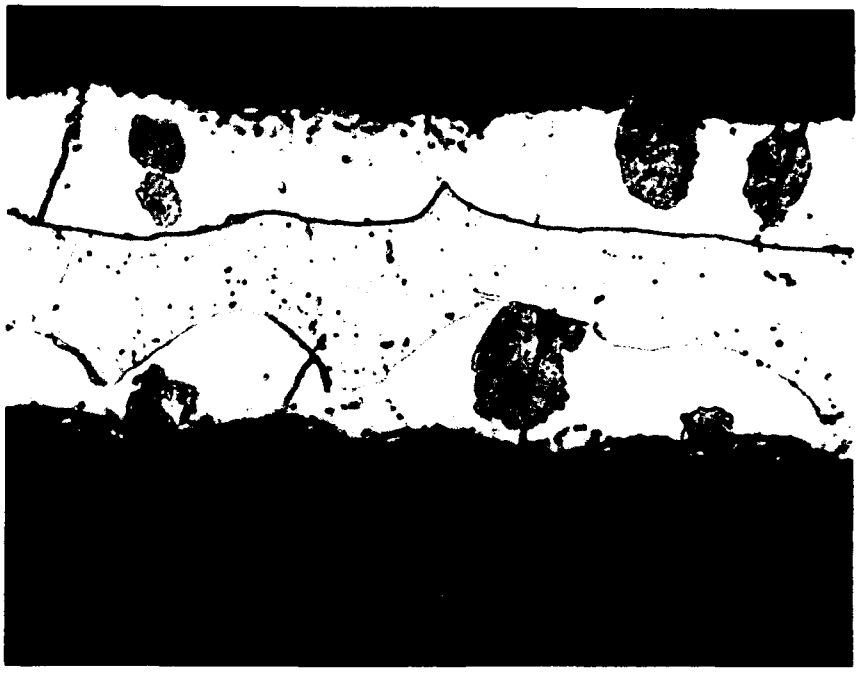

(b)

Figure 4-41. Thick Nb_xSi_y films deposited on niobium from the hydrogen reduction of the halides showing minimal void formation (sample JD300-36): (a) SEM photomicrograph (1000X); (b) optical photomicrograph (1000X).

the formation of voids at the deposit/niobium interface. In some cases (Figures 4-37, 4-38), most of the niobium was consumed. In others (Figures 4-39 through 4-41), an adherent interface was formed between the niobium and intermetallic. Sample deposits were visually uniform over a 2- to 3-inch span of substrate that was in the hot zone of the deposition chamber.

Niobium/silicon ratios were reproducible within the process parameter variability of these experiments except when clogging of the $NbCl_5$ generator occurred. Varying the $SiCl_4$ flow from 3.8 cc/min to 10.4 cc/min with approximately the same $NbCl_5$ flow changed the amount of void volume but had a minor effect on the niobium/silicon ratio.

The approach taken in these experiments to prepare niobium silicide foils appears to be a reasonable one. With process parameter control, niobium silicide foils with a niobium-rich core can be generated. The niobium cores provide toughness to the otherwise brittle niobium silicide intermetallic.

4.4 DEPOSITION OF $Nb_xAl_yTi_z$ TERNARY ALLOYS

Production of alloy films in the Nb-Ti-Al system requires consideration of possible products. According to the 1200°C section of the ternary phase diagram shown in Figure 4-42, nine phases are possible. The Nb-Al coordinate shows the expected Nb_3Al, Nb_2Al, and $NbAl_3$ compounds and how they are extended toward the Ti apex with Ti additions. This diagram also shows the other single phase regions, such as Al(l), ß(Nb-Ti), mixed TiAl, Ti_3Al, and two ternary phases, B_2 and τ_2, as well as invariant three-phase and two-phase deposition regions including some tie lines. Clearly, it would be difficult to deposit precise single phases except perhaps ß[Ti,Nb,(Al)]. Although control of stoichiometry sufficient to produce other single phases using AlCl(g) must still be learned, certainly Nb-Ti-Al products can be made using AlCl(g), $TiCl_4$, and

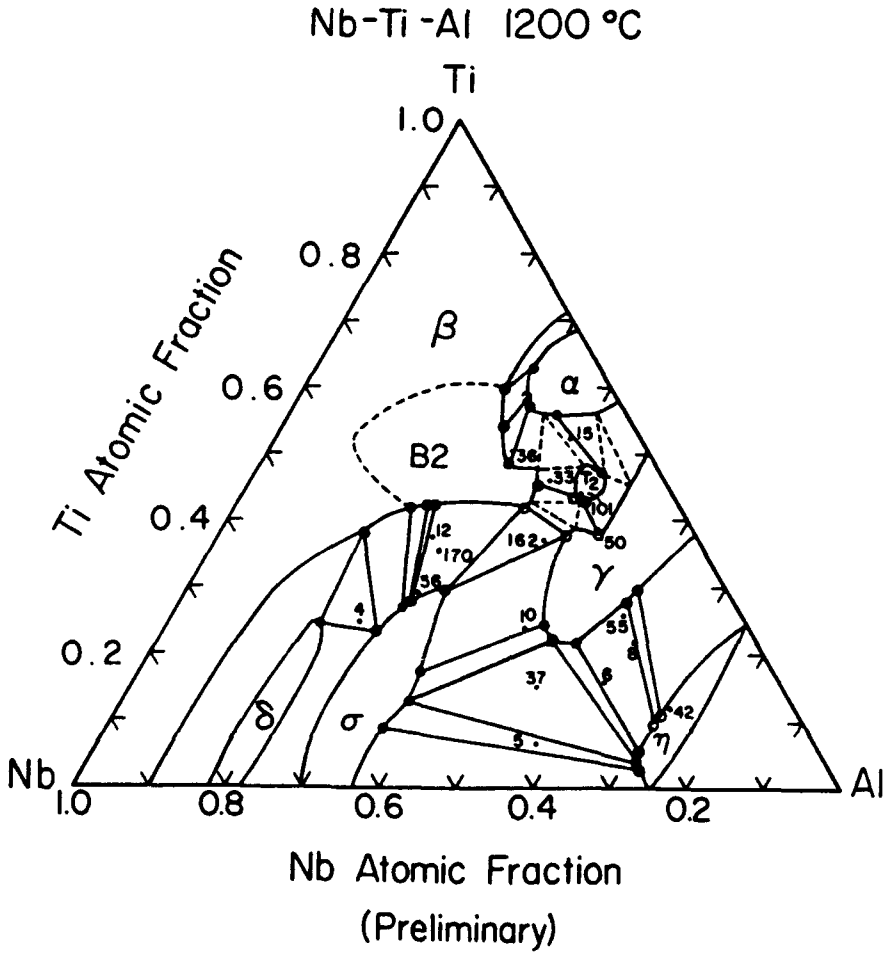

Figure 4-42. The 1200°C section of the Nb-Ti-Al system phase diagram (Ref. 4-1).

$NbCl_5$. This task is much more difficult to control in terms of product composition in the ternary system than in the two component systems.

These depositions were performed using the same apparatus that was used in the formation of niobium aluminides by the AlCl reduction of $NbCl_5$. AlCl was generated by passing He through a temperature controlled $AlCl_3$ vaporizer. Helium passing through a temperature controlled $NbCl_5$ vaporizer and $TiCl_4$ at room temperature completed the reactant gas mixture. Process parameters used to deposit $Nb_xAl_yTi_z$ by the reduction of mixed titanium and niobium chlorides with AlCl are given in Table 4-11.

The results of these experimental trials are shown in Figures 4-43 to 4-47 and Table 4-12. When high concentrations of $TiCl_4$ were attempted (sample JD300-14), a black sooty deposit resulted. Figures 4-43 and 4-44 show that inclusion of a small amount of titanium in the deposit made an improvement in the apparent density of the intermetallic deposit when compared with deposits (Figures 4-18 to 4-24) made with nearly the same process parameters without titanium. This densification was less when higher concentrations of titanium were added to the intermetallic. The tendency to form multiple layers was very strong in these deposits. With higher titanium in the deposit, porous inner layers developed and are believed to have been the cause of missing coating layers in samples JD300-18 and JD300-24.

Deposition of $Nb_xTi_yAl_z$ ternary compositions is thus feasible, but the compositional limits of this process are unknown at this time.

Table 4-11. Ternary Alloy Deposition

Sample Number	Temperature (°C)				Gas Flow (cc/min)							Time (min)	Pressure (torr)
	Substrate	$AlCl_3$	$NbCl_5$	Al	He in $AlCl_3$	$AlCl_3$	He in $NbCl_5$	$NbCl_5$	He in $TiCl_4$	$TiCl_4$ (at 20°C)	He		
JB300-14	900	132	105	955	100	3.2	100	0.23	200	4.0	2000	240	4
JB300-16	945	134	107	965	100	3.6	100	0.25	50	1.0	1950	240	4
JB300-18	950	132	97	965	100	3.2	100	0.16	50	1.0	1950	250	4
JD300-20	900	130	106	955	100	2.7	100	0.24	100	2.0	1900	243	4
JD300-22	900	131	107	955	100	3.0	100	0.25	150	3.0	1850	240	4
JD300-24	950	131	99	955	100	3.0	100	0.17	100	2.0	1900	245	5

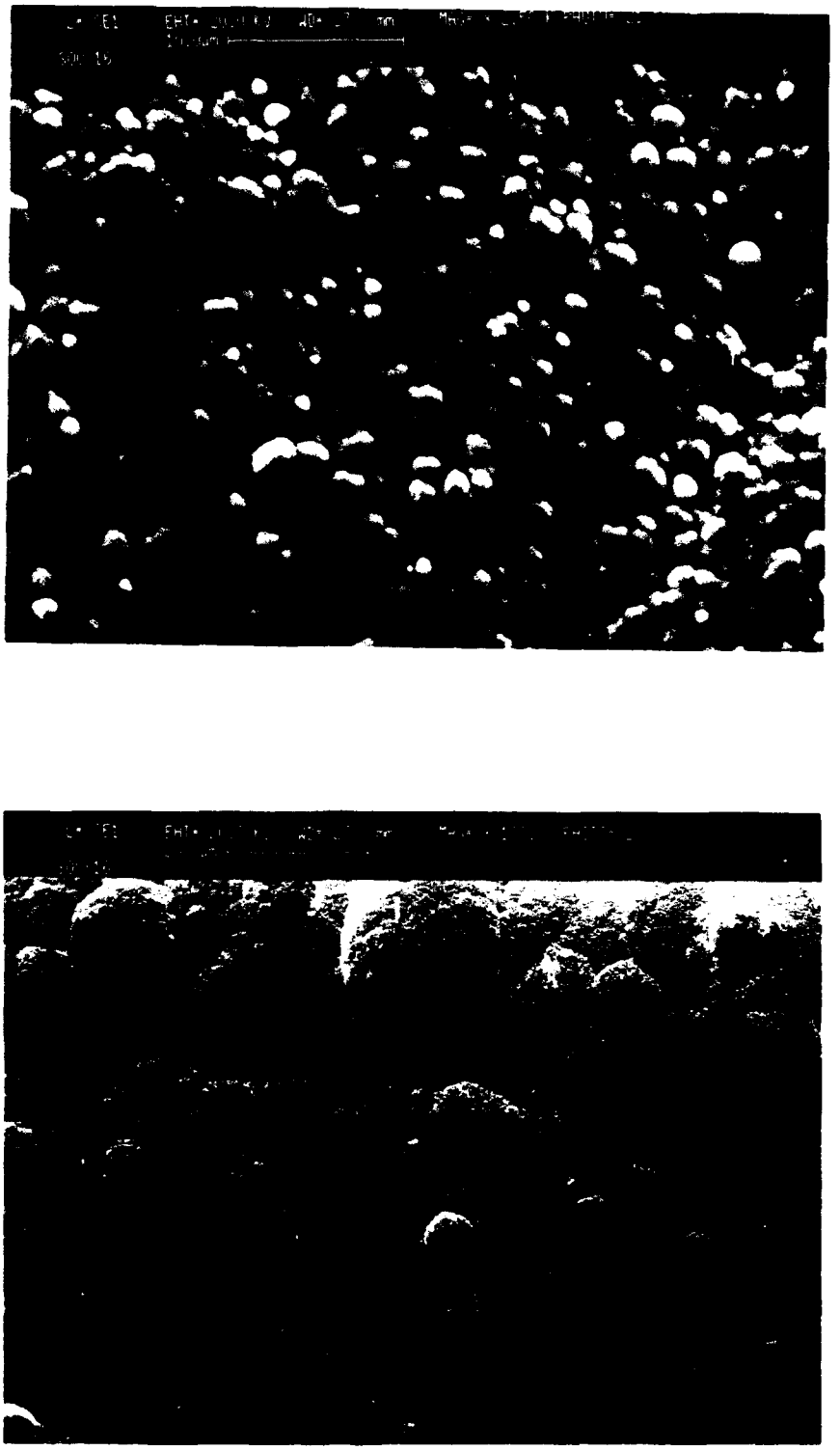

Figure 4-43. SEM photomicrograph of an NbTiAl intermetallic film containing 58.6 at. % Nb, 35.5 at. % Al, and 5.9 at. % Ti.

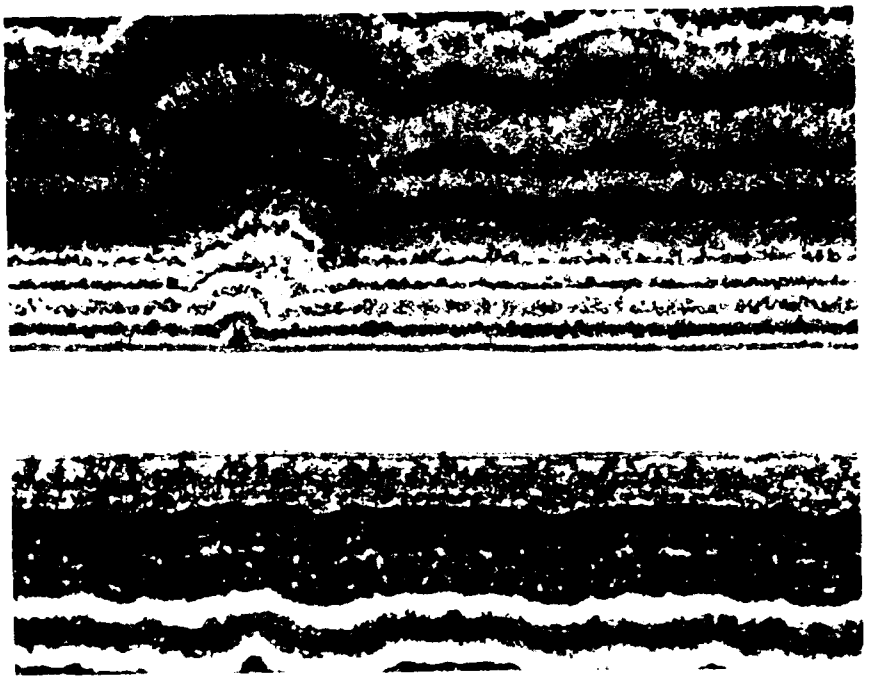

(a)

(b)

Figure 4-44. Cross sectional views of vapor deposited $Nb_xAl_yTi_z$ (sample JD300-16) on niobium foil: (a) optical photomicrograph of an etch sample at 500X; (b) SEM photomicrograph.

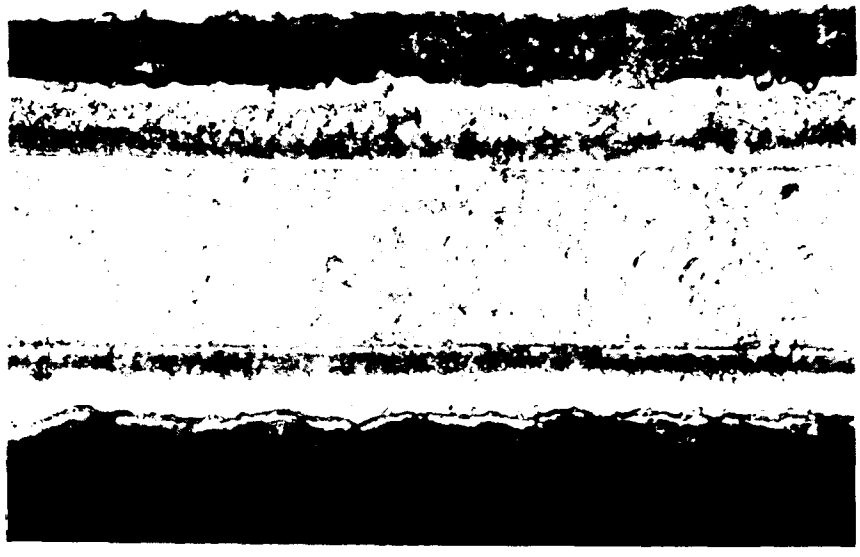

(a)

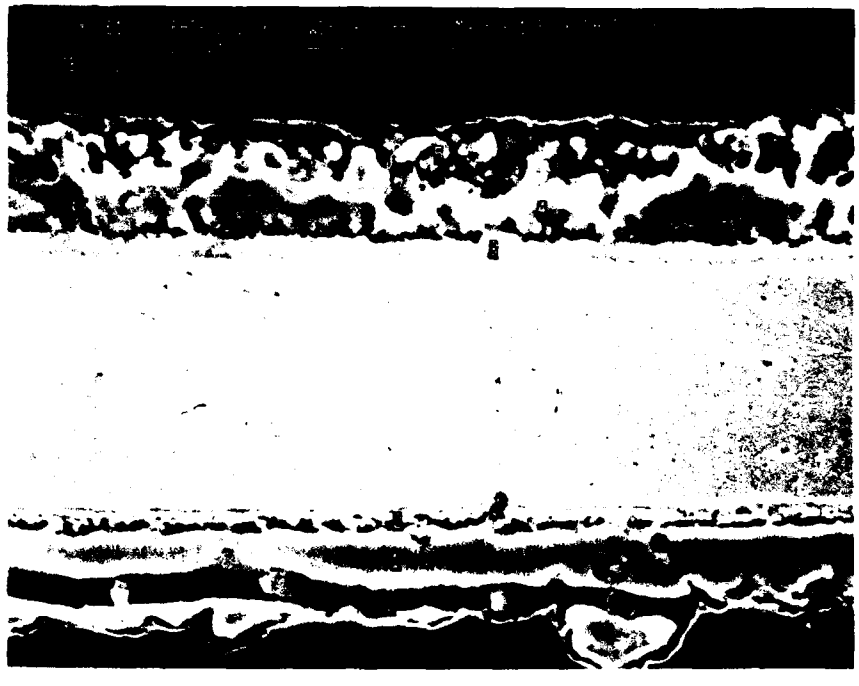

(b)

Figure 4-45. Cross sectional views of $Nb_xAl_yTi_z$ (sample JB300-20) deposited on niobium showing porosity in high titanium concentration areas: (a) optical photomicrograph at 1000X; (b) SEM photomicrograph.

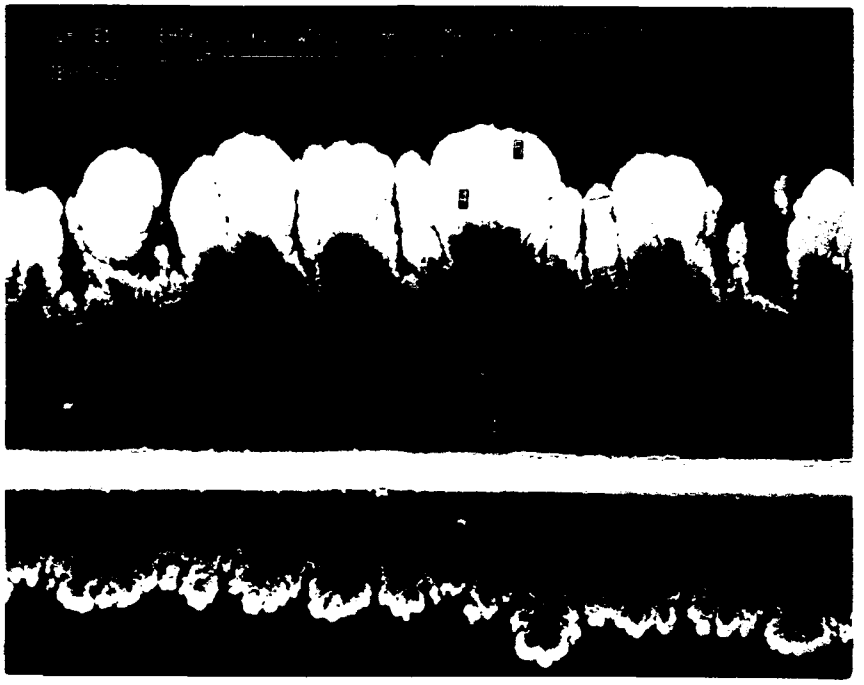

Figure 4-46. SEM photomicrograph of a cross section of $Nb_xAl_yTi_z$ (sample JB300-22) deposited on niobium showing the formation of a porous high titanium content material between the niobium substrate and the outer intermetallic deposit.

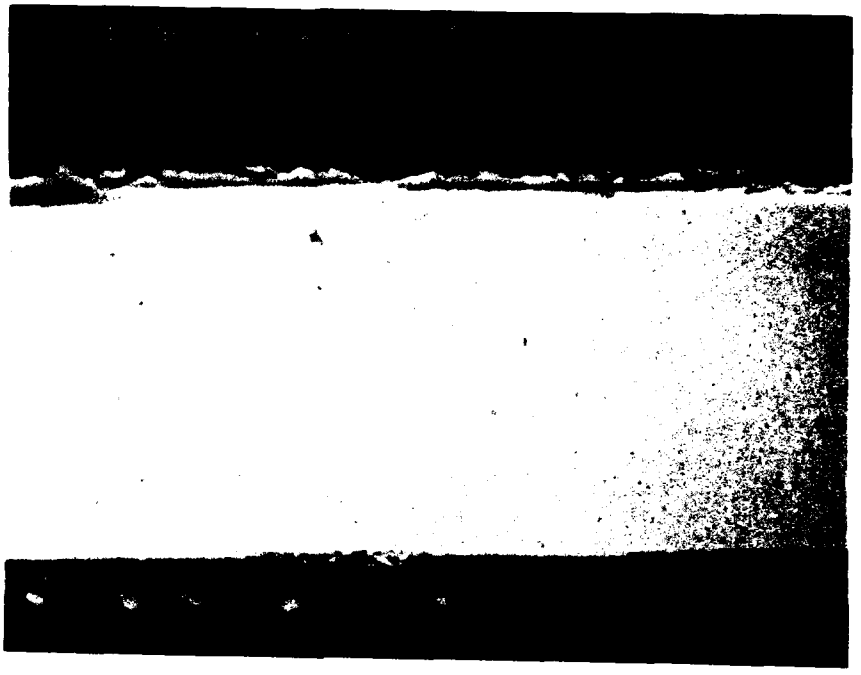

Figure 4-47. SEM photomicrograph of high titanium content $Nb_xAl_yTi_z$ (sample JB300-24) deposited on niobium without porous and multiple $Nb_xAl_yTi_z$ layers previously observed in equivalent experimental trials.

Table 4-12. Results of $Nb_xAl_yTi_z$ Deposition Experiments

Sample Number	Layer	Deposition Rate (μm/min)	Layer Composition (at. %)			Micro-hardness	Remarks
			Nb	Al	Ti		
JD300-14	Coating						Sooty deposit
JB300-16	Substrate		100			73	
	Inner transition	0.33	54.77	42.62	2.61	360	Many more than two layers in the transition. The separation into inner and outer was arbitrary.
	Outer transition		51.43	43.49	5.08	686	
	Coating		58.64	35.49	5.87	599	
JB300-18	Coating						Coating missing
JB300-20	Substrate		100			63	
	Inner transition	0.04	28.23	50.04	21.73		Too soft for microhardness
	Outer transition		4.47	43.16	52.39		Porous sooty layer
	Coating		8.92	36.29	54.79		
JB300-22	Substrate		100			60	
	Outer transition	0.08	29.85	12.16	57.98		Very porous
	Coating		54.32	42.50	3.18	710	
JB300-24	Coating		4.42	30.20	65.38		Coating thin or missing

5. COMPOSITE MATERIAL FORMATION (CVI)

An effort was made to determine the feasibility of using processes for making niobium aluminide intermetallics to infiltrate fiber preforms. Alumina is a candidate as a reinforcing filament for these intermetallic matrix composites. Alumina tow made by 3M was chosen for these examinations. The AlCl reduction of $NbCl_5$ was the process chosen for these chemical vapor infiltration (CVI) experiments.

Process parameters used for these experimental trials are given in Table 5-1. The alumina tow was held vertically in the deposition system, supported only at the top end, in experimental trials JB300-4 to JB300-8. The first deposits coated the filaments with niobium aluminide as shown in Figures 5-1 and 5-2 but did not form an infiltrated intermetallic matrix material. Efforts made to secure both ends of the alumina tow with carbon yarn still did not provide filaments which coated uniformly. A dense matrix linking the individual filaments was not achieved. The chemical compositions of these deposits are shown in Table 5-2.

To keep the fiber tow held firmly during attempted CVI processing, the tow was wound around alumina tubes used for gas inlets as shown in Figure 5-3. Carbon yarn was used to fasten the alumina filaments to the alumina tow supports. Metallographic cross sections of the resulting materials are shown in Figures 5-4 and 5-5. The deposits were nonuniform and generally porous along the length of the tow. Most of the deposits were on the exterior of the fiber tow. The substrate material also influenced the deposit. The deposit readily formed on the carbon yarn used to fasten the alumina tow on the alumina tubes, as it had in previous depositions on niobium substrates. The coating was more sparse on the alumina tow. Nucleation on the substrate may be more difficult on these filaments than on carbon or niobium. There was no evidence of damage to the fibers in optical and SEM photomicrographs.

Table 5-1. Process Parameters for Chemical Vapor Infiltration of 3M Alumina Tow

Sample Number	Substrate	Temperature (°C)				Gas Flow (cc/min)					Time (min)	Pressure (torr)
		Substrate	$AlCl_3$	$NbCl_5$	Al	He in $AlCl_3$	$AlCl_3$	He in $NbCl_5$	$NbCl_5$	He		
JB300-4	3M Al_2O_3	918	130	107	955	100	2.7	100	0.25	2000	255	6
JB300-6	3M Al_2O_3	918	135	107	960	100	3.9	100	0.25	2000	487	6-7
JB300-8	3M Al_2O_3	910	133	105	965	100	3.4	100	0.26	2000	1085	6-7
JB300-10	3M Al_2O_3	895	131	104	950	100	2.9	100	0.21	2200	660	6-7
JB300-12	3M Al_2O_3	885	132	106	955	100	3.2	100	0.47	2200	600	6-7
JD300-92	3M Al_2O_3	1305	124	130	-	100	1.7	300	2.2	800 (H_2)	120	40
JD300-93	3M Al_2O_3	1315	123	131	-	100	1.6	300-211	2.3-1.6	800 (H_2)	150	39-23
JD300-94	3M Al_2O_3	1300	133	127	-	100	3.4	300	2.0	800 (H_2)	150	37

Table 5-2. Composition of Nb_xAl_y Deposits on 3M Alumina Tow

Sample Number	Composition (at. %)	
	Nb	Al
JB300-4	28.52	71.48
JB300-6	41.30	58.70
JB300-8	64.70	35.30

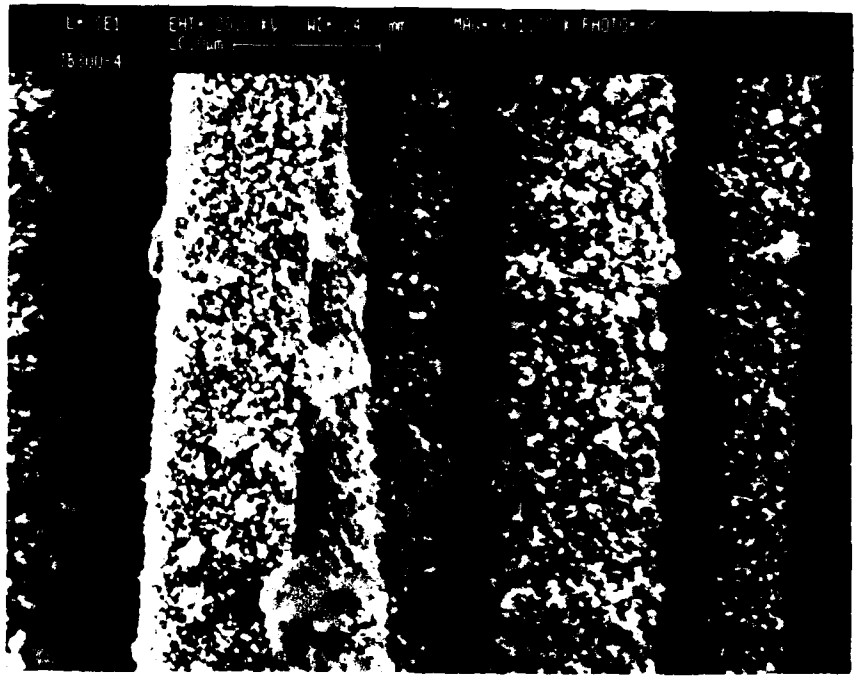

(a)

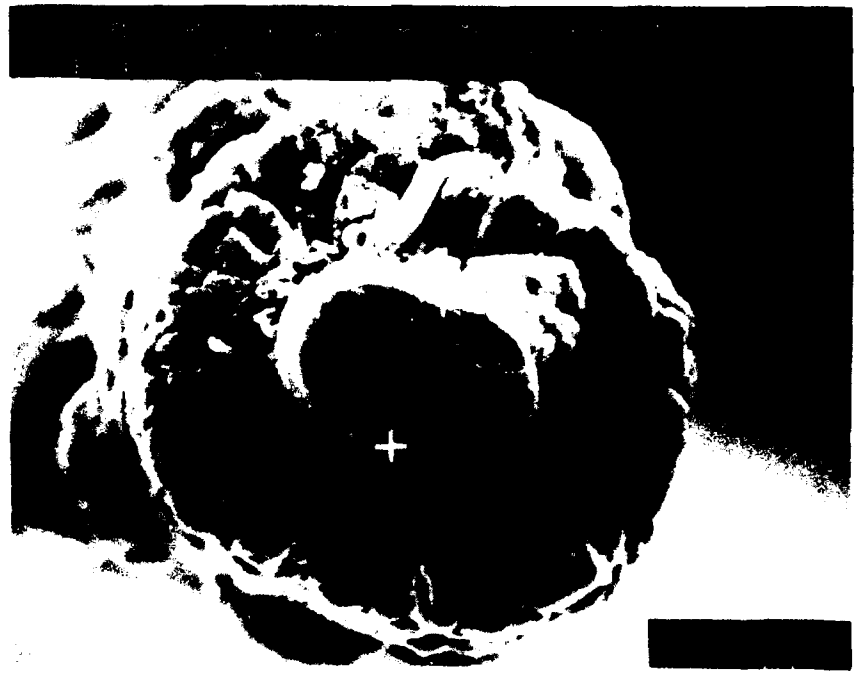

(b)

Figure 5-1. SEM photomicrographs of niobium aluminide infiltrated 3M alumina tow as processed in experiment JB300-4.

(a)

(b)

Figure 5-2. SEM photomicrographs of niobium aluminide infiltrated 3M alumina tow as processed in experiment JB300-6.

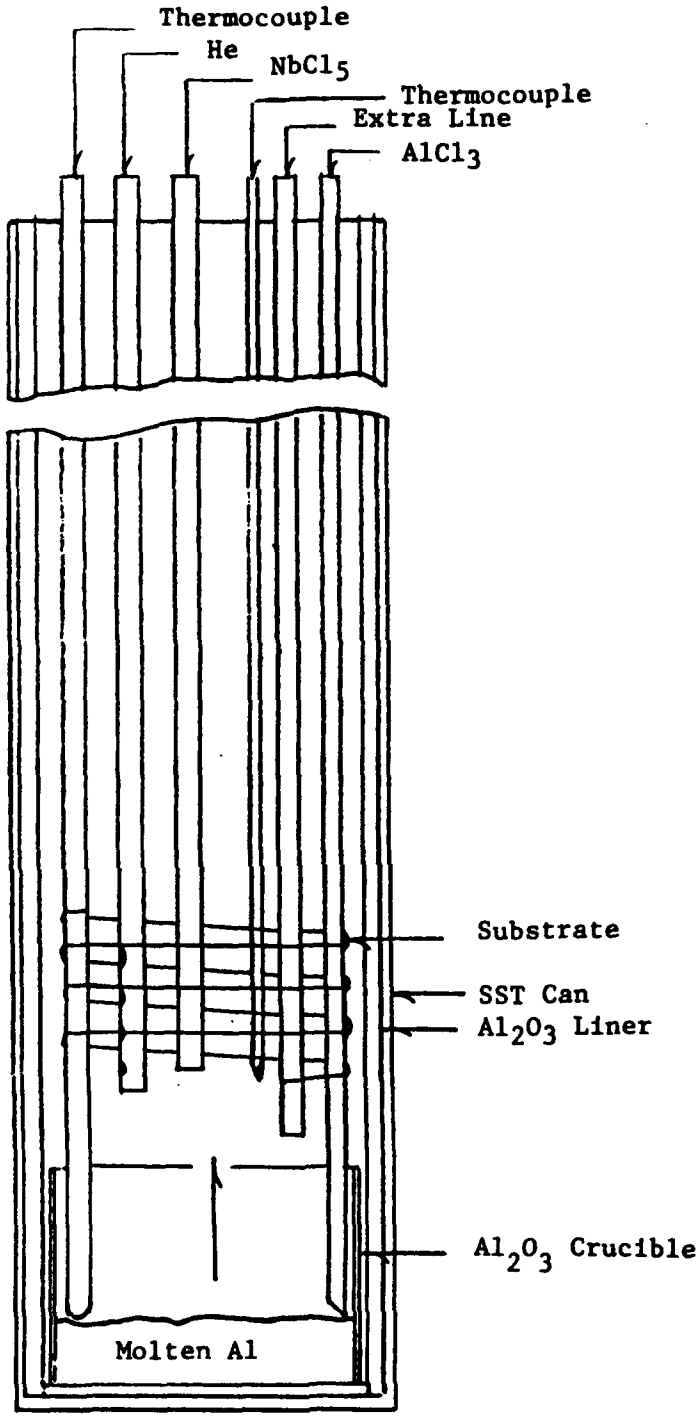

Figure 5-3. Schematic diagram of the experimental setup used for vapor infiltration of alumina tow.

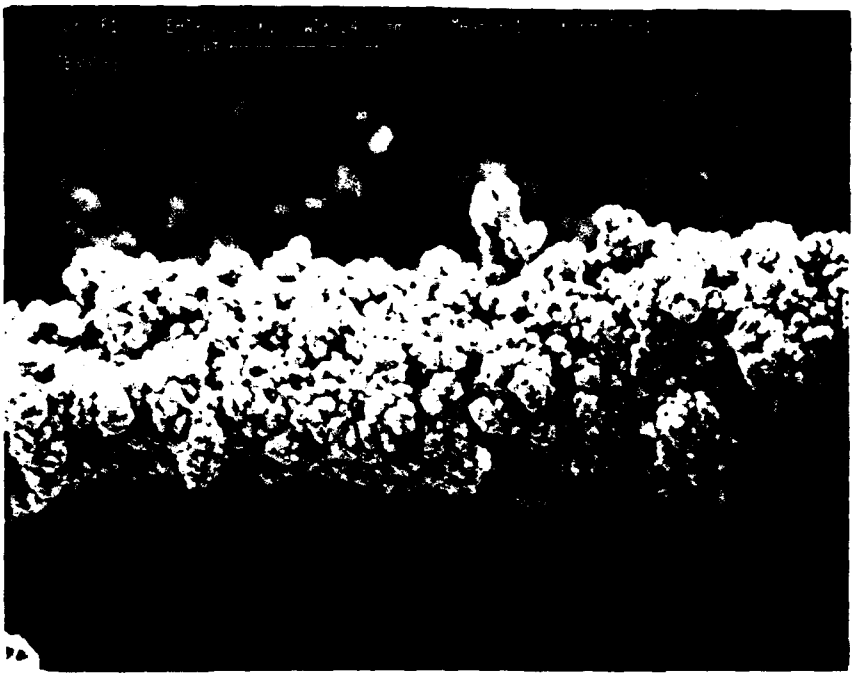

(a)

(b)

Figure 5-4. Examples of porous niobium aluminide deposits on 3M alumina from experiments (a) JB300-8, (b) JB300-10-1.

(a)

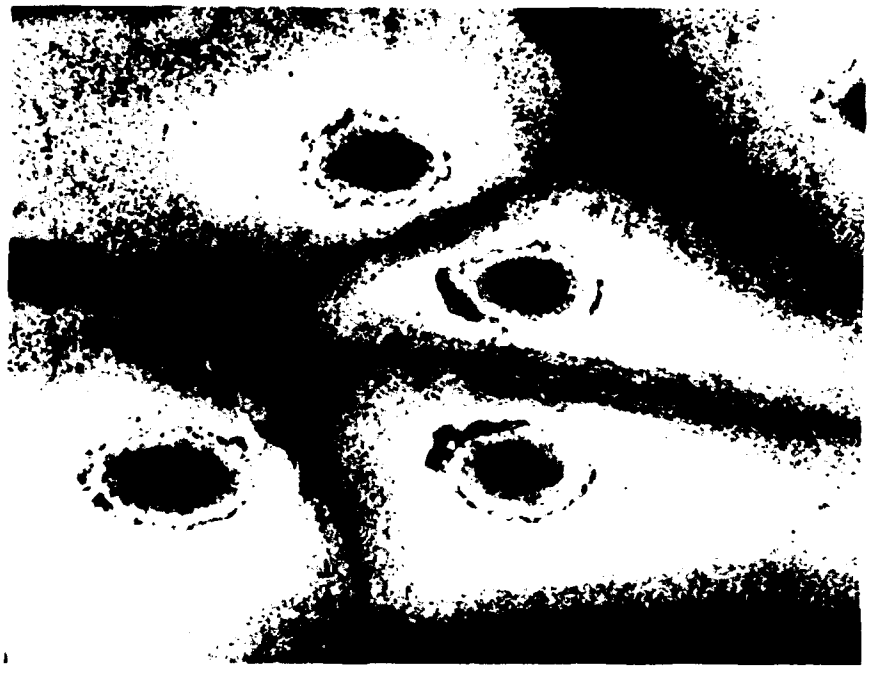

(b)

Figure 5-5. Metallographic photomicrographs at 500X of chemical vapor infiltrated 3M alumina tow from experiments (a) JB300-10-1 and (b) JB300-12-1 showing partial infiltration and nonuniform deposition of the exterior of the fiber tow.

Three experimental trials, JD300-92 to JD300-94, were made to form the niobium aluminide matrix composite by the hydrogen reduction of AlCl3 and NbCl5. These deposits were made on 3M alumina fiber tow suspended along the axis of a cylindrical graphite susceptor. Damage to the filaments from the high temperature processing is unknown.

6. MECHANICAL TESTING OF FOILS

Most of the foil samples that could be removed from the substrate were either porous or brittle. Measuring the mechanical properties of these foils by conventional means did not seem feasible. The decision was made to use a single filament tester to measure the tensile properties of the foils. The objective was to accommodate the anticipated low failure loads and fragile nature of the specimens by minimizing the stress needed to hold the sample in the tester. One way of doing this is to use an adhesive to bond the specimen to a holder. The apparatus used for these tests is shown in Figure 6-1. Specimen JB200-44 was epoxy bonded to a paper holder as shown in Figure 6-2, and the assembly was then clamped in the tester as shown in Figure 6-3. When the paper tab was cut to begin the test, relief of stress in the paper broke the sample. A second sample was mounted in the tensile tester and the specimen holder was burned instead of cut with a scissors to release the sample. The load needed to test the sample exceeded the load limit of the tester. This work was discontinued when it was realized that none of the experimental deposits produced foils which were uniform enough or strong enough to be testable using this procedure.

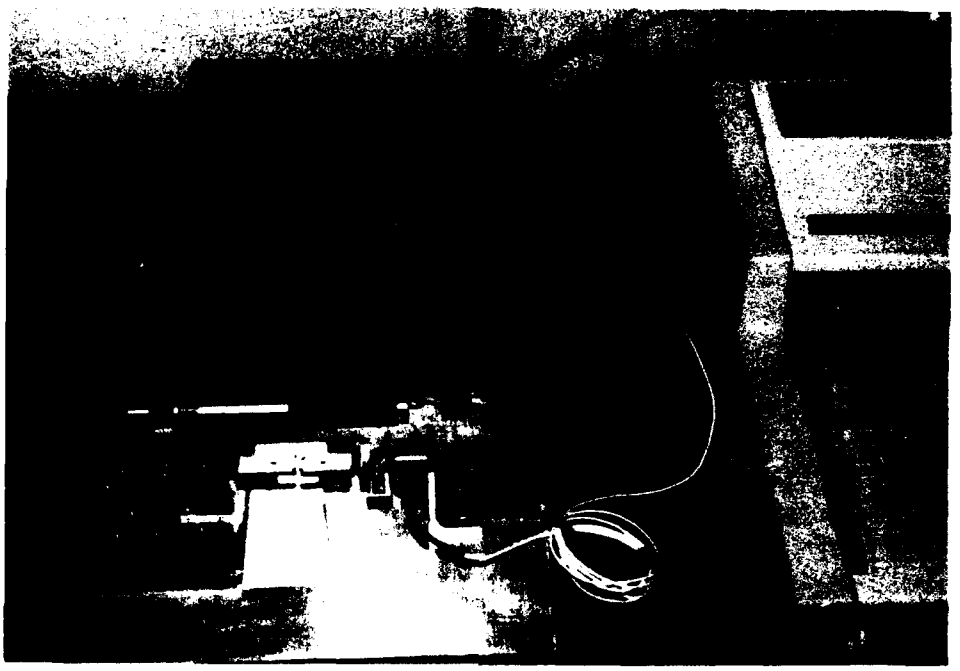

Figure 6-1. Single filament tensile tester used for Nb_xAl_y foil tensile tests.

Figure 6-2. Nb_xAl_y foil sample epoxy bonded to a paper template.

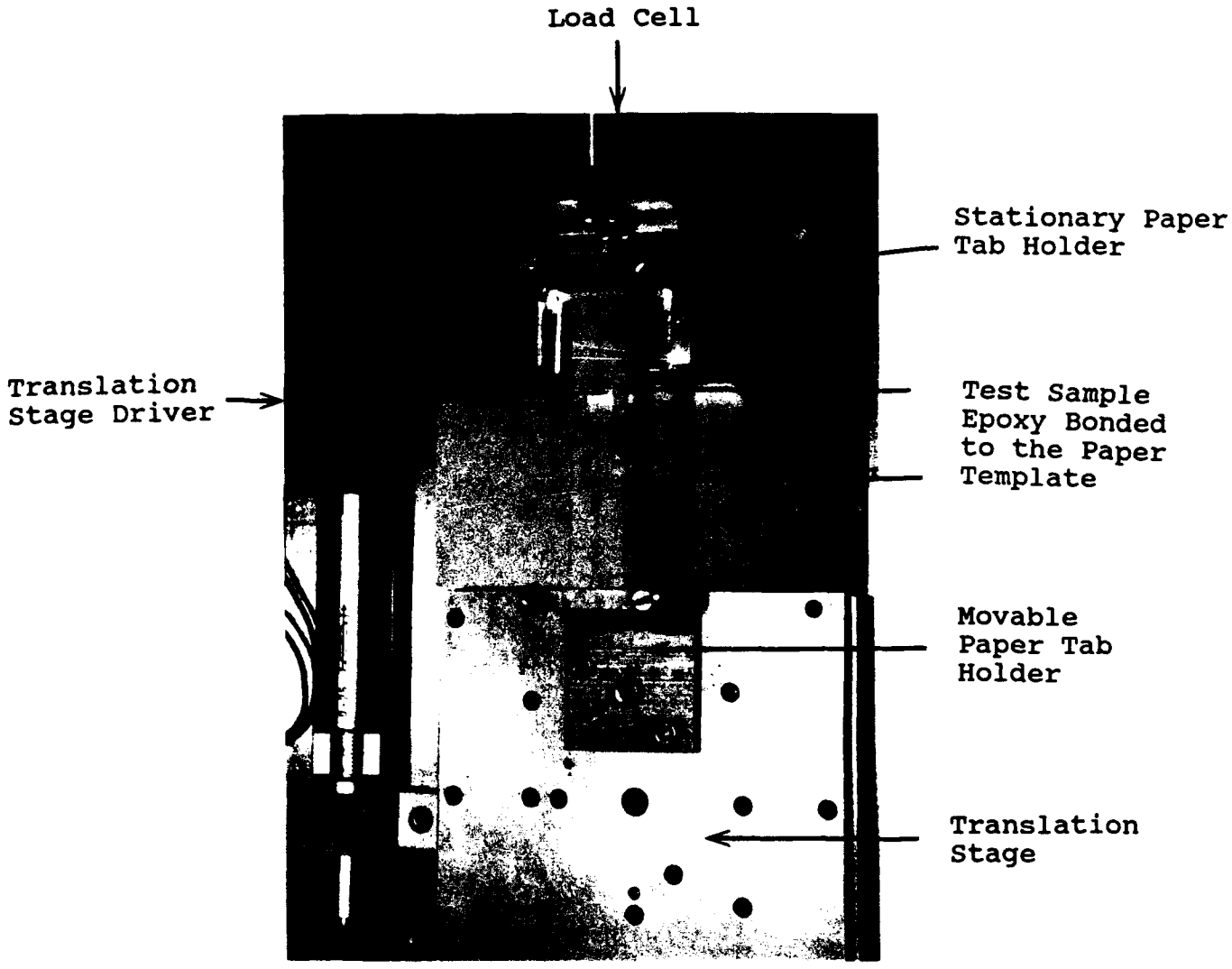

Figure 6-3. Test sample epoxy bonded to a paper template and mounted in the test fixture.

7. SUMMARY

The Phase II effort improved both the understanding and control of processes developed in Phase I for the preparation of NbAl intermetallics. Emphasis was given to the deposition of the niobium aluminides by the reduction of niobium pentachloride with aluminum monochloride. Other experiments examined the preparation of niobium aluminide by the hydrogen reduction of the metal chlorides. The deposition of niobium silicides and ternary niobium-titanium-aluminum intermetallics was also investigated.

The results of this Phase II program are summarized below.

Task 1. Process Modeling

- Equilibrium thermodynamic modeling of the formation of niobium aluminides by the reduction of $NbCl_5$ with AlCl and the hydrogen reduction of the metal chlorides was completed. Experimental parameter selections based on these model predictions proved to be correct.
- Alternative processes for forming niobium aluminide intermetallics from the reduction of $NbCl_5$ with aluminum metal and MCl_x metal chlorides were also modeled.

Task 2. Process Optimization

- Niobium aluminide intermetallics were deposited by two processes: (1) the formation of AlCl, which in turn was used to reduce $NbCl_5$, and (2) the hydrogen reduction of aluminum and niobium chlorides.
- Handling molten aluminum for the required generation of AlCl(g) involved an extra process step and extra equipment. It also imposed some limitations on the materials used in the construction of the apparatus.
- For Phase II, the Phase I apparatus used in the deposition of $NbAl_x$ was modified to replace quartz in the system with alumina. It was found experimentally and shown theoretically early in the Phase II effort that AlCl(g) would reduce SiO_2 and thus was unacceptable as a containment

vessel material for these experiments. Other improvements made in the apparatus used to deposit materials in the Phase II studies included (1) deposition at both atmospheric and reduced pressures, (2) better temperature monitoring of the input gases and the substrate during deposition, and (3) use of multiple gas inputs to improve flow controls and the orientation of gases introduced into the chamber. (This improved process control permitted the formation of ternary intermetallics.)

- Contamination in the product intermetallics was reduced primarily through better control of the deposition environment and adjustments in the substrate temperature.

- Correlations were found between modeling predictions and experimental results for process conditions which favored the formation of niobium aluminum in both AlCl and hydrogen reduction processes. The AlCl process did not require the high temperatures that the hydrogen reduction process did, but as predicted the chemical compositions of these deposits were more sensitive to the gas flow dynamics and system geometry than deposits formed by the hydrogen reduction process.

Task 3. Deposition of Nb-Si Compositions

- Deposition of niobium silicides by the hydrogen reduction of the chlorides was straightforward. Forming foils of this material is difficult because of the reactivity of silicon with most materials that would be used as substrates. The selection of a niobium substrate for these deposits eliminates the inclusion of a third material and may be the best option for foil preparation.

- Niobium silicides with compositions corresponding roughly to $NbSi_2$ were deposited on niobium substrates.

Task 4. Deposition of Ternary Intermetallic Compsitions

- Ternary intermetallics containing niobium, aluminum, and titanium were formed by the reduction of the chlorides of niobium and titanium with AlCl.

- The addition of titanium tetrachloride to the aluminum monochloride process for forming niobium aluminide initially increased the density of the deposit, then caused the formation of multiple layers and high titanium content porous layers.

- The process is a complex one; thus, the degree of control one has over the composition is unknown at this time.

Task 5. Deposition of Intermetallic Compounds Containing Dispersed Metallic Phases

- Niobium aluminide deposits formed by the AlCl reduction of the chlorides corresponding to niobium-rich niobium aluminide (Nb + Nb_3Al) compositions were successfully produced but were mostly porous. Even when the composition corresponded to Nb-Nb_3Al, discrete dispersed particulate phases were not detected by the characterization methods used.

- Niobium aluminide deposits formed at high temperatures by the hydrogen reduction of the chloride and niobium silicide deposits reacted with the niobium substrates. In some cases layered structures were formed with niobium at the core and the intermetallic on the surfaces, and in other cases the niobium substrate disappeared, leaving a large void between layers of intermetallic.

Task 6. Chemical Vapor Infiltration of Ceramic Fiber Tow

- Alumina tow was infiltrated with niobium aluminide from the AlCl reduction process. Filaments were coated with niobium aluminide by both AlCl and H_2 reduction processes. With the AlCl process, infiltration of the tow was generally poor and the tows were not sufficiently rigidized to qualify as "chemically vapor infiltrated" composites. Infiltration by the hydrogen reduction process coated the filaments more uniformly than the ymonochloride process, but high temperature process damage to the filaments is unknown.

- Intermetallic foils deposited in the program were mostly porous or integral with, and difficult to remove from, the substrate. Tensile testing of these materials as thin foil specimens was not successful.

Task 7. Material Characterization

- Characterization of the niobium aluminide films was primarily by optical metallography, SEM, and EDAX examinations.

- Intermetallic foils deposited in the program were mostly porous or integral with, and difficult to remove from, the substrate. Tensile testing of these materials as thin foil specimens was not successful.

8. REFERENCES

1. Lundin, C.E., and A.S. Yamamoto, Trans. Met. Soc. AIME **236**, 863 (1966).

2. Malets, G.A., Vesti. Akad. Nauk., B. SSR, Ser. Khim. Nauk. **6**, 127 (1974).

3. JANAF Thermochemical Tables, M.W. Chase et al. (eds.), Dow Chemical Company, 3rd edition, Supplement 1, 1985.

4. Perepezko, J.H., Y.A. Chang, L.E. Seitzman, J.C. Lin, N.R. Bonda, T.J. Jewett, and J.C. Mishurda, "High-Temperature Phase Stability in the Ti-Al-Nb System," in High Temperature Aluminides and Intermetallics, S.H. Whang, C.T. Liu, D.P. Pope, and J.O. Stiegler (eds.), The Minerals, Metals & Materials Society, 1990, p. 19.

☆U.S. Government Printing Office:1992—648-127/62283